A Study on System-Level Energy Management Methodology for Demand-Side Flexibility

Submitted to
Graduate School of Information Science and Technology
Osaka University

January 2023

Daichi WATARI

Publications

Journal Article (Refereed)

[J1] Daichi Watari, Ittetsu Taniguchi, Francky Catthoor, Charalampos Marantos, Kostas Siozios, Elham Shirazi, Dimitrios Soudris, and Takao Onoye, "Thermal-comfort aware online co-scheduling framework for HVAC, battery systems, and appliances in smart buildings," *IEICE Transactions on Fundamentals of Electronics, Communications and Computer Sciences*, vol. E106-A, no. 5, pp. -, 2023. (to appear)

[J2] Daichi Watari, Ittetsu Taniguchi, Hans Goverde, Patrizio Manganiello, Elham Shirazi, Francky Catthoor, and Takao Onoye, "Multi-time scale energy management framework for smart PV systems mixing fast and slow dynamics," *Applied Energy*, vol. 289, p. 116671, 2021.

[J3] Daichi Watari, Ittetsu Taniguchi, and Takao Onoye, "SOH aware system-level battery management methodology for decentralized energy network," *IEICE Transactions on Fundamentals of Electronics, Communications and Computer Sciences*, vol. E103-A, no. 3, pp. 596-604, 2020.

International Conference Papers (Refereed)

[I1] Daichi Watari, Ittetsu Taniguchi, and Takao Onoye, "Improving duck curve by dynamic pricing and battery scheduling based on a deep reinforcement learning approach," in *Proceedings of the 8th ACM International Conference on Systems for Energy-Efficient Buildings, Cities, and Transportation (BuildSys)*, pp. 232–233, 2021.

[I2] Daichi Watari, Ittetsu Taniguchi, Francky Catthoor, Charalampos Marantos, Kostas Siozios, Elham Shirazi, Dimitrios Soudris, and Takao Onoye, "Thermal comfort aware online energy management framework for a smart residential building," in *Proceedings of the 2021 Design, Automation and Test in Europe Conference (DATE)*, pp. 535–538, 2021.

[I3] Daichi Watari, Ittetsu Taniguchi, Patrizio Manganiello, Hans Goverde, Francky Catthoor, and Takao Onoye, "An online multi-scale optimization framework for

smart PV systems," in *Proceedings of the 36th European Photovoltaic Solar Energy Conference and Exhibition (EUPVSEC)*, 6CO.15.1, pp. 1681–1684, 2019.

[I4] Daichi Watari, Ittetsu Taniguchi, and Takao Onoye, "SoH aware battery management optimization on decentralized energy network," in *Proceedings of the 9th ACM/IEEE International Conference on Cyber-Physical Systems (ICCPS)*, pp. 337–338, 2018.

Domestic Conference Papers (Unrefereed)

[D1] Daichi Watari, Ittetsu Taniguchi, Francky Catthoor, Charalampos Marantos, Kostas Siozios, Elham Shirazi, Dimitrios Soudris, and Takao Onoye, "Thermal comfort aware real-time co-scheduling of HVAC, battery system, and smart appliances for smart building," *IEICE Technical Report*, vol. 121, no. 92, MSS2021-8, pp. 36–41, 2021 (in Japanese).

[D2] Daichi Watari, Ittetsu Taniguchi, Patrizio Manganiello, Hans Goverde, Francky Catthoor, and Takao Onoye, "An online multi-scale optimization framework for smart PV systems," *SICE Symposium on Systems and Information (SICE-SSI)*, 2020 (in Japanese).

[D3] Daichi Watari, Ittetsu Taniguchi, and Takao Onoye, "A battery degradation aware system level battery management methodology," *IEICE Technical Report*, vol. 118, no. 457, VLD2018-104, pp. 67–72, 2019 (in Japanese).

Summary

Towards a sustainable future, renewable energy, especially solar and wind power, increasingly emerge as a clean energy source without emitting carbon dioxide. In some countries, renewable generation has already reached grid parity, where their generation costs are the same or less than that of conventional power plants. From the perspectives of cost and cleanliness, the penetration rate of renewable generation is expected to grow further. However, renewable energy depends on environmental conditions such as weather and wind speed and is often intermittent and uncontrollable. The variable renewable generation risks destabilizing the energy system. In particular, the demand-supply mismatch caused by the massive solar integration is called the duck curve problem, and it brings severe cost increases to supply-side management, such as the more active operation of power plants. To smoothly integrate renewable energy more and more, promoting the acquisition and utilization of demand-side flexibility (DSF) is required, which refers to the portion of the demand load that can be shifted, curtailed, or adjusted from their normal consumption patterns.

With the development of information and communication technology (ICT), local energy systems on the demand side are becoming more intelligent. Consumers turn into prosumers with a controllable distributed energy resource (DER) such as renewable generation, a battery system, and controllable demand. Accordingly, the prosumers can bidirectionally exchange information and electrical energy with the supply side. The most promising application for the demand side energy system is an energy management system (EMS) that enables the monitoring, planning, and controlling of various DERs. For instance, the EMS schedules battery systems and electric vehicles (EVs) as an energy buffer to effectively use renewable generation. In addition, such controllable demands as appliances and heating, ventilation, and air conditioning (HVAC) systems can be shifted or reduced following price signals and user preferences. In this way, the demand side can manage DERs to reduce their system and electricity costs while maximizing user convenience. However, thermal comfort sensation and the DER's characteristics, such as battery degradation effects and uncertainties of demand-supply patterns, often lead to higher costs and dissatisfaction. Therefore, the EMS must consider such system dynamics when optimizing operational planning and real-time operation.

On the other hand, the supply side desires to utilize the part of demand-side DERs as DSF to meet the purpose of the global energy system. A demand response (DR)

program is one of the promising solutions to exploit DSF, organized by the supply side or aggregators. The DR program uses various signals/requests, including time-varying electricity prices or incentives for demand change. These signals could encourage the demand-side end users to reduce, shift, or increase their load patterns. Depending on the types of signals, there are mainly two types of DR programs: price-based DR and incentive-based DR. Each program has both good points and shortcomings, and an appropriate DR program should be designed to treat a specific supply-side problem such as the duck cure. Furthermore, the optimized interaction between the supply and demand sides through the DR and EMS development will unlock the potential of DSF.

This dissertation presents a system-level energy management methodology for smart energy systems with DERs, concerning the planning and real-time operation in the demand-side EMS and developing a DR program to exploit DSF. As for operational planning, a battery degradation-aware operational planning methodology for a smart energy system is proposed to estimate the system performance and minimize the system costs. In particular, the state-of-health (SOH) model is introduced to represent the capacity-fading effect of the battery system caused by the charging/discharging cycle and the battery state-of-charge (SOC) level. This model enables quantitatively observing the battery degradation factors and evaluating the system performance of the operational planning in terms of the battery system cost. The proposed method formulates the mixed-integer programming (MIP)-based two-stage optimization problem; the first stage minimizes energy purchase while the second stage minimizes the battery degradation factor with the constraint of the amount of the energy purchase. The simulation result shows that the proposed method can reduce the annual battery degradation costs by 14.1% without increasing the energy purchase compared to the baseline method that does not consider battery degradation. As a result, a better trade-off between battery degradation and the amount of energy purchased can be obtained.

To realize the real-time operation of DERs to compensate for the renewable fluctuation and reduce electricity costs, this dissertation proposes a multi-time scale energy management framework for scheduling a battery system and shiftable appliances with variable renewable generation. The proposed framework especially integrates the photovoltaic (PV) forecasting model and the accurate-parameterized equivalent circuit model of the battery system, which enables incorporating the real-time change of the system state. Moreover, a multi-time scale structure is proposed to reduce computational complexity without sacrificing the solution quality by considering a mix of fast and slow system dynamics. The simulation result shows that the proposed framework can reduce electricity costs by up to 47.5% compared to the five baseline methods. In addition, the proposed framework takes only 20 seconds of computational time at a maximum, satisfying the computational requirement (< 15 min).

For the real-time operation of DERs, thermal comfort, as well as electricity costs, should be considered through the heating/cooling system management. This dissertation also proposes a comfort-aware electrical and thermal energy management frame-

work for the energy system with a controllable HVAC system. The proposed framework is extended based on the above framework to schedule HVAC systems for optimal temperature set points. In the proposed framework, the thermal comfort estimation model based on linear regression techniques predicts the comfortable temperature that maximizes occupancy thermal comfort. The multi-objective optimization problem is formulated to minimize electricity costs and maximize thermal comfort simultaneously. The simulation result shows that the proposed framework can improve the trade-off relationship between electricity costs and thermal comfort. In the case study, the proposed method can reduce the electricity costs by up to 14.0% within the same comfort level compared to the baseline.

To meet the grid purposes through exploiting DSF, the optimal design of the DR program is required. As for the DR program, this dissertation proposes an optimal aggregator's strategy on the price-based DR and battery scheduling for improving the duck curve. The hierarchical energy market model is modeled as a Markov decision process (MDP), which represents the interaction between prosumers, an aggregator, a wholesale electricity market, and an independent system operator. In this work, the aggregator learns an optimal strategy using a model-free deep reinforcement learning (DRL) approach with the MDP model. The obtained strategy can calculate the retail prices to prosumers as a DR program and the schedule of the aggregator's battery power station to maximize social welfare, including the aggregator's profit, the prosumer's cost, and the improvement of the duck curve. Moreover, owing to the model-free DRL approach, the proposed method can capture the complex prosumer responses to the prices without the detailed privacy information of the prosumers, such as the system configuration and the prosumer preferences. The simulation result shows that the proposed method with the carefully designed reward function can reduce the duck curve index, i.e., the standard variation and the peak-to-average ratio of the net load are reduced by up to 57.1% and 20.8% compared to the baselines.

Acknowledgments

First of all, I would like to express my gratitude and owe special thanks to my supervisor Associate Professor Ittetsu Taniguchi, Department of Information Systems Engineering, Graduate School of Information Science and Technology, Osaka University. He did for me what the best supervisors always find the way to do. If it wasn't for his kind support I would not be the person I am today and live the life I have today. His valuable guidelines and supports enable me to achieve sophisticated results in my research.

I would like to show my appreciation to my supervisor Professor Takao Onoye, Department of Information Systems Engineering, Graduate School of Information Science and Technology, Osaka University, who provided carefully considered feedback and valuable comments. His technical insight is always on target, and I am deeply in debt to him for his careful guidance for this work.

I am very grateful to Professor Francky Catthoor, Department of Electrical Engineering (ESAT) at KU Leuven, and also an imec fellow. His invaluable ideas and advice helped me and my research on numerous occasions. He always facilitates collaborations with EnergyVille and NTUA/AUTH colleagues and contacts researchers in related fields. based on linear regression techniques. Clearly, this dissertation could not have grown as large as it has without him. In addition, he really supported my life when I was staying in EnergyVille, Belgium.

I would like to appreciate Professor Tatsuhiro Tsuchiya, Department of Information Systems Engineering, Graduate School of Information Science and Technology, Osaka University, for his detailed reviews and insightful suggestions that can drive my dissertation in a better and new direction.

I am grateful to Assistant Professor Hiroki Nishikawa, Department of Information Systems Engineering, Graduate School of Information Science and Technology, Osaka University, for his precious suggestions and his enormous help. I have always learned a lot from his insightful views on doing research and his constructive comments.

I would like to thank Professor Yuichi Itoh, Department of Integrated Information Technology, Aoyama Gakuin University, and Associate Professor Masahide Hatanaka, Faculty of Informatics, The University of Fukuchiyama, for their kind advice and valuable comments on my research.

I would like to acknowledge members of imec for their contribution to multi-time scale energy management. I wish thanks to Assistant Professor Patrizio Manganiello,

Department of Electrical Sustainable Energy, TU Delft. He gave me proper advice at the meeting and advanced various things related to the research, such as paperwork, code validation, and literature survey. I am sure that this work could not have progressed without him. I would also like to thank my colleagues who belong to EnergyVille, Dr. Imre Horvath, Dr. Gofran Chowdhury, Mr. Laxmikant Radkar, Mr. Ioannis Oroutzoglou, Mr. Apostolos Bakovasilis, Mr. Barış Akyüz, and Mr. Dávid Máté Parragh for the wonderful time and for helping me greatly when I was working as the intern in EnergyVille. I would like to thank Assistant Professor Elham Shirazi, Faculty of Engineering Technology, University of Twente, for her cooperation in this work by giving valuable feedback, preparing the dataset, and managing Skype meetings. I would like to thank Dr. Hans Goverde, who was working at imec. He gave me the PV forecasting data and helped me during my stay at imec. His advice is always helpful in developing my work. The forecasting data of the PV panel is provided by Dr. Dimitrios Anagnostos, who was working at imec. I would like to acknowledge him for making the PV forecasting data to simulate the framework proposed in this dissertation while he was very busy.

I would like to thank members of the National Technical University of Athens (NTUA) and the Aristotle University of Thessaloniki (AUTH), Dr. Charalampos Marantos, NTUA, Professor Dimitrios Soudris, School of Electrical and Computer Engineering, NTUA, and Associate Professor Kostas Siozios, Department of Physics, AUTH, for their contribution to the collaboration on the online HVAC management. Meeting calls with them always motivated me and gave me insights.

I would also like to appreciate Professor Yoshiyuki Shimoda in the Division of Sustainable Energy and Environmental Engineering, Graduate School of Engineering, Osaka University, Associate Professor Toshihiro Suzuki in the Campus Sustainability Office at Osaka University, and the employees of DAIKIN Industries, Ltd., Mr. Shinya Harada, Mr. Sumio Shiochi, Mr. Tadao Tsuji, Mr. Yoshinori Yura, Mr. Masakazu Okamoto, Mr. Yasuhiro Sugimoto, Mr. Minoru Tomoda, and Mr. Hidekazu Kozuma for the precious suggestions and enormous help throughout on-site HVAC experiment in another project.

I would like to thank all members of Onoye Laboratory for the brilliant and lovely time. Mrs. Yuki Yoshida, the secretary of Onoye Laboratory, supported me in all of my laboratory life. Thanks to her kind support, I could concentrate on my research. I also thank members of Group CPS, Assistant Professor Dafang Zhao, Mr. Kenshiro Kato, Mr. Yuki Ozawa, Mr. Koki Iwabuchi, Mr. Kaneko Naoya, Mr. Shunsaku Miyatake, Mr. Kazuki Okazawa. Their comments and suggestions at the meeting always help me and my research, and a great time with them is a delight to me and always gives me motivation. Special thanks to my classmate in the laboratory, Mr. Yoshitaka Ishihara, Mr. Masahiro Itoh, Mr. Shori Ueda, Mr. Yoshinori Kamizono, and Mr. Kento Sakurauchi. After completing the master's program, we continued to go to a lot of Ramen restaurants and get a drink. It made me feel relaxed.

To all my wonderful friends, thank you always for the warm friendship and the fun

time. I owe a great debt of gratitude to my dearest friend Mr. Ryo Shinohara for giving me a big motivation towards each other's dream. I am especially grateful to have you in my life and to be able to say that you are part of my family. To my friends in the cycling club, Mr. Tomohiro Iguchi, Mr. Yutatsu Oe, Ms. Madoka Okumura, and other members, your friendship is one of the most precious things that I got at Osaka. I indeed thank my childhood friends in the T. group, Mr. Hiroki Tsutsumi, Mr. Yuki Obayashi, Mr. Hiroki Obayashi, Mr. Ryo Matsui, Mr. Takumi Yoshiie, Mr. Akira Morimatsu, despite the distances and seldom getting all together, great times with them and their funny jokes take my mind off any worries.

I would like to extend my gratitude to my family (Cruise, Mr. Hirotaka Watari, Mrs. Mika Watari, and Mr. Shuji Watari), Thank you for your endless love and patience which give me strength every day. Without my family's support, I would have never seen the end of this voyage.

Last but not least, I would like to offer my special thanks to my beloved wife Natsuki. Thank you for encouraging me to pursue the Ph.D and for your understanding over the last five years combined with my master's degree program. You are always there for me, bring so much happiness to my life, and supported me whenever the work was not going well. I could not have done this dissertation and my Ph.D journey without her warm and endless support and encouragement.

Contents

List of Figures

List of Tables

Chapter 1

Introduction

1.1 Background

Nowadays, the penetration rate of renewable energy is growing more and more for a sustainable future [1, 2]. As illustrated in Fig. 1.1, the global installed capacity of renewable energy has continuously increased in the past decades [3, 4]. In particular, wind and solar energy, which have expanded by 807 GW and 854 GW between 2000 and 2021, are promising energy resources because of their low operating cost and easy installation. Such renewable energy is also attractive in terms of sustainability since it is clean energy without CO_2 emissions and is not dependent on finite fossil fuels required to mine or import.

Despite its cleanliness, however, renewable energy has significant challenges from the perspective of the network capacity and the stable operation of the power grid [5]. Renewable generation is often intermittent and variable depending on environmental conditions, e.g., wind speed, solar irradiation, and cloud movement. In addition, they have uncontrollable characteristics, whereas such traditional power plants as coal-fired power generation can quickly ramp up/down and turn on/off. The variable renewable generation would cause severe grid stability issues such as frequency disturbance, overloading on the grid lines, and supply and demand mismatch [6]. In particular, the California independent system operator (CAISO) has reported that increased solar generation leads to the duck curve problem, which shows a steep net load graph representing total power consumption minus renewable generation [7]. Consequently, the power grid suffers from the rapid integration of renewable energy. To address the renewable variability, the supply-side utilities are responsible for keeping the supply-demand balance using their power generation system [8]. Also, they reserve their capability of power ramping up/down by building more new power plants and retrofitting the old power plants in advance. However, the profitability of having large-capacity power plants that are generally not used is particularly low. Not only supply-side management but also the use of demand-side energy resources is more critical.

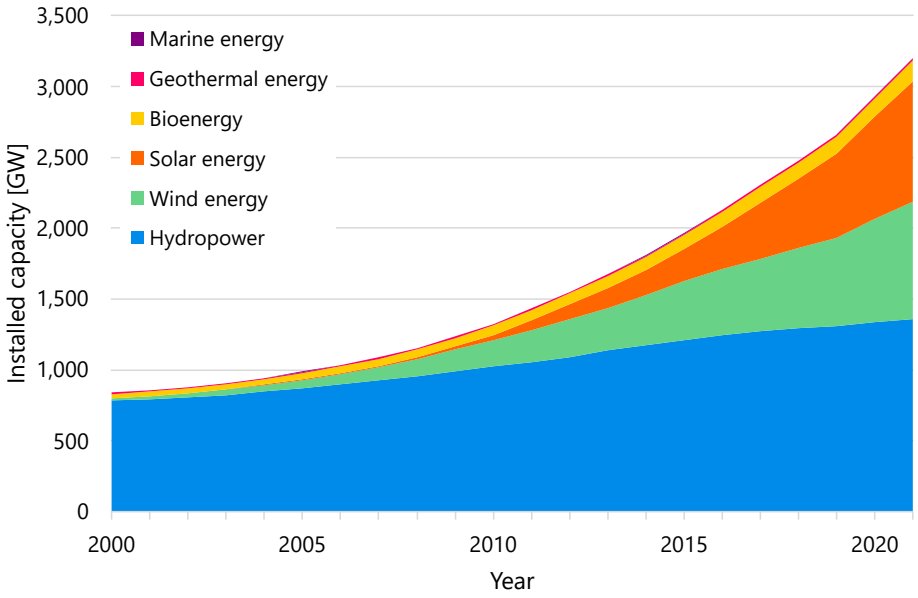

Figure 1.1: Installed global renewable energy capacity by technology.

On the other hand, with the development of information and communication technology (ICT), renovation of the conventional energy system towards the next-generation energy system is also being promoted [9]. In particular, the transition of local energy systems has been remarkable. To enhance energy security and resilience, the local energy system integrates a controllable and flexible energy resource, generally called distributed energy resources (DERs). The representative DERs include a battery system, heating, ventilation, and air conditioning (HVAC) systems, electric vehicles (EVs), controllable appliances, and so on. A consumer with smart metering technology and DERs shifts into a prosumer that can produce energy and can communicate with others. Furthermore, an energy management system (EMS) provides various vital applications, including monitoring energy and system states and controlling DERs. The EMS can make local energy systems more flexible in their energy use and reduce power and system costs.

The relationship between the supply and demand side has also been changing. Fig. 1.2 shows the diagram of the energy system renovation. As shown in Fig. 1.2a, the conventional energy system has only unidirectional (one-way) power and information flow from power plants to consumers. The generated power by central power plants is delivered to consumers through a power company. Although the power company is responsible for balancing electricity demand and supply, the recent diversification of energy demand has made management more difficult. Meanwhile, as for the next-generation energy system shown in Fig. 1.2b, wholesale and flexibility markets play an important role in ensuring reliable electricity trading at an efficient cost through market

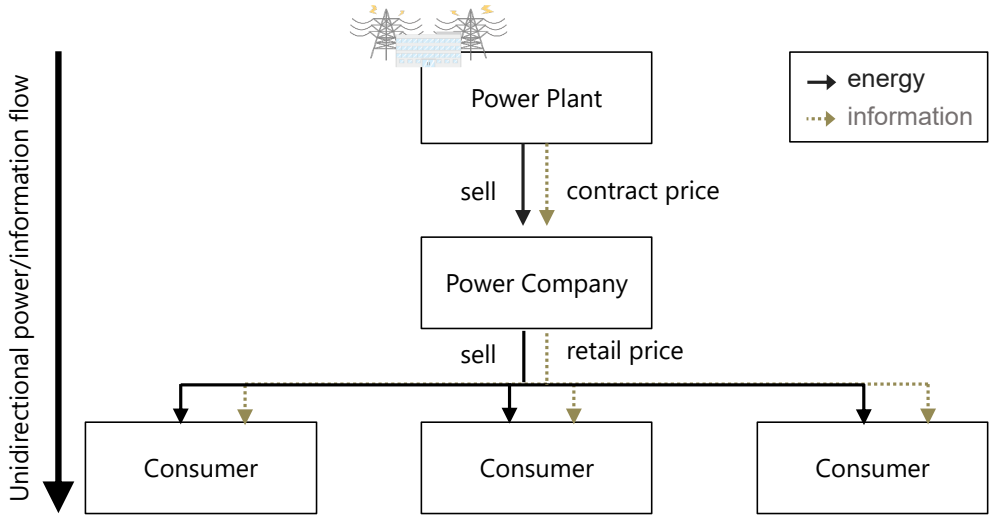

(a) Conventional energy system.

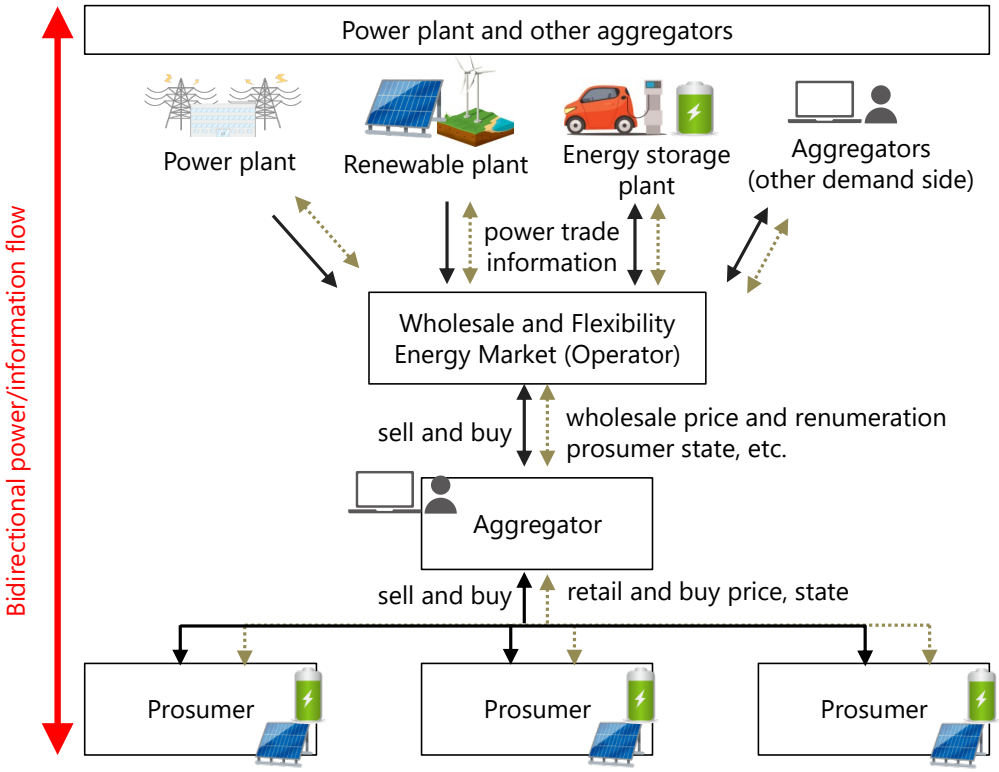

(b) Next-generation energy system.

Figure 1.2: Renovation of energy system.

mechanisms. An aggregator coordinates the market entry of end users and provides financial and systematic benefits to both the demand and supply side as an intermediate entity [10]. The local energy system composed of prosumers is still connected to the conventional power grid, and energy shortages and surplus generation could be traded in the market. The renovation makes both power and information flow bidirectional between the global power grid and the local energy system. Owing to the bidirectional flow and the market entry of the demand side, the demand side can engage in the management of the grid stability issues.

Demand-side flexibility (DSF) is one of the promising solutions to mitigate the mismatch of demand and supply. DSF refers to the portion of demand-side load patterns that can be adjusted, shifted, curtailed, or increased than a normal shape of their demand load [11]. The supply side aims to achieve the desired load pattern through DSF collection and utilization., e.g., peak cut and reduction of power change rate (ramp rate) through the acquisition and utilization of DSF. Exploiting DSF could be motivated by price signals or non-price signals with incentives. For instance, time-varying electricity prices encourage prosumers to control the end user's behavior indirectly. In addition, incentives or compensation are sometimes paid to prosumers who respond to the requests for grid purposes [12]. Such a mechanism is normally called a demand response (DR) program, and the DR program serves as a means of leveraging DSF. To improve grid stability, designing appropriate DR programs considering the characteristics of end users and faced issues are necessary.

According to the reports, the installed capacity of DERs has been increasing day by day [13–15]. The sales of heat pumps in 2021 increased by more than 13% globally, and its market is expected to continue to grow [13]. Also, the total number of EVs in the world increased from 5.5 million to 16.5 million between 2018 and 2021 [14]. According to the Stated Policies Scenario (STEPS) discussed in [15], the International Energy Agency (IEA) estimates that DSF will provide roughly a quarter of power system flexibility in 2050. Hence, the capacity of the DSF will become even more significant in the future. The optimized interaction between the supply and demand side through the DR and EMS development will unlock the potential of DSF.

1.2 Smart Energy Systems and Applications

This section describes the background of smart energy systems and their applications. First, types of DERs on the demand side are introduced. As energy system applications, the functions and effectiveness of the EMS and DR are explained. Then, an aggregation process of demand-side energy resources for maximizing the potential of DSF is described.

1.2.1 Types of Energy Resources on Demand Side

In addition to renewable generation such as solar and wind power, the representatives of DERs on the demand side are battery systems, controllable appliances, HVAC systems, and EVs.

Battery System

Energy storage technology such as battery systems is a crucial technology as the central pillar in the energy system. The rechargeable property of the battery system provides a role as an energy buffer to change the demand load pattern. The battery system can stabilize the sudden power change and the voltage fluctuations due to renewable generations by charging/discharging electrical energy. In addition, it can reduce the demand load during peak hours by shifting the energy to off-peak hours. There are various types of battery systems according to the materials from which the battery system is made, e.g., lead-acid, nickel-metal hydride, and Li-ion batteries. Among them, the Li-ion battery is the most commonly used for EVs and energy system operation thanks to its superior power and energy density.

However, most batteries suffer from the degradation effects that cause capacity fading, making running costs expensive. Generally, battery degradation is defined by state-of-health (SOH), which is the ratio of the current battery capacity to the initial battery capacity. Many works have reported that the factors of battery degradation are depth-of-discharge (DoD) and a high state-of-charge (SOC) level, which is the ratio of the remaining energy to the battery capacity, as well as operating temperature [16]. Although the usage restriction of battery systems will reduce battery degradation effects, electricity costs and the DSF potential will worsen conversely. The dynamics of battery degradation are relatively long effects over the years, and it should be addressed in a long-term schedule plan. Hence, a battery planning methodology that improves the trade-off relationship between battery degradation and electricity costs is important. The real-time operation of the battery system is also vital to manage actual demand load and renewable fluctuation.

Controllable Appliance

Many electrical appliances are on the demand side to make user life more convenient and comfortable. From the viewpoint of energy management, appliances can be classified into non-controllable and controllable. Non-controllable appliances, which include lights, televisions, and refrigerators, are demand loads that continuously operate or cannot shift an operation time. Meanwhile, controllable appliances can be reduced or shifted their operation time to other time slots, including washing machines, tumble dryers, and dishwashers. Well-developed ICT enables demand-side users to schedule

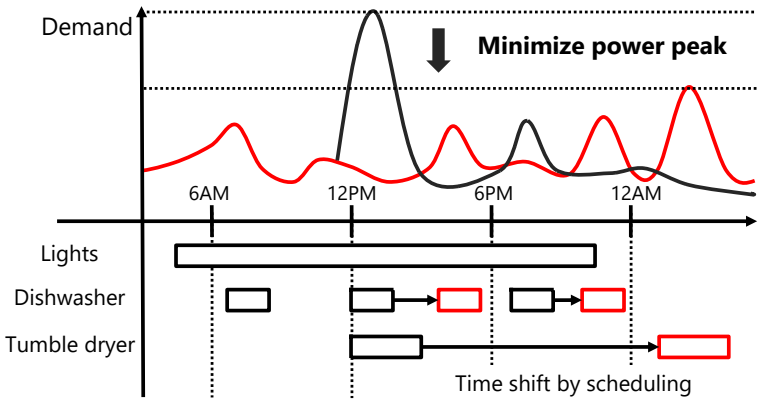

Figure 1.3: Appliance scheduling.

their controllable appliances automatically based on price signals and demand load profiles [17].

Fig. 1.3 shows a conceptual view of the scheduling of controllable appliances. The appliance scheduling is expected to mitigate power peak by spreading demand with respect to a time horizon. To do so, demand-side users are motivated by time-varying electricity prices or other mechanisms. They can shift their appliances from peak price hours to off-peak price hours to minimize electricity costs. When scheduling the appliances, the main concern of users is whether the operation of appliances is completed by the time they set. It is required to optimize appliance schedules to keep such user preferences while minimizing electricity costs.

HVAC System

Heating and cooling systems, such as heating, ventilation, and air conditioning (HVAC) systems, are necessary to improve the living environment and occupancy comfort. Generally, HVAC systems account for 30-40% of the total energy consumption in the building sector. Hence, managing HVAC systems has significant potential as flexibility while controlling the indoor climate, especially in summer and winter. Recently, HVAC systems can easily obtain environmental information from sensors and the internet and calculate effective schedules, owing to the ICT. For instance, if a power peak is likely to occur, the operation of HVAC systems can be reduced immediately. Also, to reduce electricity costs, a pre-cooling/pre-heating scheme is an effective solution where the HVAC operates during a low price period in advance. In this way, the demand load of HVAC systems can be managed for multiple purposes.

Despite the development of HVAC management, thermal comfort is the most important objective to preserve occupancy health and productivity [18]. As for indoor climate control, a comfortable temperature range is often set as a hard constraint that must not be violated. Thermal comfort is defined by various comfort indices such as the pre-

dicted mean vote (PMV) and predicted percentage of dissatisfied (PPD) [19]. As they have indicated, thermal comfort is a complex phenomenon and is affected by many factors such as indoor temperature, humidity, wind speed, metabolic rate, etc. Therefore, it is necessary to control HVAC systems taking into account not only maximizing DSF potentials and minimizing electricity costs but also the most comfortable conditions.

Electric Vehicle

Electric vehicles (EVs) are vehicles fully powered by electrical power, which is one of the promising DERs to address large-scale supply-side issues. All EVs have a battery system as a power source and are electrically connected via EV chargers to the energy system. The charging sources of EVs are the electricity purchased from the grid and generated by renewable sources. Since the capacity of the installed battery system is larger than commercial household batteries to maximize the driving range, the charging demand of EVs has a significant effect on the power grid.

On the other hand, vehicle-to-grid (V2G) is a key technology to manage EVs as DSF, which enables EVs to discharge the energy to the energy system or grid [20]. With the implementation of the V2G, EVs can be used as battery systems when connecting to the energy system as well as vehicles. The charge/discharge coordination of EVs can realize power grid stabilization by mitigating high ramp rates and power peaks. Meanwhile, range anxiety is known as the main issue of EV management [21]. Range anxiety is the concern of EV drivers that the remaining energy in the battery is insufficient to reach their destination. Besides, the arrival time and the charging requirements are different for each EV driver. Hence, an EV management methodology, which considers driver satisfaction and these uncertainties, is required.

1.2.2 Energy Management System

To enhance the operational planning and decision for DERs, an energy management system (EMS) has the most critical role on the demand side [22]. With the development of ICT and the integration with a smart meter, the EMS usually provides four main functions as follows.

- Real-time monitoring of user's energy usage and system behavior.
- Operational Planning of the energy resources considering their long-term characteristics.
- Real-time operation compensating for fluctuation of renewable generation and load and reflecting the actual system state.
- Providing useful applications, e.g., visualization, communication with outside, and automation of energy usage.

In particular, the EMS is expected to automatically and comprehensively optimize various DERs such as renewable generation, battery systems, appliances, and heating/cooling systems while satisfying user preferences.

Despite the high functionality of the EMS, the uncertainties that will be in the energy system make the operation of EMS a difficult task. For instance, the unpredictability and short-term variability of renewable generation may cause energy loss and mismatches. The EMS currently relies on energy storage in battery systems to deal with the uncertainty of renewable sources. Hence, the improvements of the battery control in the EMS are desirable, as this leads to better overall energy efficiency.

The system scales targeted by the EMS range from a single house to a medium-scale system, i.e., local energy systems. For a single house and building, the EMS is required to reduce electricity costs by scheduling their energy resources such as a battery system. Besides, demand control, which includes the scheduling of appliances, HVAC systems, EVs, and so on, is an efficient way to achieve low electricity costs by changing their demand shape according to electricity prices. In addition, other goals of prosumers than electricity costs can be achieved through energy-efficient and user-friendly EMS, including the serious system costs such as battery degradation and investment cost and user preferences such as thermal comfort, appliance usage-timing preference, and EV charging requirement. In local energy systems, multiple prosumers are electrically connected, and the EMS aims to reduce demand peak, mitigate the mismatch of energy balance, and minimize investment costs. In particular, improving the reliability of the energy system is one of the main goals for independence from the conventional power grid. The excess and shortage of energy will be compensated by exchanging it with each other and trading it in the wholesale electricity market. Also, a hundred or thousand DERs in the local energy system should be coordinated towards these goals.

The time scale of the control sequence of the EMS is also a non-negligible factor in the performance of EMS. For a long time scale covering several months, the EMS application should consider a seasonal change of renewable generation and demand load and long-term effects of system components such as degradation. On the contrary, for a short time scale with a time resolution of a second, the energy imbalance between renewable generation and demand can cause energy loss directly. Also, ramp rates (power change rate) on the local energy system are important issues that should be met for system stability. Therefore, precise control for compensating for real-time changes in the energy balance is required. As described above, the system and time scale managed by the EMS varies widely, and their purpose of them also differs. Therefore an EMS design suitable for each purpose and each time scale is required for the improvements of the EMS performance.

1.2.3 Demand Response Program

The demand response (DR) program is a measure that exploits DSF in response to power grid constraints and purposes, e.g., peak-shaving, valley filling, and load shifting [23]. To achieve that, the DR programs encourage the demand side to change the electrical demand load into the desired shape by sending price or non-price signals.

There are mainly two types of schemes: incentive-based and price-based. The incentive-based DR aims to induce demand load modifications by non-price signals, and the involved users receive compensation when responding to the signals. A representative example of the incentive-based DR is the direct load control (DLC) [24], which directly controls the demand-side resources such as on/off switching of appliances and air conditioning and force charging/discharging of the battery and EVs. Also, emergency demand response (EDR) is a contract that requires immediate demand load changes instead of providing compensation to the demand side in emergency events including frequency disturbance and power outages [25]. Since the incentive-based DR usually makes a contract with prosumers, the amount of available DSF is reliable and controllable. However, it requires well-developed infrastructure including EMS and tailored communication lines, and the implementation cost is relatively high.

On the other hand, the price-based DR aims to control the demand load using price signals indirectly and has been employed in residential and commercial sectors because of its scalability and efficiency. In the price-based DR, time-varying price signals are announced to the demand side, and the indirect control of the demand load is anticipated. Generally, setting a high price during peak hours is a widely-used approach to reduce power peak. Depending on the degree of dynamic pricing, the price-based DR programs are mainly categorized into critical peak pricing (CPP), time of use (TOU), and real-time pricing (RTP) [26]. In particular, the RTP has significant potential for changing end-user behavior, as demonstrated in the literature [27]. In addition, the price-based DR can be easily implemented without any specialized infrastructure. However, the effect of the price-based DR is unreliable since the participation of prosumers is voluntary. These existing (incentive- and price-based) programs have both pros and cons, and the design of the DR program is required according to the issues to be solved.

1.2.4 Demand-Side Flexibility

This section introduces demand-side flexibility (DSF) and system-level processes for exploiting DSF, which are the main focus of this dissertation. In general, DSF means the ability of demand-side users to change their load patterns from current and normal patterns. Responding to the signals of DR programs, the willing demand-side users including residential, commercial, and industrial sectors can curtail, adjust, or shift their demands and DERs. If DSF can be effectively utilized, it will help to realize the high penetration of renewable generation and ensure energy system stability [11]. To acquire and utilize the DSF, the aggregator and the supply side organize DR programs to motivate the demand-side prosumers to change their electricity load.

Fig. 1.4 shows a schematic view of system-level processes for exploiting demand-side flexibility. There are three entities regarding DSF exploitation; the supply side (the power grid and the market), the aggregator, and the prosumers. The system-level processes are as follows. First, the supply side sends the price signals in wholesale

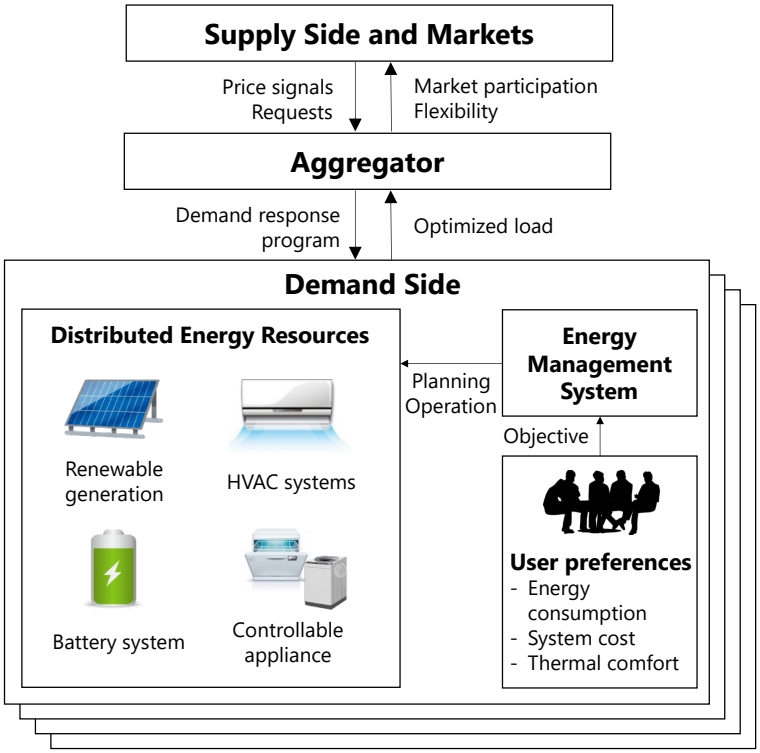

Figure 1.4: Schematic view of system-level processes for exploiting demand-side flexibility.

electricity markets and requests to meet the grid purposes, such as peak power shaving and ramp rate reduction. Then, the aggregator decides and announces DR signals to the prosumers, e.g., time-varying retail price signals, incentive payment, and other compensation, based on the obtained and observable information from the supply and demand side. According to the DR signals, prosumers may change their load patterns using the EMS. Depending on their willingness to participate in the DR programs, there are typically two types of prosumers: reactive and proactive prosumers. The reactive prosumers aim to optimize their energy balances by scheduling their energy resources without looking at the DR signals and global grid concerns. Meanwhile, proactive prosumers make a plan and operate DERs to maximize their preferences that include electricity and system cost minimization and comfort maximization. Finally, the aggregator coordinates the optimized load of the prosumers and provides DSF to the supply side.

Through these processes, the social welfare of energy systems can be maximized. For the supply side, the utilization of DSF reinforces the stability of the energy system by contributing to resolving the supply-side issues in the global power grid, e.g., power peak, frequency regulation, and high ramp rates. The DSF can be an alternative to expensive additional power plants for ramping up/down the network electricity load. As for the demand side prosumers, they can reduce electricity costs when participating

in the DR programs, i.e., scheduling their DERs to the lower price period or getting compensation for DER control. Besides, the aggregator is strongly motivated to perform these processes. This is because the aggregator can profit from intermediating energy trades in the market and flexibility transactions between the supply and demand side. Thus, unlocking the potential of DSF is a win-win for all entities.

1.3 Research Questions and Issues

This section describes the remaining research questions to maximize the potential of DSF in system-level energy management for smart energy systems. Fig. 1.5 shows the study scope of this dissertation. This dissertation addresses three questions regarding the planning and real-time operation of energy demand on the demand side and the DR program offered by the aggregator for changing prosumer behavior to meet the grid goal.

Question 1: How could prosumers make a plan for their DERs to reduce system costs?

As for the prosumer on the demand side, making an operational plan for DERs such as battery systems is essential to evaluate the system performance and estimate the electricity costs/profits over the long term for more than months. However, there is an important issue when making the operational plan; the energy loss due to DER characteristics, especially battery degradation. Many works have reported that the degradation rate of battery systems varies greatly depending on their usage history [28]. The initial costs of a battery system, are too expensive to neglect the degradation effects. In addition, the power output of renewable generation, especially PV generation, significantly varies in different seasons due to the temperature and solar irradiation variation. This seasonal variation will make optimal operational plans differ depending on the season. To address these issues, a long-term operational planning decision method is required to minimize the total costs that involve the system and electricity costs by considering the seasonal variation of renewable generation and the critical energy loss including battery degradation. Along with the planning of energy resource operations, the sizing of systems such as renewable energy generation and battery systems and cost-optimal working points that consider longer system characteristics can be explored. On the other hand, in the context of DSF, such operational planning also enables the prosumers to estimate the potential of their flexibility under various scenarios. It helps to choose an appropriate DR program among multiple program options provided by aggregators and supply-side entities.

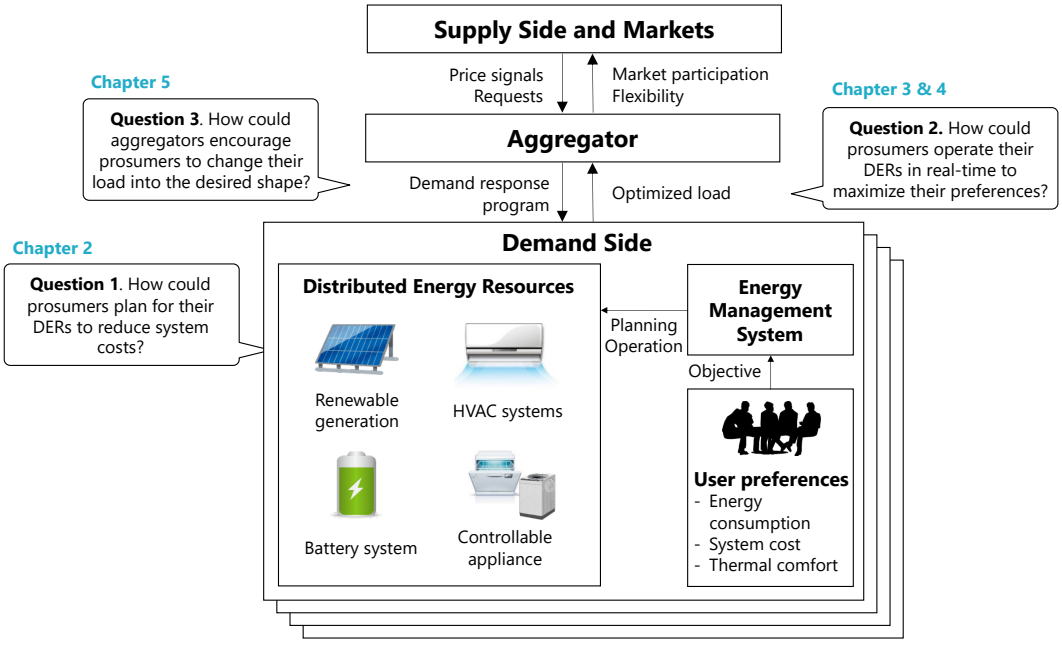

Figure 1.5: Study scope of this dissertation.

Question 2: How could prosumers operate their DERs in real-time to maximize their preferences?

Since electricity demand and renewable energy fluctuate in real time, it is necessary to mitigate the demand and supply mismatch even on the demand side to avoid energy losses. To address this issue, in addition to operational planning, real-time operation of energy systems is a very important application in EMS. However, the complex characteristics of DERs make energy management more dynamic [29]. Controllable appliances and heating/cooling systems need to be scheduled on a daily scale to follow the price signals considering user preferences. In addition, battery systems must consider not only a day-scale load variation due to periodic user behavior and solar cycle but also a real-time scale that covers renewable energy fluctuations and transient responses of the battery system. To solve such complex problems, a real-time operation method is required, which guarantees solution quality while reducing computational costs.

On the other hand, more objectives than minimizing electricity and system costs must be considered. The objectives also include user preferences such as thermal comfort realized by HVAC systems, the timing preferences of controllable appliances, and the charging requirement of EVs [30]. These objectives often conflict with each other and have a trade-off relationship that should be improved through smarter energy management. Furthermore, the characteristics of the energy resources corresponding to these preferences are completely different and have a significant impact on the EMS performance. Therefore, it is essential to develop a decision-making tool that simulta-

neously meets these multiple objectives while considering the different characteristics of the energy resources explicitly.

Question 3: How could an aggregator encourage prosumers to change their load into the desired shape?

From the aggregator's perspective, the question remains as to what DR strategies will achieve the maximum utilization of DSF for improving the supply-side issue. One such supply-side issue is the duck curve due to the high penetration of PV generation. The duck curve is a graph of demand load, which shows a sharp change in the ramp rate in the morning and evening and an imbalance between demand and PV generation [31]. To address such issues, aggregators typically implement DR programs to encourage prosumers to change their behavior and demand load patterns. The implicit price-based DR, namely dynamic pricing, is particularly promising since it can be applied regardless of prosumer type or capacity. Time-varying electricity prices indirectly control the load shape, e.g., shaving power peak with a higher price while filling load valley with a lower price. However, it is unclear what price patterns will resolve the duck curve, and modeling how prosumers respond to the prices is challenging. Privacy concerns also make it difficult to access detailed information on prosumers or directly control their energy resources. Therefore, a model-free dynamic pricing strategy is required to improve the duck curve from minimal information on the prosumers.

1.4 Objective and Organization

This section summarizes the objectives of the following chapters and outlines how to address the questions described in Chapter 1.3. The objective of this dissertation is to develop a system-level energy management methodology for DSF in smart energy systems to maximize social welfare that includes system cost minimization, thermal comfort maximization, and grid stabilization. To this end, this dissertation addresses three questions, as shown in Fig. 1.5.

Battery degradation aware operational planning method for battery system on EMS to address Question 1

For operational planning, the battery degradation issue that causes serious cost increases should be addressed. This dissertation proposes a battery degradation-aware operational planning methodology for the planning stage of the energy management system. The battery state-of-health (SOH) model, which can calculate an amount of battery capacity fade based on battery operation profiles, is integrated to treat battery degradation in the optimization problem and evaluate system costs quantitatively. The two-stage optimization problem is formulated as a mixed-integer programming (MIP) and incorporates

the novel objective function and constraints to reduce battery degradation. The simulation results show that the proposed method can reduce battery degradation without increasing the electricity purchase. Note that the proposed method in this chapter is limited to minimizing battery degradation under static load with hourly changes; dynamic workload-based improvement of battery lifetime is out-of-scope of this dissertation and will be addressed in future work.

Online and real-time operation methods for battery system, appliances, and HVAC systems on EMS to address Question 2

This dissertation investigates two methods to achieve real-time operation of DERs by EMS for maximizing user preferences. For the first method, an online optimization framework is proposed for scheduling a battery system and controllable appliances to minimize electricity costs. To address the fluctuation of renewable generation and real-time energy loss, this work incorporates a forecasting model of PV generation and an accurate battery model. Moreover, the time scale is divided into two time scales: coarse and fine-grained time scales. Compared to the state-of-the-art single-time scale structure that ignores fast system dynamics, the proposed multi-time scale structure enables considering both fast and slow system dynamics with reasonable computational complexity. The simulation results show that the proposed method can reduce electricity costs in real-time and has scalability for a number of shiftable appliances and a length of the planning period.

As for the second method, to consider other objectives, such as thermal comfort than electricity costs, the scheduling of HVAC systems is integrated into the framework. In general, HVAC systems, which significantly affect the thermal comfort of occupants, account for 40% of residential and commercial buildings. This work aims to improve the trade-off relationship between minimizing electricity costs and maximizing thermal comfort. Thermal comfort is modeled as a predicted mean vote (PMV) and predicted percentage of dissatisfaction (PPD) indices, widely used as comfort criteria. Moreover, a multi-objective optimization problem is formulated to adjust the balance between electricity costs and thermal comfort. The simulation experiments show that the proposed method can improve the trade-off relationship between electricity costs and thermal comfort. Finally, this work provides a complete energy management framework for typical buildings. Note that integrating more energy resources, such as wind power and electric vehicles, into the framework is not addressed in this dissertation and is of interest in future work.

Price-based DR strategy of aggregators for duck curve improvement to address Question 3

This dissertation proposes a price-based DR strategy to improve the supply-side duck curve problem through DSF exploitation. The duck curve is a graph of the steep curve

in a net load of demand-side (users) due to high penetration rates of PV generation. Massive PV generation reduces the net load at noon, while it causes a ramp rate in the morning and evening by increasing/decreasing the energy production of PV panels. This work tries to improve the duck curve by battery scheduling and dynamic pricing, which is a kind of price-based DR program that indirectly controls DSF by changing retail prices. This chapter formulates the hierarchical energy market model, which consists of electricity markets, a resource aggregator (RA), and prosumers. Then, a duck-curve improving strategy of RA for dynamic pricing and battery scheduling based on deep reinforcement learning (DRL) is proposed. Thanks to DRL, the proposed method can learn optimal retail prices and schedule of RA's battery to improve the duck curve using only data and to preserve prosumer privacy. The simulation results show that the proposed method can reduce the standard deviation and the peak-to-average ratio of net load compared to baseline methods. Note that this chapter mainly focuses on price-based DR programs; incentive-based DR will be investigated and integrated in the future.

Dissertation Text Organization

The rest of this dissertation is organized as follows. Chapter 2 proposes the battery degradation-aware operational planning method for the demand-side energy sources, which solves the two-stage optimization problems based on the battery degradation model. The proposed method reduces the battery degradation costs without increasing the electricity purchase, and the obtained solution is helpful for battery planning as reference working points.

Chapter 3 investigates the online multi-time scale energy management framework to realize the real-time operation of the demand-side energy sources, which integrates PV forecasting and accurate parameterized battery models. The results show that the proposed multi-time scale structure reduces both electricity costs and computational complexity.

Chapter 4 presents the electrical and thermal energy management framework based on the framework developed in Chapter 3 and introduces the thermal comfort estimator that predicts comfortable temperature set points. The proposed framework improves the trade-off relationships between electricity costs and thermal comfort.

Chapter 5 proposes the DRL-based aggregator's strategy for dynamic pricing and battery scheduling to improve the duck curve issue. The results show that the proposed strategy improves the duck curve through the price-based DR interaction between the aggregator and prosumers. Finally, Chapter 6 summarizes this dissertation and refers to the extensions for future work.

Chapter 2

SOH-Aware Optimal Two-Stage Planning for Battery System

In smart energy systems, battery degradation is a serious issue due to its high initial costs. Battery degradation is a relatively long-term effect, and this issue should be addressed in the planning stage of energy management. This chapter proposes a state-of-health (SOH)-aware two-stage operational planning methodology to minimize battery degradation[1]. First, a battery SOH model is introduced, which can express battery capacity fade based on battery operation profiles. Second, a two-stage optimization problem is formulated as a mixed-integer programming (MIP) by integrating a new objective function and constraints extracted from the SOH model. The case study is performed for the local energy community using the measured data in Japan for one year. The results show that the proposed method leads to improvements in the trade-off between battery degradation and electricity purchase and that the battery aging cost is reduced by 14% at the same electricity purchase amounts.

2.1 Motivation and Objective

Lithium-ion batteries are one of the core components in demand-side flexibility (DSF) of smart energy systems to provide flexible energy applications such as energy arbitrage and ancillary services. Although advanced manufacturing processes have made lithium-ion battery systems cheaper, the introduction cost and the lifetime of the batteries remain issues for wide introduction to the real world [33]. In particular, battery degradation is a phenomenon that the battery capacity reduces with daily use and leads to serious cost increases for smart energy systems.

Battery degradation is generally expressed in two terms: calendar aging and cycle aging [34]. Calendar aging is a degradation process that occurs with elapsed time,

[1]This chapter is a refined and reproduced version of the paper to be published in IEICE Transactions on Fundamentals of Electronics, Communications and Computer Sciences [32] copyrighted by IEICE.

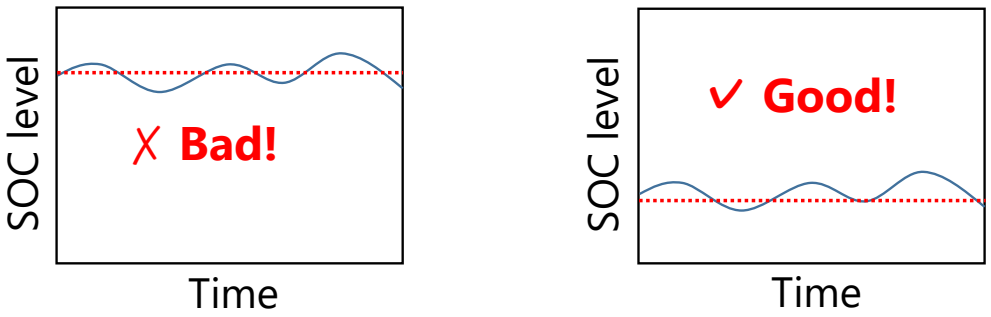

(a) Average SOC effect on battery degradation.

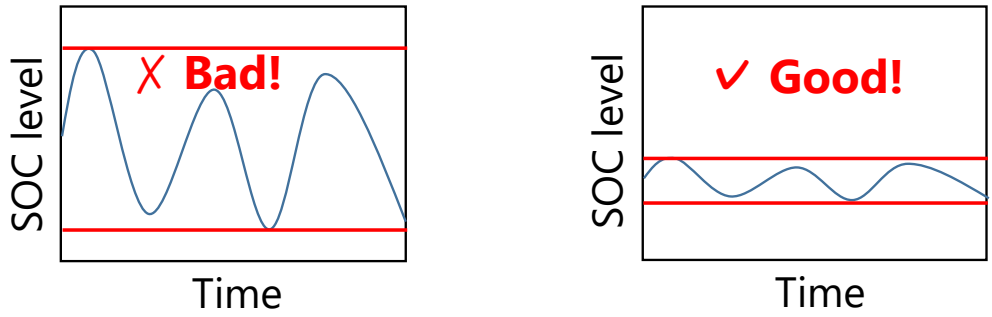

(b) SOC swing effect on battery degradation.

Figure 2.1: Battery SOC patterns.

regardless of charge/discharge cycles [35]. On the other hand, cycle aging occurs during the charging and discharging of a battery, and the main factors are operation states, e.g., operation temperature, depth of discharge, charge/discharge rate, and state-of-charge (SOC) levels [36–38]. Therefore, even though the mechanism of battery degradation is chemical and physical changes within battery cells, the battery lifetime can be improved through system-level battery management, i.e., scheduling of battery charge/discharge.

To indicate a degraded state of a battery, a state-of-health (SOH) index is used, which is usually defined as the ratio of the current capacity to the capacity when the battery is new. Millner developed an SOH model of a battery to calculate the amount of SOH reduction caused by calendar and cycle life [39]. Fig. 2.1 shows four battery SOC patterns as an example of typical battery usage. According to this work, the high average level of SOC usually has a greater effect on battery degradation than the low average SOC, as shown in Fig. 2.1a. Likewise, as illustrated in Fig. 2.1b, the large swing of SOC levels generally has a negative influence on battery lifetime. To extend the battery lifetime, both the average SOC level and the SOC swing should be maintained low.

This chapter proposes an SOH-aware operational planning methodology for the smart PV system. Battery degradation and the amount of electricity purchased are in a trade-off relationship. Therefore, the objectives of the proposed method are to reduce battery degradation and to minimize the electricity purchase from the power company.

To evaluate and control the battery aging accurately, the battery SOH model proposed in the literature [39] is introduced to the energy management problem. Since such a battery degradation model is generally nonlinear, integrating it into optimization problems is especially challenging. This chapter addresses this issue by deriving new objectives and constraints based on the analysis of the SOH model. The optimization problem with them is formulated to minimize the average SOC level and SOC swing, which are the aging factors of the battery. The proposed method is a two-stage MIP optimization problem; (1) the first stage calculates the minimum purchased energy and (2) the second stage recalculates the battery schedule to minimize a battery aging function with a constraint of the minimum purchased energy. Finally, the proposed method explores effective battery schedules to obtain a better trade-off between battery degradation and the amount of electricity purchased.

The main contributions of this work are as follows:

- Battery degradation model [39] is introduced to consider battery degradation phenomena and evaluate system performance quantitatively.
- Two-stage MIP-based optimization problem is formulated to minimize battery degradation without increasing energy purchase.
- Simulation experiments are conducted to show the proposed method outperforms the conventional method that only considers energy purchase minimization in terms of battery degradation costs.

The remainder of this chapter is organized as follows. Section 2.2 introduces related works of battery management systems and energy management systems. Section 2.3 describes the battery aging factor and introduces the battery SOH model. Next, Section 2.4 explains system models of a local energy community. Section 2.5 derives the proposed SOH-aware two-stage operational planning methodology. Then, Section 2.6 evaluates the proposed method through simulation experiments using real measured data in Japan. Finally, Section 2.7 concludes this chapter and states the outlook.

2.2 Related Works

Many battery management methods have been proposed to reduce electricity costs. Zhang et al. [40] proposed a day-ahead distributed battery scheduling algorithm on the smart grid. Kanchev et al. [41] studied a scheduling method of battery charge/discharge based on a heuristic approach. Silvente et al. [42] formulated a mixed-integer programming (MIP)-based optimization problem to schedule electricity demand and a battery system to reduce electricity costs. Harsha et al. [43] presented an optimal battery management method to integrate renewable energy under a dynamic pricing policy. They also investigated the optimal sizing of a battery through sensitive analysis. The main objective of these papers is to minimize the total system operation cost. However, they have not considered battery degradation, and the degradation issue should be tackled to reduce high battery running costs.

As for battery degradation-aware battery management, Michelusi et al. [44] proposed a stochastic Markov chain framework to capture a degradation process of a battery in wireless sensor devices and also presented a heuristic policy to improve battery lifetime. Vatanparvar et al. [45] investigated an optimized charge and drive management methodology for an electric vehicle (EV), which decides an optimal route, a departure time, and an EV charging schedule while improving battery lifetime. Park et al. [46] formulated an optimization-based method of battery assignment and battery scheduling for a drone delivery business. They introduced a battery SOH model and demonstrated that their proposed method reduces electricity costs and battery purchasing costs. To improve battery lifetime effectively, a specific SOH model should be considered in the management problem. The studies above tried to solve the battery degradation issue; however, there are a few studies that focus on the EMS with considering renewable generation and a stationary battery system in households and buildings.

On the other hand, Kato et al. [47] mathematically formulated an energy management problem as MIP with the battery charge/discharge cycle limitation. The number of charge/discharge cycles is also a degradation factor, and they achieved the quarter numbers of the battery charge/discharge cycles. The results show that their method can potentially inhibit battery degradation qualitatively. However, the average SOC level and the SOC swing are also important factors in battery degradation that should be considered in system-level management. Besides, they did not consider any specific battery degradation models, and the theoretical background of mathematical formulation and quantitative evaluation of battery degradation is lacking.

To overcome the challenges mentioned above, in this chapter, a battery degradation-aware optimization method is investigated by introducing the SOH model of the battery. Compared to the conventional approach, the proposed method reduces battery degradation in a quantitative manner that uses the battery aging models. Moreover, introducing the battery SOH model enables an evaluation of the proposed method in terms of battery degradation. This integration enables evaluating the system performance quantitatively in terms of battery degradation.

2.3 Battery Aging Factor

This section introduces battery degradation as SOH and a battery SOH model, which expresses the relationship between the battery aging factor and battery capacity degradation. After that, a preliminary simulation of the SOH model is performed to identify the most influential factor on battery degradation.

2.3.1 Battery Degradation Model

In general, battery degradation is represented by SOH, which is a key quality indicator of a battery. The SOH is defined as the ratio of the current battery capacity to its initial

capacity, and is given by the following equation:

$$SOH^m = \frac{X_m^{full}}{X_{init}^{full}}, \tag{2.1}$$

where SOH^m and X_m^{full} are the SOH and the actual capacity after m charge/discharge cycles, respectively. X_{init}^{full} is the initial nominal capacity of the battery. The SOH of the new battery is 1.0 (100%), and the SOH degradation refers to the loss of capacity as the battery ages. According to the literature [39], when the SOH reaches 80%, the battery is generally considered useless for energy management applications due to significant capacity fading and an increase in the battery's internal resistance.

Estimating the SOH can be a challenging task because the complex physical and chemical reactions inside battery cells cause the capacity to degrade.

SOH estimation is a difficult task because complex physical and chemical reactions inside battery cells cause SOH degradation. Some electrochemical-based SOH models proposed in [48, 49] accurately model the changes in the cathode, anode, electrolyte, and solid electrolyte layers. Additionally, data-driven approaches proposed in [50, 51] derive a black-box model from historical and empirical data, which can be fairly accurate without a full understanding of the aging mechanism. However, these models are unsuitable for optimization problems since these models consist of complex nonlinear equations and are too computationally complex to solve.

Then, this work introduces Millner's SOH model [39] to capture the battery degradation effect. The Millner's model calculates the SOH degradation during the charge/discharge cycle based on the battery's SOC trace [39]. While this model consists of nonlinear equations, it is not too complicated and can be applied to MIP formulation using a linear-approximation technique. In addition, this model shows good agreement with experimental data, making it suitable for optimization problems.

The following explains the SOH model proposed by Millner. First, the SOC represents the amount of remaining energy in the battery and is defined as follows:

$$SOC = \frac{X}{X_m^{full}}, \tag{2.2}$$

where X is the current stored energy in the battery. The variable SOC_{avg} denotes the average SOC over a charge/discharge cycle, and SOC_{swing} denotes the range between the maximum and minimum SOC levels in the cycle. The SOH degradation in the m-th charge/discharge cycle, represented by $L_{cycle,m}$, is calculated as follows:

$$L_1 = K_{CO} \cdot \exp\left[(SOC_{swing} - 1) \cdot \frac{T_{ref} + 273}{K_{EX} \cdot (T_B + 273)}\right] + 0.2 \cdot \frac{\tau}{\tau_{life}}, \tag{2.3}$$

$$L_2 = L_1 \cdot \exp\left[4K_{SOC} \cdot (SOC_{avg} - 0.5)\right] \cdot SOH^m, \tag{2.4}$$

$$L_{cycle,m} = L_2 \cdot \exp\left[K_T \cdot \left(T_B - T_{ref}\right) \cdot \frac{T_{ref} + 273}{T_B + 273}\right], \tag{2.5}$$

where L_1 and L_2 represent the degradation effects due to the SOC swing and the average SOC level and calendar life, respectively. After calculating L_1 and L_2, $L_{cycle,m}$ is determined by taking temperature effects into consideration. It is important to note that the value of $L_{cycle,m}$ represents the percentage of capacity degraded, i.e., the drop rate of the SOH. The constants K_{CO}, K_{EX}, K_{SOC}, and K_T are the coefficients of the battery degradation model. The symbol τ represents the duration of the m-th charging/discharging cycle, and τ_{life} represents the total expected calendar life, or the amount of time the battery can be stored until end-of-life. T_B and T_{ref} represent the battery temperature and the reference operation temperature, respectively. The values of these coefficients can be found in the literature [39].

Finally, the SOH level after M charging/discharging cycles, denoted by SOH_m, can be defined by:

$$SOH_m = 1 - \sum_{m=1}^{M} L_{cycle,m}. \tag{2.6}$$

In this way, Millner's model estimates the current value of the battery SOH based on historical operation profiles.

2.3.2 Preliminary Experiment

In this section, the preliminary simulation of the SOH model described in the previous section is performed in order to identify the most influential factor for battery degradation. Battery life cycles, which mean the number of the charge/discharge cycles from the initial state to the end-of-life, are calculated while repeating charging/discharging with fixed values of SOC_{swing} and SOC_{avg}. The value of SOC_{swing} and SOC_{avg} increments from 0.3 to 0.6 ($30\% - 60\%$). The end-of-life of the battery is assumed until the SOH reduces to 80%. Other parameters are set to the value that appeared in the literature.

Fig. 2.2 shows the battery life cycles until the end-of-life. In Fig. 2.2a, the x-axis is the value of the SOC swing, and the y-axis is the number of life cycles until the end-of-life of the battery. As the SOC swing value is increasing, the life cycles are slowly decreasing. In Fig. 2.2b, the x-axis is the value of the average SOC, and the y-axis is also the life cycle. As the average SOC value is increasing, the life cycles are rapidly decreasing. The average SOC seems to have a greater impact on the battery life cycles than the SOC swing. As a result, the larger SOC_{swing} and SOC_{avg}, the less the life cycles until the end-of-life; i.e., the higher average SOC and the higher SOC swing accelerate the SOH degradation. Moreover, compared to the effect of SOC_{swing} and that of SOC_{avg} on the battery degradation, SOC_{avg} has a greater impact on the battery aging than SOC_{swing}. Following these results, it is shown that the proposed method needs to reduce both SOC factors and especially minimize the average SOC in order to suppress battery degradation.

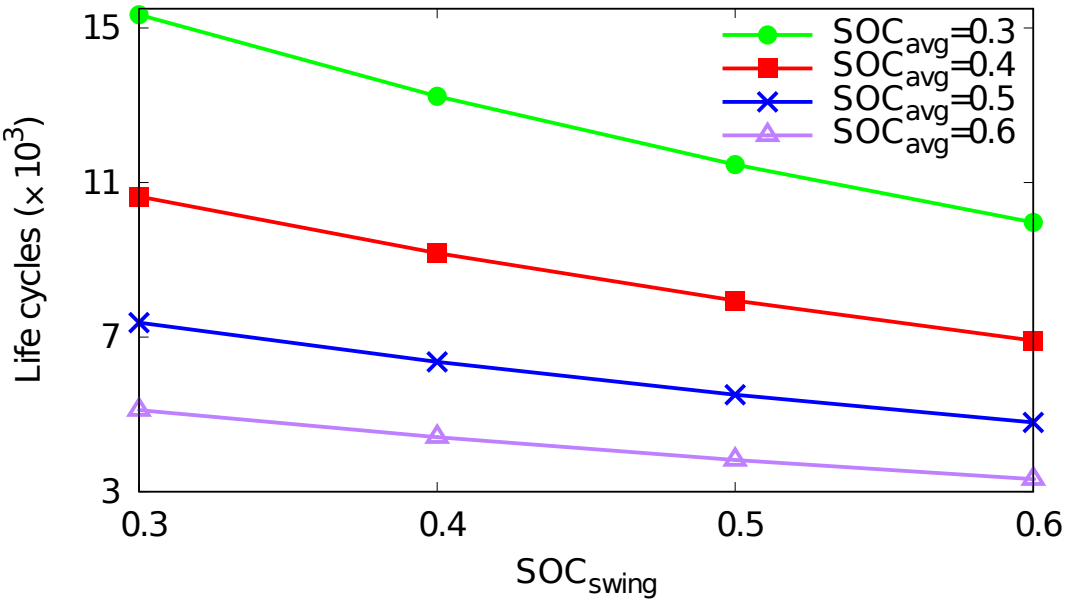

(a) Relationship of life cycles and SOC_{swing}.

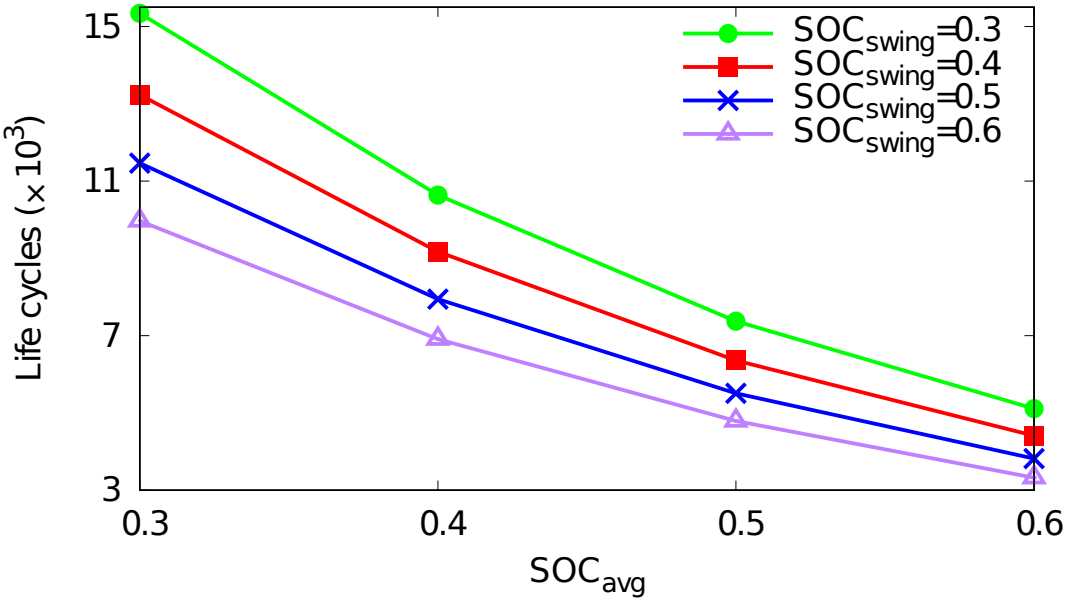

(b) Relationship of life cycles and SOC_{avg}.

Figure 2.2: Battery life cycles until end-of-life.

Such results are not limited to Millner's results, and many studies have reported that these SOC factors have a significant impact on battery aging [52–54]. Thus, the energy management problem that reduces both the average SOC and the SOC swing is formulated for minimizing battery degradation.

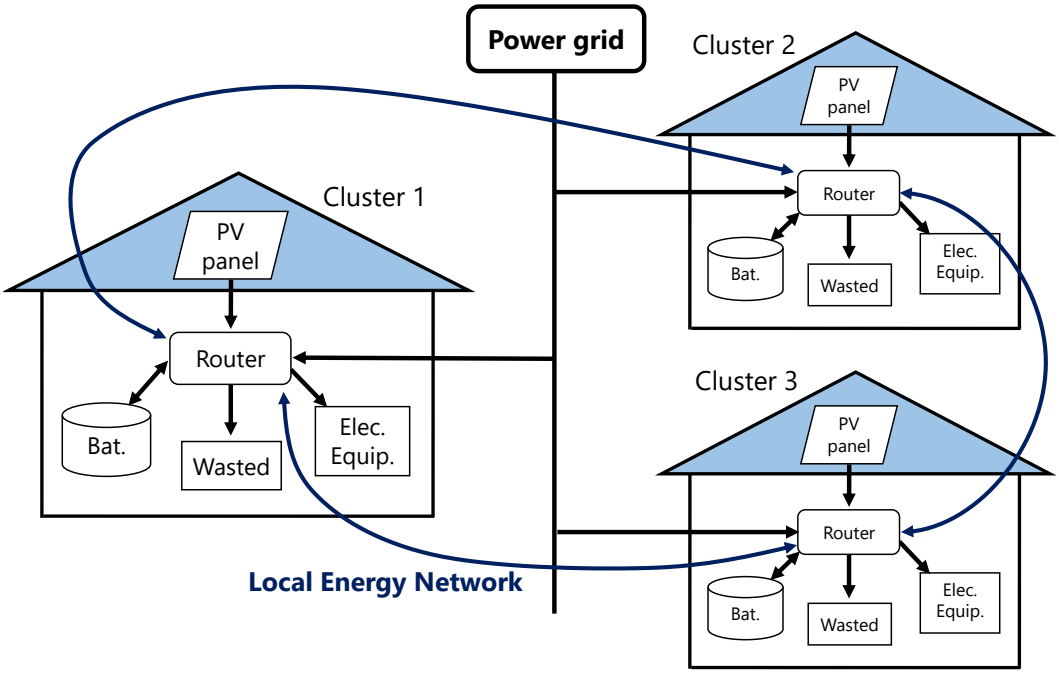

Figure 2.3: Smart PV system model.

2.4 System Model

This section describes the overview of a targeted system and the mathematical formulation.

2.4.1 Overview

This section presents a model for a smart PV system, as shown in Fig. 2.3. The system consists of N clusters [9, 55, 56], which represent households in the real world and are connected to each other through a local energy network. To effectively utilize renewable energy, inter-cluster energy transmission is enabled through the local energy network lines. In case of excess or deficiency of electricity, clusters can exchange electric energy with each other.

The details of power flow within each cluster are shown in Fig. 2.4. Each cluster consists of a photovoltaic (PV) panel, a battery, electric equipment that consumes energy, and a router that monitors and controls power flow in the system. The router, which is a common component in such smart energy systems and includes several AC/DC converters and power metering units [57, 58], connects all devices in the cluster and all clusters to each other via the local energy network. The router controls the power flow between devices and clusters based on control commands received from a control center.

As for energy sources, a cluster primarily uses the power generated by its PV panels

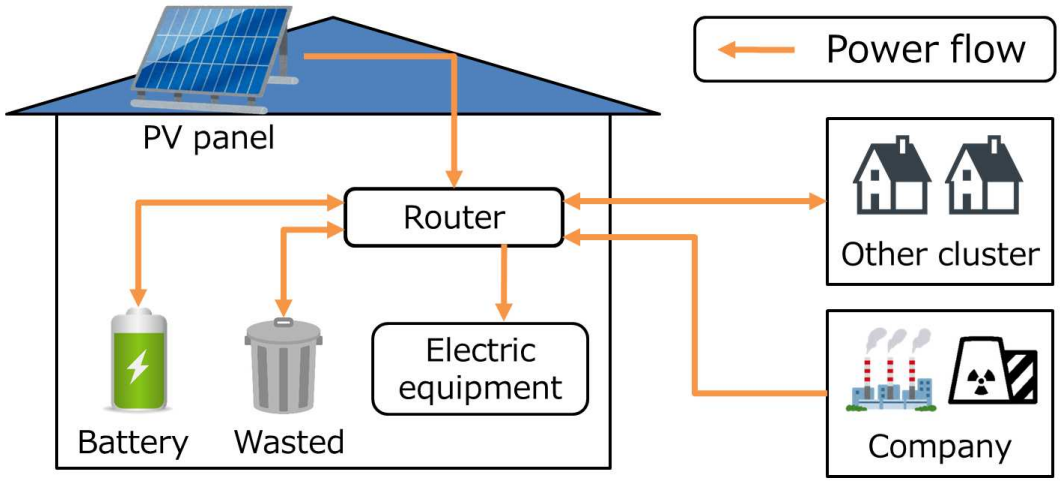

Figure 2.4: Power flow in each cluster.

or purchases electricity from the power grid. This smart PV system does not allow for selling surplus PV generation to the power grid. Any surplus PV generation is either stored in the battery, transmitted to other clusters, or wasted in the cluster. The concept of wasted energy is introduced to consume excess energy within the cluster and prevent reverse power flow to the power grid. The main focus of this system is deciding how much energy to send to which batteries or clusters, known as the energy management problem. The general objective of this system is to effectively utilize uncontrollable renewable energy and minimize the amount of energy purchased from the power company. Minimizing purchased energy can help optimize the performance of the smart PV system. However, battery degradation is a significant issue due to the high cost of batteries. Therefore, it is desirable to include battery degradation control in the energy management problem.

2.4.2 Mathematical Model

This section outlines the fundamental mathematical formulation of the energy management problem. The variables i, t, and u represent cluster number, day, and time, respectively. Their ranges are $1 \leq i \leq N$, $1 \leq t \leq T$, and $1 \leq u \leq U$. The variable j is used to represent the cluster number in the formulation of inter-cluster energy exchange, with a range of $1 \leq j \leq N, i \neq j$. Inputs, decision variables, and parameters used in the proposed formulation are listed in Table 2.1. The units of value not mentioned in the table are kWh. All inputs are assumed to be perfectly predicted and the measured values are used. While this assumption is not practical for real-time control, it allows for the evaluation of the system performance and the potential for reducing battery degradation.

Battery behavior is not ideal, and some electrical energy is lost during charging.

Table 2.1: Mathematical symbols used in formulated optimization problem.

Inputs	Description
$D_{i,t,u}$	Electricity demand of cluster i at day t, time u
$G_{i,t,u}$	Energy generated from PV panel of cluster i at day t, time u
Variables	**Description**
$S_{i,t,u}$	Energy purchased from utility grid by cluster i at day t, time u
$Y_{i,t,u}$	Wasted energy of cluster i at day t, time u
$X_{i,t,u}$	Stored energy in battery of cluster i at day t, time u
$B^{in}i,t,u$	Energy charged to battery of cluster i at day t, time u
$B^{out}i,t,u$	Energy discharged from battery of cluster i at day t, time u
$Z_{i,j,t,u}$	Energy transmitted from cluster i to cluster j at day t, time u
$SOC_{i,t,u}$	SOC level of battery in cluster i at day t, time u [%]
$Z^T i,t,u$	Energy transmitted from cluster i to other clusters at day t, time u
$Z^R i,t,u$	Energy received by cluster i from other clusters at day t, time u
Parameters	**Description**
$X^0 i$	Initial stored energy in battery of cluster i
$\underline{Xi}$	Lower bound for stored energy in battery of cluster i
$\overline{X_i}$	Upper bound for stored energy in battery of cluster i
XC_i	Charge/discharge speed for battery in cluster i
α_i	Charging efficiency of battery in cluster i [%]
$\beta_{i,j}$	Loss rate of energy exchange between cluster i and cluster j [%]
$\gamma_{i,j}$	Capacity for energy exchange between cluster i and cluster j

The stored energy at the next time $u+1$ and the SOC level at time u of the battery are calculated using equations (2.7) and (2.8), respectively. As described in the previous section, the SOC level represents the ratio of the stored energy to the battery capacity.

$$X_{i,t,u+1} = X_{i,t,u} + \alpha_i \cdot B^{in}_{i,t,u} - B^{out}_{i,t,u},\ \forall i,t,1 < u \leq U \tag{2.7}$$

$$SOC_{i,t,u} = \frac{X_{i,t,u}}{\overline{X_i}}.\ \forall i,t,u \tag{2.8}$$

To avoid over-charge/discharge, the battery capacity and the maximum charge/discharge rate, which are given by a manufacturer, should be kept.

$$\underline{X_i} \leq X_{i,t,u} \leq \overline{X_i},\ \forall i,t,u \tag{2.9}$$

$$0 \leq B^{in}_{i,t,u} \leq XC_i,\ \forall i,t,u \tag{2.10}$$

$$0 \leq B^{out}_{i,t,u} \leq XC_i.\ \forall i,t,u \tag{2.11}$$

The formula (2.9) ensures that the stored energy in the battery remains within the minimum and maximum limits. The formulas (2.10) and (2.11) are constraints on the charge

and discharge rate for each time u.

In addition, the following equations must also be satisfied for the battery:

$$X_{i,1,1} = X_i^0, \ \forall i \tag{2.12}$$
$$X_{i,T,U+1} = X_i^0, \ \forall i \tag{2.13}$$
$$X_{i,t+1,1} = X_{i,t,U+1}. \ \forall i, \ 0 \leq t < T \tag{2.14}$$

The equation (2.12) sets the initial stored energy of the battery at the beginning of the day. The equation (2.13) defines that the end value of the stored energy is the same as the initial stored energy X_i^0. The equation (2.14) takes over the stored energy to the next day $t+1$ at the end of each day.

The inter-cluster energy exchange is facilitated by the local energy network, which is composed of private electric cables. Such a local energy network typically has a maximum limit for transmitted energy. The energy loss occurs during the energy exchange due to cable resistance as follows:

$$0 \leq Z_{i,j,t,u} \leq \gamma_{i,j}, \ \forall i, j, t, u, i \neq j \tag{2.15}$$
$$Z_{i,t,u}^T = \sum_{j=1, j\neq i}^{N} Z_{i,j,t,u}, \ \forall i, t, u \tag{2.16}$$
$$Z_{i,t,u}^R = \sum_{j=1, j\neq i}^{N} \beta_{j,i} Z_{j,i,t,u}. \ \forall i, t, u \tag{2.17}$$

The formula (2.15) is the constraint of the transmission capacity between the cluster i and j. The formula (2.16) calculates the transmitted energy from the cluster i. The formula (2.17) calculates the received energy from the other clusters to the cluster i with the energy exchange loss.

As for the energy management by the router, the following equations must be satisfied.

$$S_{i,t,u} \geq 0, \ \forall i, t, u \tag{2.18}$$
$$Y_{i,t,u} \geq 0, \ \forall i, t, u \tag{2.19}$$
$$S_{i,t,u} + G_{i,t,u} + B_{i,t,u}^{out} + Z_{i,t,u}^R = Y_{i,t,u} + D_{i,t,u} + B_{i,t,u}^{in} + Z_{i,t,u}^T. \ \forall i, t, u \tag{2.20}$$

The formula (2.18) shows that the cluster can only purchase electricity from the power company. The formula (2.19) indicates that the wasted energy must be a positive value. The equation (2.20) is the router equation, which states that the sum of incoming energy equals the sum of outgoing energy on the router.

2.5 Mathematical Formulation of SOH-Aware Two-Stage Optimization

This section presents the SOH-aware two-stage planning method as a MIP formulation. To reduce SOH degradation, the most effective approach is to directly incorporate the SOH degradation model into the optimization problem. However, this non-linear optimization problem is difficult to solve in a reasonable amount of time as the problem is quite complex even using a commercial solver. Therefore, the proposed method aims to reduce SOH degradation indirectly by controlling battery aging factors.

As previously mentioned in Section 2.3, higher SOH degradation is caused by both higher SOC swing and higher average SOC level. Moreover, reducing battery degradation actively would lead to suppressing battery usage, which in turn leads to an increase in electricity costs. These are in a trade-off relationship. To find the optimal trade-off, the proposed method mainly focuses on controlling the SOC swing, which affects both purchased energy and battery degradation. For example, a larger SOC swing reduces purchased energy but also increases battery deterioration. On the other hand, a smaller SOC swing reduces battery degradation but also increases purchased energy. Thus, the optimal solution for this trade-off can be found by introducing a constraint on the SOC swing to keep it below a certain upper bound. This approach allows us to easily explore the trade-off by adjusting the upper bound of the SOC swing.

The proposed method also considers the average SOC, which has a relatively small impact on purchased energy. To minimize the degradation effect of the average SOC, the proposed method uses a penalty function based on the SOH model proposed by Millner [39]. In summary, the proposed approach consists of (1) a constraint for SOC swing control and (2) a penalty function for the average SOC, which are described in Section 2.5.1 and Section 2.5.2, respectively. The detailed formulation of the proposed optimization problem is presented in Section 2.5.3.

2.5.1 Constraint for SOC Swing Control

This section describes the constraints for SOC swing control. Firstly, the SOC swing, denoted by $SOC_{i,t}^{swing}$, is given as follows.

$$SOC_{i,t}^{swing} = \max_{1 \leq u \leq U} SOC_{i,t,u} - \min_{1 \leq u \leq U} SOC_{i,t,u}. \ \forall i,t \tag{2.21}$$

For simplification, $SOC_{i,t}^{swing}$ is defined as the ranges between the maximum and the minimum SOC level of cluster i at the day t. Note that the formulation internally contains several binary variables in order to express the equation (2.21); hence, the proposed optimization problem is MIP.

To limit $SOC_{i,t}^{swing}$ and control the battery usage, the following constraint is introduced:

$$0 \leq SOC_{i,t}^{swing} \leq SWING_{max}, \ \forall i,t \tag{2.22}$$

where $SWING_{max}$ is the upper bound of SOC swing for a day, which can range from 0 to 1. If the value of $SWING_{max}$ is low, the SOC swing is heavily restricted, and a value of 0 means that the battery is unable to be used due to the constraint. The balance between battery degradation and purchased energy can be easily examined by adjusting the single parameter of $SWING_{max}$.

2.5.2 Penalty Function of Average SOC

The average SOC is a significant factor contributing to battery degradation. Because the average SOC has a relatively small impact on the purchased energy, the proposed method minimizes the damage caused by the average SOC in order to reduce battery degradation. As shown in the equation (2.4) of the SOH model, the battery degradation effect is regarded as an exponential function of the average SOC. Assuming that minimizing the equation (2.4) is more effective in reducing battery degradation than simply minimizing the sum of the average SOC. Therefore, a penalty function based on the equation (2.4) is set as the objective function. Initially, the average SOC, denoted by $SOC_{i,t}^{avg}$, is defined as follows:

$$SOC_{i,t}^{avg} = \sum_{u=1}^{U} \frac{SOC_{i,t,u}}{U}. \ \forall i,t \tag{2.23}$$

The average SOC originally refers to the average SOC level for each charge/discharge cycle. For simplicity, the average SOC is treated as a daily average in this formulation.

The penalty function of the average SOC is defined based on the equation (2.4) of the SOH model as follows:

$$P(x) = \exp\left[4K_{SOC} \cdot (x - 0.5)\right], \tag{2.24}$$

where x represents the average SOC, which ranges from 0 to 1.0, and this function represents the battery damage caused by the average SOC level. Since $P(x)$ is an exponential function, it cannot be directly introduced into the MIP formulation. Thus, to linearize this non-linear function, the functuion is approximated by a set of linear lines using a piecewise-linear approximation technique.

Let N be a number of sampling coordinates $x_1, \ldots, x_N$. Here, x_0 and x_N correspond to the average SOC of 0 and 1.0, respectively. Then, the function is approximated by a set of linear functions for each interval $[(x_n, P(x_n)), (x_{n+1}, P(x_{n+1}))]$ $(k = 0, \ldots N-1)$. These sets of linear functions are defined as the approximated penalty function $\tilde{P}(x)$. To minimize the battery damage caused by the average SOC level, the sum of $\tilde{P}\left(SOC_{i,t}^{avg}\right)$ is set to an objective function in the optimization problem. Note that it is

required to introduce several binary variables internally in the formulation to express the equation $\tilde{P}(SOC^{avg}i,t)$. The final formulation is MIP due to the equation (2.21) and the piecewise-linear function.

2.5.3 Proposed Two-Stage Optimization Problem

This section presents the proposed SOH-aware two-stage operational planning formulation based on the energy management problem. There are two objectives for this problem: 1) minimizing the purchased energy from the power company and 2) reducing the SOH degradation. To achieve a balance between these two objectives, the optimization problem is divided into two stages:

- Stage 1: Minimizing the purchased energy from the power company.
- Stage 2: Reducing the battery aging factors.

In Stage 1, the minimum amount of purchased energy needed to operate the system is calculated. In Stage 2, the schedule of the battery is determined to reduce the aging factors, subject to the constraint of the minimum purchased energy obtained in Stage 1. The constraint on the SOC swing (2.22) is introduced in both stages to explore the trade-off, and the penalty function of the average SOC $\tilde{P}\left(SOC_{i,t}^{avg}\right)$ is set as the objective function in Stage 2 to reduce battery degradation. In this way, the proposed method obtains the minimum purchased energy and minimum battery degradation, which represent the trade-off relationship.

This two-stage structure is reasonable from time scales and system dynamics perspectives. The purchased energy should not rapidly change in this context where PV generation does not fluctuate greatly, and electricity prices are fixed. In contrast, the battery degradation is actively controlled, and the time constant of the stage 2 is smaller than that of the stage 1. The faster problem of battery aging factor reduction should be solved for a given working point of the slower problem of purchased energy minimization.

Alternatively, a one-stage optimization approach could be used where the objective function is a weighted sum of the purchased energy and the penalty function for battery degradation. However, finding the optimal weight parameters for each term is a challenging task, as the scales of the purchased energy and the penalty functions are significantly different (i.e., the former is a cost and the latter is an aging factor). The two-stage structure avoids the need for searching for optimal weights and allows for easy exploration of the trade-off. Therefore, the two-stage structure is more suitable for this purpose. The details of the proposed formulation are described in the following sections.

Stage 1: Purchased Energy Minimization

In Stage 1, the minimum purchased energy is obtained by solving the following optimization problem:

$$\begin{aligned}
&\text{minimize} && S_{total} = \sum_{i=1}^{N}\sum_{t=1}^{T}\sum_{u=1}^{U} S_{i,t,u}, && (2.25)\\
&\text{subject to} && (2.7)-(2.20),(2.21),(2.22),\\
&\text{input}\\
&&& \{G_{i,t,u}, D_{i,t,u}\},\ \forall i,t,u\\
&\text{decision variables}\\
&&& \{S_{i,t,u}, Y_{i,t,u}, X_{i,t,u}, B^{in}_{i,t,u}, B^{out}_{i,t,u}, Z_{i,j,t,u}\}.\ \forall i,j,t,u, i \neq j,
\end{aligned}$$

This problem includes the constraints for SOC swing with the upper bound $SWING_{max}$ as a parameter. The objective function (2.25) seeks to minimize the total purchased energy of all clusters over the planning period. The proposed method uses the obtained minimum purchased energy, denoted by S^*_{total}, as a reference point to keep the purchased energy at a minimum.

Depending on the value of $SWING_{max}$, the minimum purchased energy S^*_{total} may vary. In Stage 1, the schedules for system operation for each cluster at each time slot are calculated. However, these schedules are then recalculated in Stage 2 to minimize battery aging.

Stage 2: Battery Aging Factor Reducing

In Stage 2, the following optimization problem is solved to minimize the battery aging factor under the minimum purchased energy:

$$\begin{aligned}
&\text{minimize} && Damage = \sum_{i=1}^{N}\sum_{t=1}^{T} \tilde{P}\left(SOC^{avg}_{i,t}\right), && (2.26)\\
&\text{subject to} && (2.7)-(2.20),(2.21)-(2.23),\ (2.25),\\
&&& S_{total} \leq S^*_{total}, && (2.27)\\
&\text{input}\\
&&& \{G_{i,t,u}, D_{i,t,u}\},\ \forall i,t,u\\
&\text{decision variables}\\
&&& \{S_{i,t,u}, Y_{i,t,u}, X_{i,t,u}, B^{in}_{i,t,u}, B^{out}_{i,t,u}, Z_{i,j,t,u}\}.\ \forall i,j,t,u, i \neq j
\end{aligned}$$

The objective (2.26) is to minimize the piecewise linear penalty function outlined in Section 2.5.2 The equation (2.27) constrains the amount of purchased energy and ensures that only the minimum necessary amount of purchased energy, S^*_{total}, is used. This

helps to keep the total purchased energy at a minimum in Stage 2. The resulting solution consists of optimal schedules for energy purchase, battery usage, energy transmission, and wasted energy. The proposed method aims to minimize purchased energy while simultaneously reducing the battery aging factor.

2.6 Simulation Experiments

In this section, the simulation experiments are performed with realistic assumptions to demonstrate the effectiveness of the proposed method.

2.6.1 Simulation Setup

To evaluate the effectiveness of the proposed method, two criteria are introduced: 1) battery aging cost and 2) total system cost. The battery aging cost, denoted by $COST_{aging}$, is defined as the product of the initial purchase cost of the battery and the decrease in battery capacity (expressed as a percentage of SOH decreases). This cost is based on the assumption that if the battery becomes degraded to the point of being useless, it will need to be replaced. Therefore, the initial cost is allocated based on the amount of battery degradation according to the following equation:

$$COST_{aging} = \sum_{i=1}^{N} \frac{1 - SOH_i}{1 - SOH_{lim}} \cdot COST_{bat}, \tag{2.28}$$

where SOH_i is the SOH of the cluster i's battery after one year of operation, SOH_{lim} is the SOH threshold indicating the end-of-life of the battery, and $COST_{bat}$ is the cost to replace the battery when it reaches its end-of-life. According to literature [39], the lifetime threshold SOH_{lim} is typically set to 0.8. The battery cost $COST_{bat}$ is set to 200 kJPY/kWh in this case.

On the other hand, to evaluate not only battery degradation but also electricity costs, the total system cost, denoted by $COST_{year}$, is defined as the sum of the electricity costs and the battery degradation costs according to the following equation:

$$COST_{year} = COST_{aging} + S^*_{total} \cdot COST_{grid}, \tag{2.29}$$

where $COST_{grid}$ is the price of electricity per unit of energy in the power grid. Assuming that the electricity price is constant regardless of time and purchase peak power, $COST_{grid}$ is set to 21 JPY/kWh.

The system model in the experiment consists of five clusters ($N = 5$) that are completely connected by the local energy network. The planning horizon is one month ($T = 31$), and hourly energy management is determined through optimization ($U = 24$). The optimization problem is solved monthly, and simulation experiments are conducted over the course of a year by applying the solution each month. The input data includes

Table 2.2: Parameter settings of smart PV system.

Parameter	Value	
Upper bound of stored energy in battery	$\overline{X_i} = 3$	$\forall i$
Lower bound of stored energy in battery	$\underline{X_i} = 0.3$	$\forall i$
Initial stored energy in battery	$\overline{X_i^0} = 0.3$	$\forall i$
Charge/discharge speed of battery	$XC_i = 3$	$\forall i$
Charging efficiency of battery	$\alpha_i = 0.9$	$\forall i$
Loss rate of energy exchange	$\beta_{i,j} = 0.95$	$\forall i, j; i \neq j$
Capacity of energy exchange	$\gamma_{i,j} = 100$	$\forall i, j; i \neq j$

real PV generation and demand profiles from five distinct houses in Shiga, Japan, which differ between the clusters. A commercial solver, IBM ILOG CPLEX v12, is used to solve the proposed MIP-based optimization problem. The parameters of the SOH model are set to the values drawn from the literature [39]. The other parameters in the simulation experiments are shown in Table 2.2.

The proposed method (labeled *Proposed*) is compared to a baseline approach (labeled *Baseline*). The baseline method only utilizes stage 1 optimization, which minimizes purchased energy while imposing the SOC swing constraint. To assess annual effects, the following steps are taken in the experiment:

1. Following optimization is performed monthly, resulting in a year-long battery charge/discharge trace.
   (a) Stage 1: Minimize purchased energy subject to the $SOC_{i,t}^{swing}$ constraint (2.22), with the upper bound $SWING_{max}$ ranging from 0.1 to 0.9.
   (b) Stage 2: Minimize the penalty function (2.26) subject to the $SOC_{i,t}^{swing}$ constraint (2.22) and the corresponding minimum purchased energy constraint (2.27).
2. Using the SOH model, the battery SOH degradation factor is calculated based on the obtained charge/discharge profiles.
3. The battery aging cost and total system cost are calculated using equations (2.28) and (2.29), respectively.

2.6.2 Results

To investigate the effect of the SOC swing constraint (2.22) on the minimum purchased energy, simulation experiments are carried out by changing the upper bound $SWING_{max}$ from 0.1 to 0.9. The results of the purchased energy are shown in Fig. 2.5. The minimum purchased energy S_{total}^{*} increases with decreasing the value of $SWING_{max}$. This is because the limitation of battery usage causes a mismatch between renewable energy and demand. Besides, for each $SWING_{max}$ setting, the purchased energy of the proposed

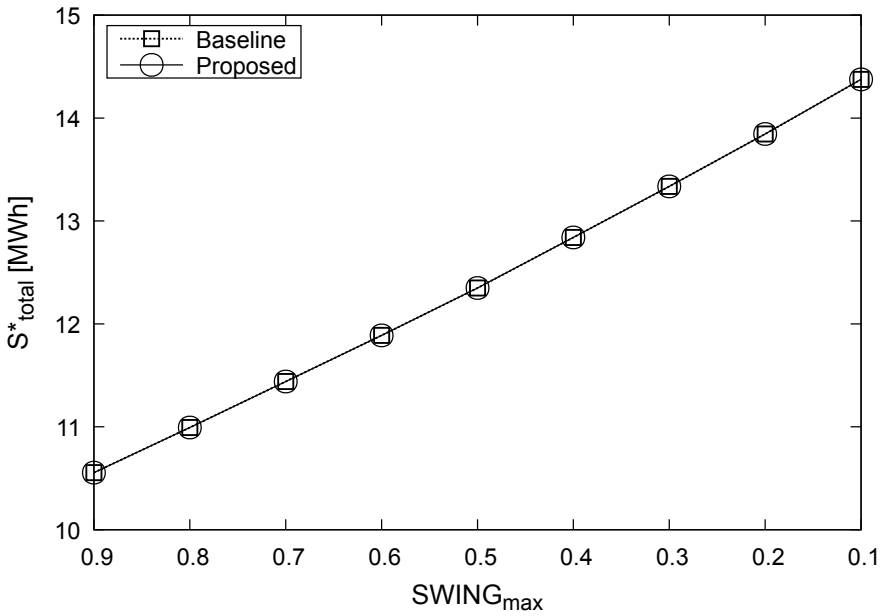

Figure 2.5: Trade-off relationship between upper bound of SOC swing and purchased energy.

method is the same as that of the baseline, i.e., the purchased energy is kept minimum, owing to the constraint (2.27).

Fig. 2.6 shows the optimized battery state-of-charge (SOC) profiles for four typical days when $SWING_{max}$ is set to 0.4 or 0.9. The x-axis represents time, while the y-axis represents the SOC level of the battery. By comparing the case with $SWING_{max} = 0.9$ to the case with $SWING_{max} = 0.4$, it can be seen that the proposed method limits and controls the range of SOC more effectively. Additionally, the proposed method consistently achieves lower SOC profiles than the baseline method. This result means that minimizing the penalty function (2.26) leads to a reduction in the average SOC level.

Fig. 2.7 shows the trade-off between the sum of the purchased energy and the SOH decrease for the given year simulation. The dotted line and solid line correspond to the proposed method and the baseline method, respectively. The x-axis shows the obtained minimum purchased energy S^*_{total}, and the y-axis represents the SOH decrease for the given year. By changing the limitations of the SOC swing $SWING_{max}$ from 0.1 to 0.9 with a 0.1 interval, the different solution points in the figure can be obtained. From the left point in the line plot, it corresponds to the case where SWINGmax is set to a low value (0.1: 10%), i.e., the strict limitation for the battery system is given. As seen in the figure, the proposed method can reduce the amount of the decrease in SOH by minimizing the battery aging factor. The proposed method can improve the battery lifetime.

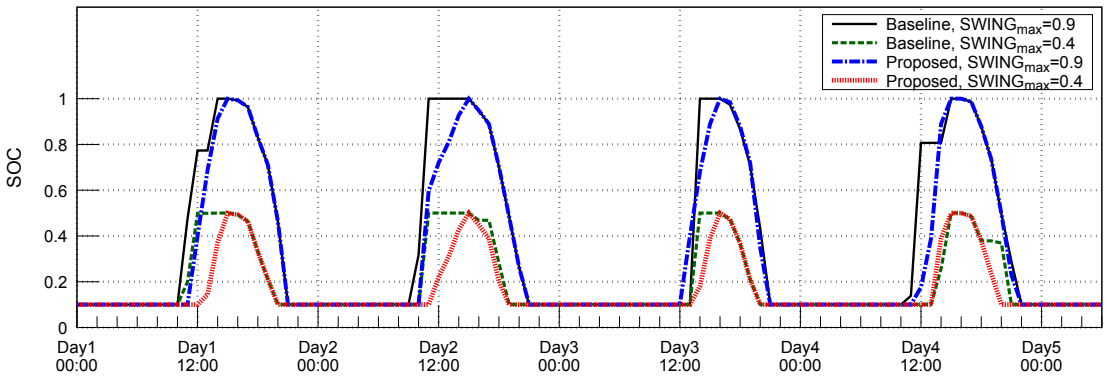

Figure 2.6: Cluster 1's battery SOC profiles of baseline and proposed methods with different $SWING_{max}$ for five days in autumn.

Next, the impact of the battery aging factors on the battery aging cost $COST_{aging}$ is demonstrated. Fig. 2.8 compares the sum of purchased energy and the battery aging cost between the proposed method (dotted line) and the baseline method (solid line). The x-axis displays the minimum energy obtained (S^*total), and the y-axis represents the battery aging cost ($COSTaging$). As in Fig. 2.7, each point in the line plot was determined by incrementally changing $SWING_{max}$ from 0.1 to 0.9 in steps of 0.1. The figure shows that the proposed method produces a more favorable trade-off than the baseline method, and can reduce the battery aging cost by up to 14.1% at the same level of purchased energy.

Finally, the total system cost for the one-year operation is calculated. Fig. 2.9 shows the total system cost for one year of operation using the proposed method. As shown in the figure, when $SWING_{max}$ is set to 0.6, the total system cost is minimized. This is because the increase in electricity cost exceeds the decrease in battery aging cost near $SWING_{max} = 0.6$. In this case study, the optimal setting for the upper bound $SWING_{max}$ is determined to be 0.6 based on the total system cost. It is worth noting that the proposed method can determine the optimal operating points for the battery to minimize degradation in the planning stage.

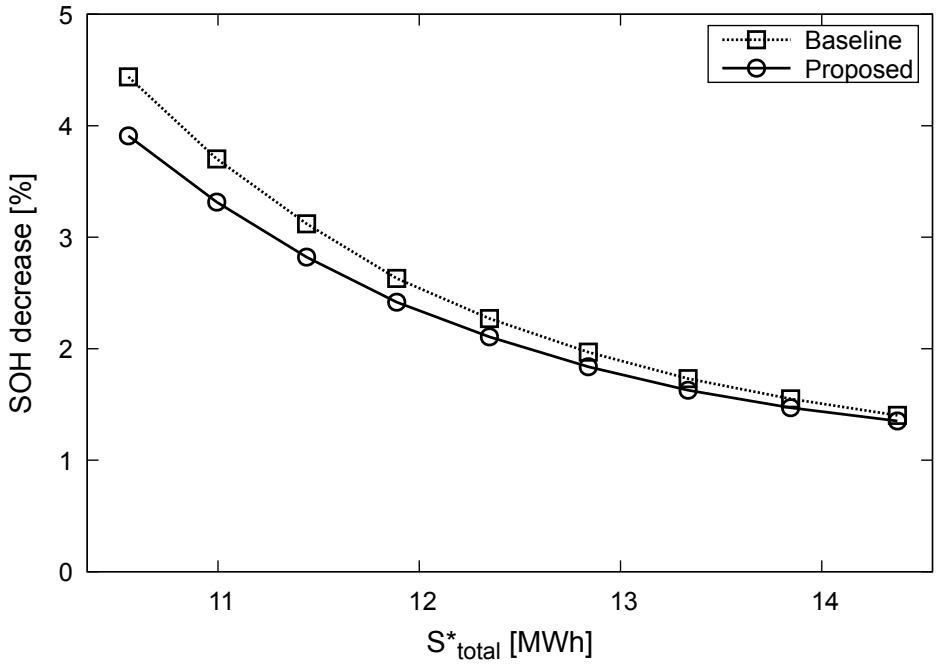

Figure 2.7: Trade-off relationship between SOH decrease for a year and purchased energy.

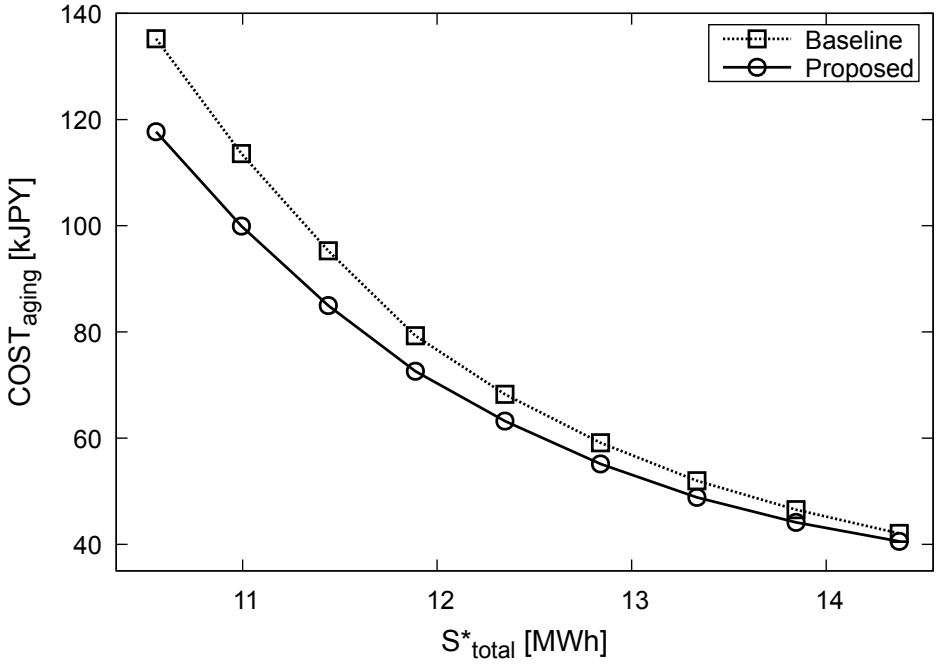

Figure 2.8: Trade-off relationship between battery aging cost for a year and purchased energy.

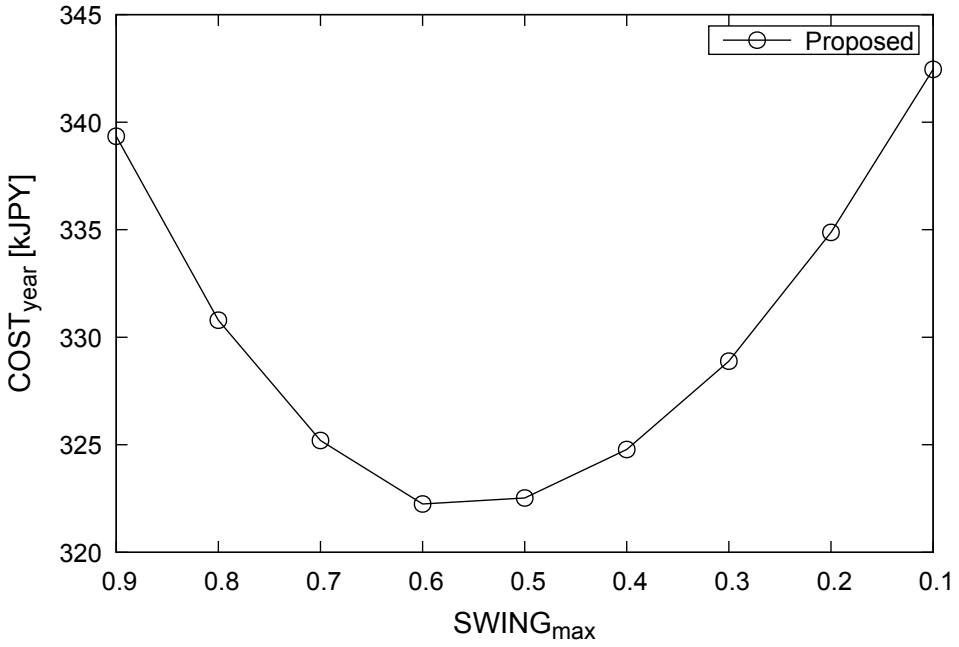

Figure 2.9: Total system cost with different upper bound of SOC swing $SWING_{max}$.

2.7 Summary

This chapter has proposed a state-of-health (SOH) aware two-stage operational planning methodology for smart photovoltaic (PV) systems with a battery system. The proposed method aims to achieve a better system-level solution for battery scheduling that extends battery lifetime. To this end, an energy management problem is formulated as a mixed-integer programming (MIP) optimization problem to minimize purchased energy from the power grid and battery aging factors. Besides, the battery SOH model is incorporated into the problem, and average state-of-charge (SOC) level and SOC swing are considered as battery aging factors. The proposed method consists of two optimization stages: (1) purchased energy minimization with SOC swing constraints, and (2) exploring solutions to minimize battery aging caused by average SOC level under the same purchased energy. Simulation results showed that the proposed method can reduce the battery aging cost by 14.1% compared to the baseline method, which aims to minimize only purchased energy. The proposed method can provide a better trade-off between battery degradation and purchased energy.

Additional research is to develop a real-time management method for EMS. The proposed method in this chapter stands on the unrealistic assumption that the amount of variable renewable generation is perfectly predicted. This assumption makes the proposed method unsuitable for real-time operation purposes. As a starting point, Chapters 3 and 4 present a real-time optimization framework that incorporates specific forecasting methods of system input and conditions

As for future work on operational planning, stochastic variations on energy profiles will be considered. Many factors, such as occupant behavior and weather conditions, can lead to uncertainties in demand and renewable generation. To avoid unexpected cost increases and grid instability, it is required to make a plan with taking uncertainties into account. Hence, an uncertainty-aware operational planning method should be developed.

Chapter 3

Multi-Time Scale Online Energy Management Framework Mixing Fast and Slow Dynamics

In real-time energy management, the fluctuation of renewable generation such as photovoltaic (PV) systems causes severe energy loss and imbalances. Meanwhile, in slower time scales, scheduling distributed energy resources (DERs) such as a battery system and shiftable appliances is important to shift energy demand from peak to off-peak hours and reduce electricity costs. To fill the gap between fast and slow time scales in energy management, this chapter presents an online multi-time scale energy management framework for smart PV systems[1]. The proposed framework consists of coarse and fine-grained time scales and repeatedly solves three consecutive optimization problems at certain time intervals. This multi-time scale structure reduces computational complexity while maintaining solution quality. In addition, a short-term PV forecasting model and an equivalent-circuit battery model are introduced for precise energy management. The proposed framework can improve both modeling capability and computational complexity in real-time EMS. The results show that the proposed framework can reduce electricity costs by up to 48.1% compared to baseline methods with reasonable computational time.

3.1 Motivation and Objective

With the recent growth of environmental awareness, a large amount of renewable energy such as solar and wind power have been introduced to demand-side consumers to reduce CO_2 emissions and electricity costs [60]. However, renewable energy is intermittent and uncontrollable, and its generation fluctuates in the short term due to various

[1]This chapter is a refined and reproduced version of the paper to be published in Applied Energy [59] copyrighted by Elsevier.

environmental factors, e.g., cloud moving and wind speed. This fluctuation nature may cause supply-demand mismatches [61]. To address this issue, a smart energy system, which integrates renewable energy, battery system, and demand control, can make such systems energy-efficient, more resilient, and eco-friendly [62].

One of the key technology of smart energy systems is an energy management system (EMS) to manage the balance of energy in real-time among appliances, battery systems, renewable generation, and electricity purchases [63]. The EMS aims to improve several criteria, including minimizing electricity costs, reducing demand peaks, and maximizing the self-sufficiency rate of renewable sources [64]. However, the unpredictable and short-term fluctuations of renewable sources can negatively impact the performance of the EMS [65]. To mitigate these fluctuations, the EMS currently relies on battery systems on a fast time scale [66]. Therefore, it is desirable to improve battery modeling and properly incorporate workload-dependent storage in the EMS [67, 68].

Model predictive control (MPC) is a widely used control methodology in EMS due to its ability to handle the fluctuations of renewable energy and control dynamic systems. One of the main benefits of using MPC is the ability to constantly adjust control inputs based on the latest information, through iterating the prediction and optimization of future system behavior for a predetermined time period. MPC is often used in the scheduling of battery systems, in combination with forecasting techniques for renewable energy generation, to address the uncertainties of renewable energy in smart energy systems [69].

On the other hand, demand load control is recognized as a promising application of EMS [70]. One type of demand load control is appliance scheduling, which helps to match load patterns with renewable generation and electricity price signals [71, 72]. In appliance scheduling, shiftable appliances that can be moved to other time slots, such as washing machines and tumble dryers, are scheduled between configuration and deadline. This enables minimizing electricity costs and maximizing PV sufficiency rates. Such a demand control approach is performed on a slower time scale, completely different from the short-term PV fluctuation. The existence of multiple problems with different time scales makes energy management complex and intractable.

One important factor that affects EMS efficiency is the difference in time scale. Mixing fast and slow system dynamics in smart energy systems puts excessive strain on computational complexity where control performance should be preserved. EMS should take into account hourly and daily fluctuations in electrical demand and renewable generation over a longer period of time, potentially up to a week [73]. Also, appliance scheduling should be performed either daily or hourly, effectively aligning supply with demand [74]. On the other hand, at a faster time scale with a second-level resolution, the energy imbalance in real-time due to renewable fluctuation should be managed to reduce energy loss. As mentioned above, the time scales and their objectives are different from each other. Thus, combining them into one problem increases computational complexity significantly. This work addresses this issue in this chapter by implementing

a multi-time scale energy management framework.

This chapter presents a multi-time scale energy management framework for a smart PV system that takes into account both fast and slow system dynamics. The targeted system is a local energy system comprising several homes and buildings equipped with PV panels, batteries, and controllable appliances. To implement real-time control, the proposed framework employs the MPC approach using data provided by PV forecasting techniques based on deep neural networks and thermal simulation [75]. An equivalent circuit model of a battery [76] is also introduced. It enables capturing the changes in the state-of-charge (SOC) and I-V characteristics of the battery system to reduce energy loss. The proposed multi-time scale structure effectively handles different time-scale problems in energy management as an integrated loop of optimization. The time scale is divided into two: coarse- and fine-grained. This approach enhances both the computational efficiency and modeling capability.

The main contributions of this work are shown below:

- The framework introduces two-time scales: coarse-grained and fine-grained. This approach allows for the incorporation of fast and slow dynamics, such as short-term fluctuation of PV generation and demand, battery transient responses, and appliance scheduling.
- The proposed comprehensive approach includes the integration of three detailed component models: a time-shiftable appliance model, a physics-based PV forecasting model with 1 s resolution, and an equivalent circuit-based battery model.
- The proposed framework uses an MPC approach to handle PV forecasting errors and the battery's internal state change. The control processes including prediction and optimization are effectively iterated.
- Experimental result shows that the proposed framework can reduce electricity costs by 48.1% compared to single-time scale methods. It also has low computational complexity, enabling real-time control of the system. The effects of PV forecasting error and battery capacity are also explored in the simulation experiments.

The remainder of this chapter is as follows. Section 3.2 presents related works of energy management methodology for a smart PV system. Section 3.3 describes an overview of the proposed multi-time scale framework and system models. Then, Section 3.4 shows a mathematical formulation of the energy management problem in the proposed framework. Finally, the effectiveness of the proposed method by simulations with measured data is demonstrated in Section 3.5 and summarize this chapter in Section 3.6.

3.2 Related Works

EMS often uses optimization-based scheduling to manage energy for appliances and battery systems. The combination of battery and appliance scheduling has been shown

to be effective, as reported in the literature. For example, Lokeshgupta et al. [77] proposed a home energy management system (HEMS) controller based on a multi-objective mixed integer programming (MIP) problem to minimize electricity costs and power peaks. They also conducted an economic analysis of using battery investment with appliance scheduling in residential settings. Dorahaki et al. [78] presented an EMS using mixed-integer non-linear programming (MINLP) that considers both electrical and thermal demand control and day-ahead energy storage scheduling. A sensitivity analysis in their study showed that the best combination of controllable devices is to schedule both electrical demand and battery use. However, these previous studies only solve the scheduling problem once per day and do not take into account forecast errors in PV generation or the latest state of the battery system during the day.

Many control methods based on the MPC approach have been proposed for EMS applications. Godina et al. [79] proposed an MPC-based home energy management for an air conditioning (AC) system under dynamic pricing schemes. They demonstrated that the MPC approach outperforms conventional controllers, which are ON/OFF and proportional-integral-derivative (PID), in terms of both electricity costs and control capability. The MPC framework in EMS is also studied by Parisio et al. [80], and they investigated the MPC-based energy management for multiple buildings by considering weather forecasts, demand forecasts, and end-user preferences. Carli et al. [81] demonstrated that the MPC-based approach can be easily implemented in real-world buildings with achieving high performance. With the recent increase in computing resources, the scope of problems that can be addressed using an MPC approach has expanded. Gan et al. [82] investigated the integration of forecasting methods for renewable generation and demand load, as well as a MIP-based MPC problem to schedule a battery system. The performance of MPC depends on the accuracy of the prediction model. To ensure both prediction accuracy and solution quality, the planning horizon for MPC typically includes a few days with a coarse-grained resolution, such as 15 min or one hour. Although there is much literature on scheduling in smart energy systems, it mainly addresses slow dynamics.

For a shorter time scale, real-time control approaches are generally based on a rule-based controller [83] and a fuzzy logic controller [84], rather than prediction-based approaches due to computational time constraints. Since such controllers only consider simplified system models and current information, the solution optimality is not guaranteed at all.

Abreu et al. [85] introduced a hierarchical MPC method for managing various demand loads, with an upper layer that calculates the maximum power limit and a lower layer that individually optimizes schedules for demand. However, this approach does not take into account renewable generation or a battery system. Lefort et al. [86] also investigated a hierarchical EMS centered on a building, battery system, and PV generation, which included a scheduling upper layer with a 7 h horizon and a pilot lower layer with a 5 min horizon. Jin et al. [87] proposed a hierarchical EMS consisting of

day-ahead schedules and intra-hour MPC adjustment to optimize EV with PV generation. However, none of these studies consider appliance scheduling, and their demand flexibility is also limited. Furthermore, the PV forecasting models used in these works are relatively simple and do not adequately account for short-term PV fluctuations. On the other hand, Elkazaz et al. [88] developed a hierarchical two-layer home EMS with the aim of lowering daily electricity expenses and boosting PV self-consumption. Their approach involves a top layer that calculates the scheduling of the battery system and appliances for the following 24 h, using the previous day's PV generation profiles as PV forecast data. The lower layer is a rule-based real-time controller that adjusts for PV fluctuations, but it is a relatively straightforward algorithm that does not consider future PV fluctuations. Accurate PV forecasting is crucial for effective energy management, as demonstrated by Ferrarini et al. [89] and Klingler et al. [90]. These authors have noted that errors in PV forecasting can significantly impact the performance of energy management systems. Furthermore, the previous studies mentioned in this text have used linear battery models, despite the fact that battery behaviors are nonlinear. Additionally, these studies have not provided a detailed view of PV forecasting and battery states on the fast time scale, which can lead to real-time energy imbalances and energy loss if fast dynamics such as short-term PV fluctuations and battery transient responses are not accounted for.

In comparison to the previously mentioned studies, the proposed framework incorporates the fast time scale through the integration of a short-term PV forecasting model and an electrical circuit-based battery model. The multi-time scale structure of the proposed framework effectively combines fast and slow system dynamics to accurately manage the balance between supply and demand. This allows for real-time scheduling to reduce electricity costs while considering a range of fast and slow dynamics, such as PV and energy demand fluctuations and battery transient responses.

3.3 Proposed Framework for Multi-Time Scale Energy Management

This section presents an overview of the proposed multi-time scale energy management framework and discusses the key concepts behind the multi-time scale structure in this section.

3.3.1 Introduction to Proposed Framework

The overview of the proposed framework is shown in Fig. 3.1. It includes a battery model, a PV forecasting model, and a mathematical formulation of a smart PV system. The control objective is to minimize electricity costs. The inputs of the framework are forecasting data of PV generation and electrical demand profiles. The obtained solution

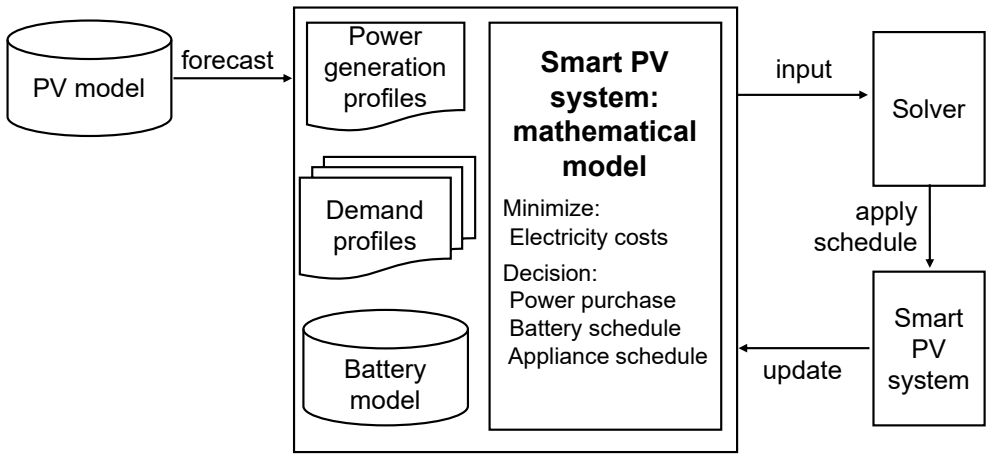

Figure 3.1: Overview of multi-time scale energy management framework.

consists of purchased power/energy, battery charge/discharge, and appliance operation timing.

The main control processes are as follows. First, the PV forecasting model provides fine-grained PV profiles upcoming half an hour or a few days. The mathematical problem to optimize the system operation is formulated, and optimal schedules are obtained by solving it with a mathematical solver. Then, the solver calculates an optimal schedule for the system to minimize electricity costs from the utility grid. Finally, the obtained schedule is employed as a system operation. These processes are iterated every time step following the MPC approach, which is introduced in the following section. This allows for real-time control that adjusts the energy balance.

3.3.2 Concept of Model Predictive Control

The proposed framework for real-time energy management uses the MPC approach to control dynamic systems. MPC is an effective method for controlling dynamic systems [91] and has been applied successfully to energy management problems in recent studies [92]. The MPC approach involves computing an optimal solution that minimizes a given objective over a finite planning period while considering future periods as well. The key idea of MPC is to improve system performance by repeating prediction and optimization steps, as illustrated in Fig. 3.2. At each sample time step, the system's predicted behavior is inputted into an optimization problem for a given period. Only the first solution is applied to the system, while the rest are discarded. At the next sample time step, the process is repeated with updated predicted inputs and a receded time period. It's worth noting that the feedback structure of MPC can potentially compensate for uncertain variables, such as load demand and PV generation [93], which is one of its main advantages.

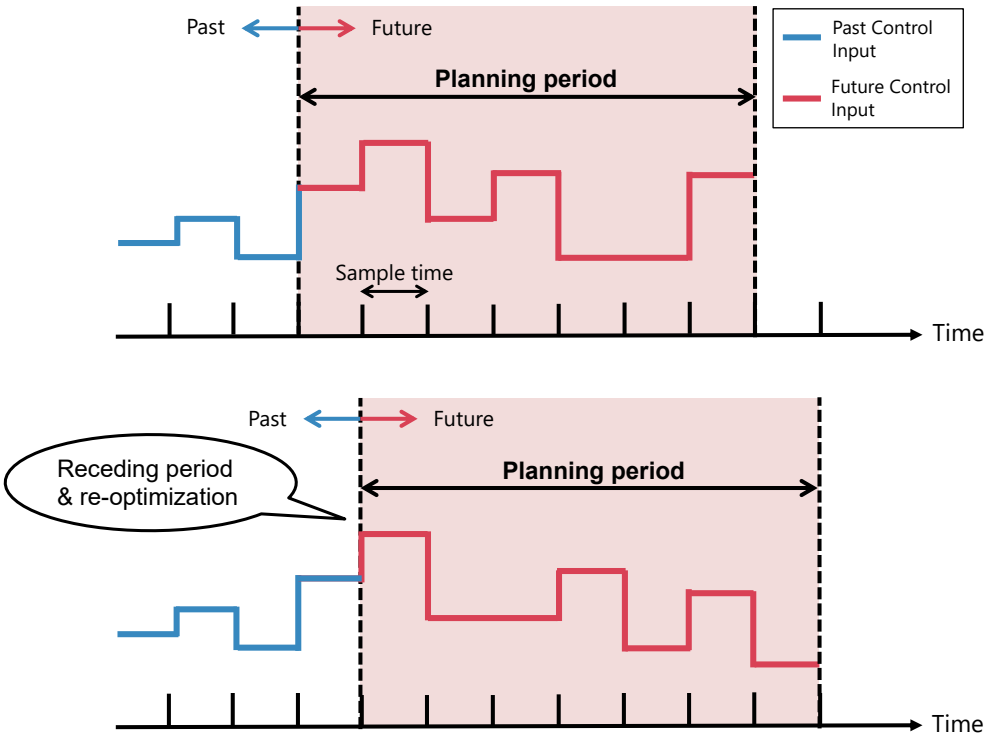

Figure 3.2: Basic concept of MPC approach.

3.3.3 Organization of Multi-Time Scale Approach

The main concept of the proposed multi-time scale structure is solving an integrated optimization loop that combines two independent time scales. The proposed structure has a coarse-grained and fine-grained time scale, as depicted in Fig. 3.3. The symbol t represents an index of time steps for the entire control procedure. At every control point, multi-time scale optimization is dispatched using the MPC approach with the input of forecast information and system states.

This structure incorporates variations in demand load and PV generation, appliance scheduling, and battery scheduling. The coarse-grained time scale, which involves coarse changes in demand and PV generation, is initially taken into consideration for scheduling appliances and batteries over a period of a few days, denoted as T_L. Long-term PV forecasting models, such as artificial intelligence [94], tend to be less accurate when the time resolution is less than minutes. Therefore, the time resolution Δt_L for the coarse-grained loops should be relatively coarse, e.g., 15 min.

The fine-grained time scale focuses on real-time control of a battery system to balance energy in the short term between PV output fluctuation and battery behavior's characteristics. In this time scale, the proposed framework uses the demand schedules obtained by the coarse-grained loop and calculates a precise battery schedule for a shorter period, T_S. To compensate for short-term PV fluctuations with battery schedul-

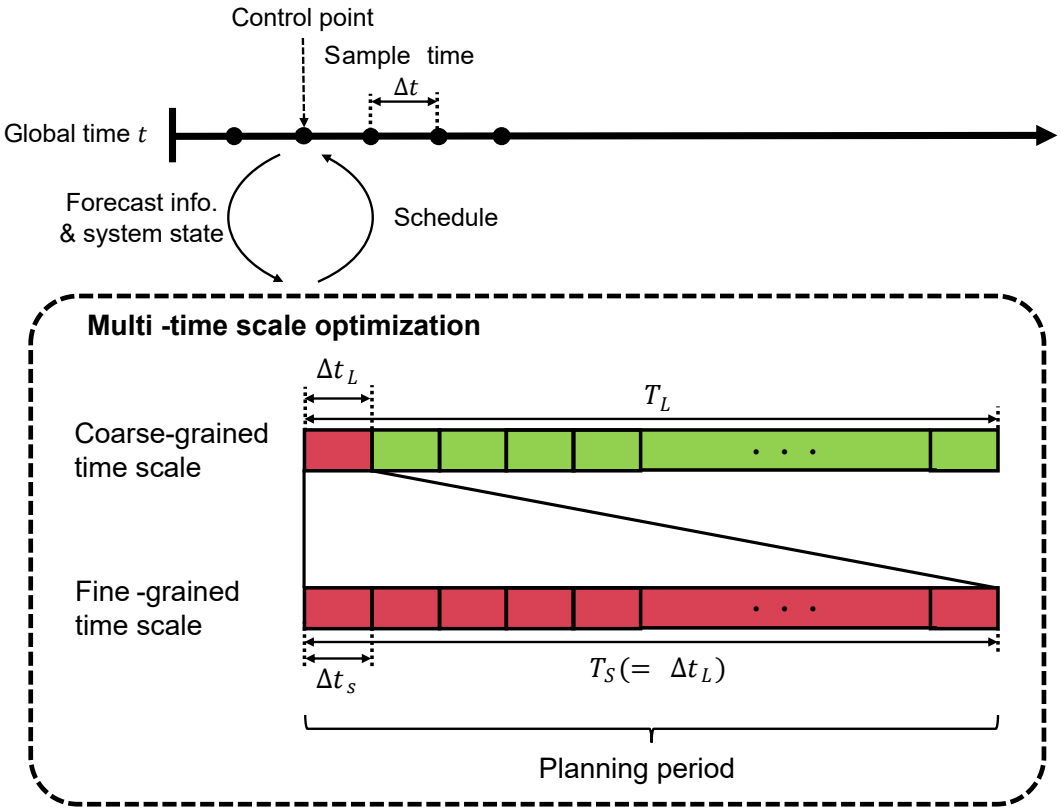

Figure 3.3: Proposed MPC approach combined with multi-time scale structure.

ing, the fine-grained loop's time resolution Δt_S should be a few seconds or less. This is because PV panels and batteries generally have electrical time constants of a few seconds or more. PV production is influenced by both solar irradiance and PV cell temperature, which can be affected by fast-changing weather conditions such as moving clouds, wind speed, etc. Their fastest time constants are usually a few seconds or higher [95, 96].

Different problems on different time scales, such as appliance scheduling, PV fluctuations, and battery operation, can be addressed by the proposed framework. However, instead of addressing these problems independently, the proposed framework can combine them into a single integrated optimization loop to obtain a high-quality solution.

3.3.4 System Model for Smart PV System

This section describes a detailed explanation of a smart PV system and mathematical formulation.

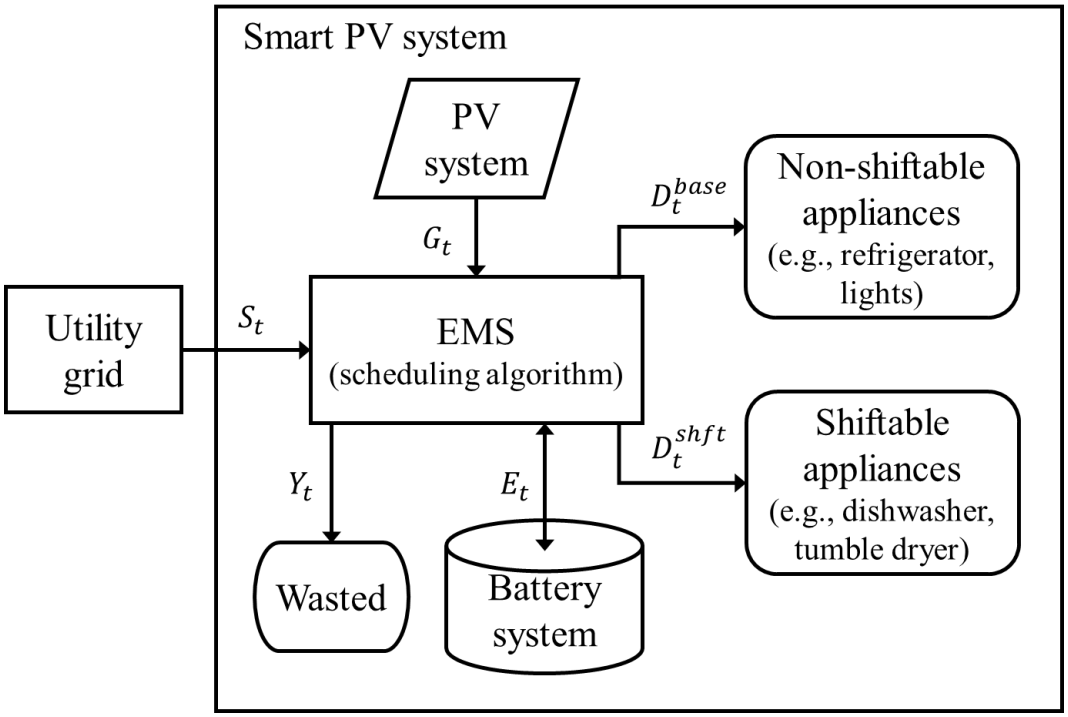

Figure 3.4: Schematic diagram of smart PV system with mathematical symbols.

Overview of Smart PV System

In this work, a PV-driven energy community made up of multiple buildings and households is called a smart PV system. The targeted smart PV system model is depicted in Fig. 3.4. The main components of a smart PV system are PV panels and a Li-ion battery system. When PV generation is insufficient or the EMS decides to supply the required demand from the battery instead of purchasing from the utility grid, the battery system supplies electrical energy. There are two categories of appliances in this system: non-shiftable and shiftable appliances. Non-shiftable appliances include refrigerators and lights whose operation and start time cannot be interrupted or deferred. Shiftable appliances, such as washing machines and dishwashers, can have their start time shifted to another time slot. During power shortages, the smart PV system buys electrical energy from the utility grid. To prevent grid instability due to reverse power flow, the system is prohibited to sell surplus energy to the grid. The surplus energy is utilized by the battery system and appliances as much as possible; otherwise, it will be wasted by additional components such as resisters, indicated by *Wasted* in Fig. 3.4. This type of system allows online data collection and control for all devices using EMS. It also connects to a network for exchanging information with other parts of the system and for obtaining external information, such as meteorological data and system states. Specifically, both shiftable appliances and a battery system can be controlled to balance PV generation

and demand load by solving optimization problems subject to user preferences.

The smart PV system is formulated as follows. First, the energy balance within the system must be maintained at all times t, which is expressed as:

$$S_t + G_t + E_t = D_t^{base} + D_t^{shft} + Y_t, \ \forall t \tag{3.1}$$

where S_t, G_t, and E_t represent the purchased energy from the utility grid, the PV energy production, and the charging/discharging energy of the battery system, respectively. D_t^{base}, D_t^{shft}, and Y_t denote the energy consumption of the non-shiftable appliances, that of the smart appliances, and the energy wasted inside the system, respectively. Charging/discharging energy E_t is positive in the case of charging and negative in the case of discharging. The purchased energy S_t and the wasted energy Y_t are only positive, as shown by:

$$0 \leq S_{t_L}, \ \forall t \tag{3.2}$$

$$0 \leq Y_{t_L}. \ \forall t \tag{3.3}$$

It should be mentioned that the system model does not explicitly manage other components such as wind turbines, electric vehicles, and air conditioning systems since this chapter focuses on the impact of PV forecasting and accurate battery models on EMS performance. These components can be easily considered by mathematically formulating their behaviors. The framework can also be extended to include management of indoor climate for air conditioning systems, as presented in Chapter 4.

Detailed Physics and Neural Network Based PV Forecasting Model

Due to meteorological random events, PV generation can fluctuate significantly. To smooth out these fluctuations and balance demand PV generation with demand and battery scheduling, real-time and precise PV forecasting data are necessary. This work uses a PV nowcasting model proposed in [75], which can predict precise and fine-grained PV generation using an all-sky camera, detailed physics-based models of PV thermal part [97], and deep neural network models. The forecasting model has the advantage of providing high temporal resolution data and making forecasts with a 1 s resolution up to a 15 min horizon. The minimum update interval is one minute, allowing for a fine-grained battery scheduling loop to be run within a reasonable time interval.

Making long-term plans for the system up to a few days requires PV forecasting for the coarse-grained time scale. It is typically obtained from a meteorological station.

Shiftable Appliance Model

Shiftable appliances are characterized by four parameters [98]: (1) operating time, (2) configuration time (T^{conf}) when the appliance is available for use, (3) deadline (T^{dead}) when the appliance must finish its operation, and (4) energy profiles for its operation.

Configuration and deadline time are considered user preferences, meaning that shiftable appliances must be scheduled between their configuration and deadline times. Finally, shiftable appliances will start based on the solution obtained automatically.

A mathematical formulation for shiftable appliances is described below. The operating cycle of each appliance is modeled rather than using a single value for appliance power consumption. To do so, the operation cycles of shiftable appliances are divided into P stages according to their operation content. The symbols m and p represent a shiftable appliance index and an operating phase index. Binary variables $q_{m,p,t}$ means the shiftable appliance's phase; if an appliance m is in operation phase p at time t, $q_{m,p,t} = 1$, otherwise it is 0. Moreover, binary variables $r_{m,p,t}$ are introduced as a finish flag; if operation phase p of appliance m is finished at time t, $r_{m,p,t} = 1$, otherwise it is 0. The shiftable appliance scheduling is then formulated as follows:

$$D_t^{shft} = \sum_{m=1}^{M} \sum_{p=1}^{P} q_{m,p,t} \cdot D_{m,p}^{app}, \ \forall t \tag{3.4}$$

$$q_{m,p,t} + r_{m,p,t} \leq 1, \ \forall m,p,t \tag{3.5}$$

$$q_{m,p,t-1} - q_{m,p,t} \leq r_{m,p,t}, \ \forall m,p, \ 2 \leq t \leq T \tag{3.6}$$

$$r_{m,p,t-1} \leq r_{m,p,t}, \ \forall m,p, \ 2 \leq t \leq T \tag{3.7}$$

$$q_{m,p,t} \leq r_{m,p-1,t}, \ \forall m,t, \ 2 \leq p \leq P \tag{3.8}$$

$$r_{m,p-1,t} - r_{m,p,t} = q_{m,p,t}, \ \forall m,t, \ 2 \leq p \leq P \tag{3.9}$$

$$\sum_{t=1}^{T} q_{m,p,t} = 1, \ \forall m,p \tag{3.10}$$

$$q_{m,p,t} = 0, \ \forall m,p, \ 1 \leq t \leq T_m^{conf}, \ T_m^{dead} \leq t \leq T \tag{3.11}$$

where $D_{m,p}^{app}$ is the consumed energy of appliance m in phase p. The equation (3.4) calculates the scheduled energy of the shiftable demand at. The formulas (3.5) - (3.8) and the equations (3.9) and (3.10) show the logic of shiftable appliance scheduling. The equation (3.11) denotes the user preference for the timing of the appliance usage. The coarse-grained time scale manages this appliance scheduling problem.

Equivalent Circuit Based Accurate Battery Model

Battery modeling is an important tool for implementing scheduling and simulation logic in EMS. This chapter's main contribution is to build a battery module based on a model of battery cell [76] for tracking SOC profiles and considering energy loss accurately. As mentioned in Section 3.2, many previous studies have utilized a basic model that only reflects the linear relationship between energy loss and the amount of charging/discharging, despite the actual relationship being nonlinear.

The battery module's configuration is illustrated in Fig. 3.5 and consists of identical cells that are connected in series and parallel. The number of series- and parallel-

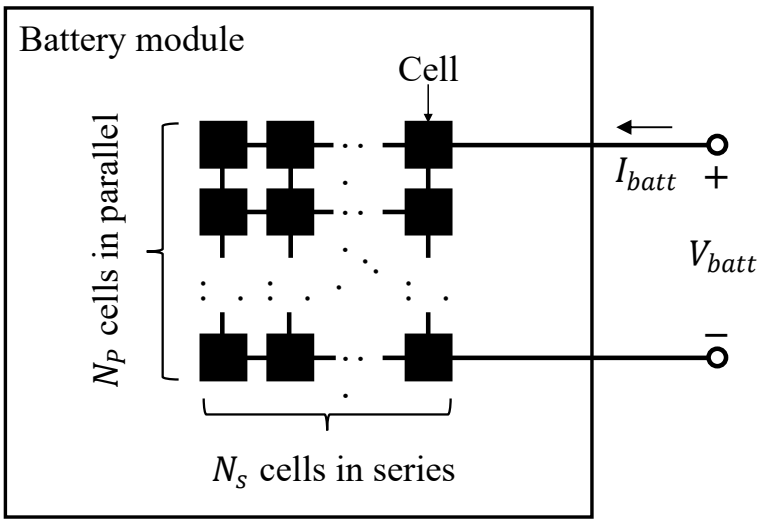

Figure 3.5: Battery module configuration composed of N_s series cells and N_p parallel cells.

connected cells is represented by N_s and N_p, respectively. The proposed framework integrates the equivalent circuit model as a battery model, showing fine agreement with the measured data regarding non-linear I-V characteristics and running time [76].

An equivalent circuit model employed in this chapter is depicted in Fig. 3.6. The battery's state of charge (SOC) change is represented by the left part of the model. The stored energy level of the battery, SOC, is indicated by the voltage source V_{SOC}, and its range is 0.0 - 1.0 ($0\% - 100\%$). The variable I_{batt} denotes the terminal current, which is positive when discharging and negative when charging. The nominal battery capacity is represented by C_{nom}, calculated based on the cell capacity, C_{cell}, and the number of parallel-connected cells, N_p:

$$C_{nom} = N_p \cdot C_{cell}. \tag{3.12}$$

Here, the SOC change is formulated as follows:

$$SOC_{t+1} = SOC_t - \int_t^{t+1} \frac{I_{batt}}{C_{nom}} dt. \; \forall t \tag{3.13}$$

The equivalent circuit's right part shows the transient response of the battery. The battery's terminal voltage is denoted by the voltage source V_{batt}. The left and right parallel RC branches handle the shorter and longer I-V characteristics, respectively. Each cell is modeled with open circuit voltage V_{OC}, resistances (R_S, R_{TS}, R_{TL}), and

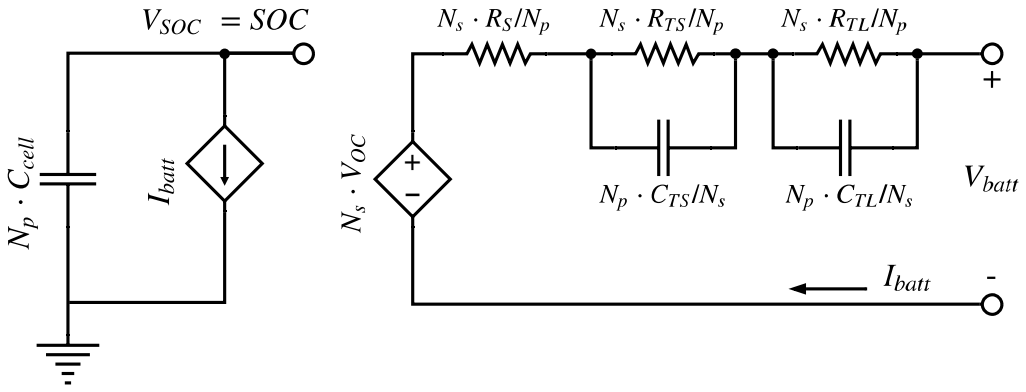

Figure 3.6: Electrical diagram of equivalent circuit-based battery model composed of $N_s \times N_p$ cells.

capacitances (C_{TS}, C_{TL}). These parameters depend on the SOC level and are given by:

$$V_{OC} = a_1 \cdot \exp(a_2 \cdot SOC) + a_3 + a_4 \cdot SOC + a_5 \cdot SOC^2 + a_6 \cdot SOC^3, \tag{3.14}$$

$$R_S = a_7 \cdot \exp(a_8 \cdot SOC) + a_9, \tag{3.15}$$

$$R_{TS} = a_{10} \cdot \exp(a_{11} \cdot SOC) + a_{12}, \tag{3.16}$$

$$R_{TL} = a_{16} \cdot \exp(a_{17} \cdot SOC) + a_{18}, \tag{3.17}$$

$$C_{TS} = a_{13} \cdot \exp(a_{14} \cdot SOC) + a_{15}, \tag{3.18}$$

$$C_{TL} = a_{19} \cdot \exp(a_{20} \cdot SOC) + a_{21}, \tag{3.19}$$

where $\{a_n, \forall n = 1...21\}$ is the set of the battery cell coefficients, which are provided in the literature [76]. The terminal voltage V_{batt} and charging/discharging energy E are given by:

$$V_{batt} = N_s \cdot V_{OC} - I_{batt} \cdot \frac{N_s \cdot R_S}{N_p} - U_{TS} - U_{TL}, \tag{3.20}$$

$$E = I_{batt} \cdot V_{batt}/1000, \tag{3.21}$$

where U_{TS} and U_{TL} represent the voltage sources of the left parallel RC branch and the right one, respectively. These values are calculated as follows:

$$\frac{dU_{TS}}{dt} = -\frac{U_{TS}}{R_{TS} \cdot C_{TS}} + I_{batt} \cdot \frac{N_s}{N_p \cdot C_{TS}}, \tag{3.22}$$

$$\frac{dU_{TL}}{dt} = -\frac{U_{TL}}{R_{TL} \cdot C_{TL}} + I_{batt} \cdot \frac{N_s}{N_p \cdot C_{TL}}. \tag{3.23}$$

In this work, the full model of the equivalent circuit is used to accurately estimate battery states through system simulation. However, in the proposed optimization problem, the modified version of the model is employed to reduce computation time while achieving efficient battery operation. A detailed explanation of the modification is described in the following sections.

3.4 Formulation of Proposed Optimization Flow

This section shows the formulation of a multi-time scale optimization problem. First, an optimization flow and a detailed mathematical formulation of the proposed framework are described.

3.4.1 Overview of Control Flow

The proposed framework aims to reduce electricity costs by finding the most efficient schedules for a smart PV system. The solution includes schedules of shiftable appliances, a battery system, and purchased energy from the grid. As previously noted in Section 3.3.3, the framework consists of a multi-time scale structure that follows an MPC approach.

The block diagram in Fig. 3.7 illustrates the control flow in the proposed multi-time scale framework. Multiple optimization problems are solved at every interval of Δt. First, the coarse-grained time scale treats two optimization problems with respect to shiftable appliances and a battery system. These are the appliance scheduling (AS) stage and the coarse-grained energy management (CGEM) stage. The AS problem determines the schedule for shiftable appliances that can be moved to a different time. The CGEM problem calculates the reference points of the battery system using the obtained appliance schedule as input. The equivalent circuit battery model is integrated into CGEM to reduce battery energy loss. The planning period of AS and CGEM should still be long to incorporate daily variations in energy profiles and appliance periodic.

Second, the fine-grained time scale treats the rapid PV fluctuation and the transient responses in the battery system. The fine-grained energy management (FGEM) problem is run using the solution from the coarse-grained optimization and the short-term PV forecasting described in Section 3.3.4. The obtained schedules, including precise battery charge/discharge, are applied to the system directly. Also, the system performance is evaluated by simulating the system behavior using the obtained solution and the battery model. The detailed formulations of AS, CGEM, and FGEM are given in the following sections.

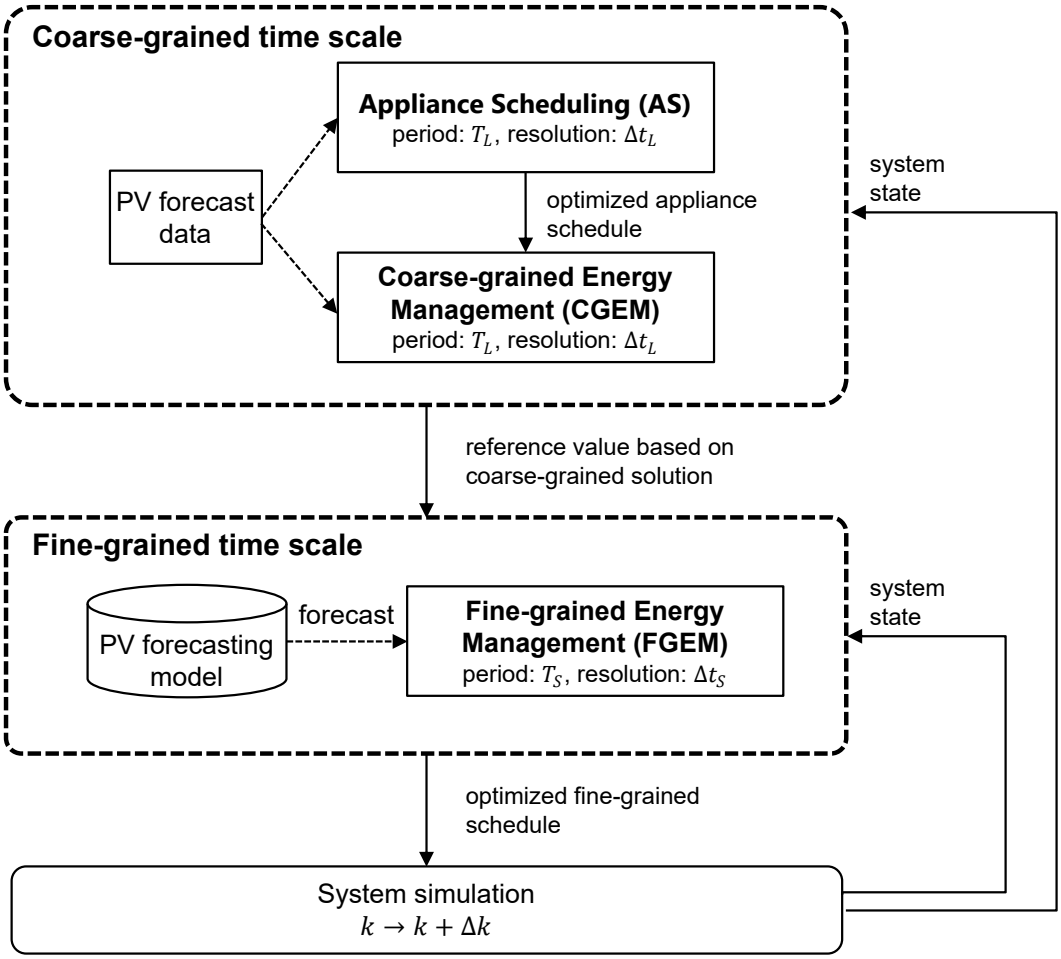

Figure 3.7: Block diagram of control flow in proposed multi-time scale framework.

3.4.2 Appliance Scheduling

Since the AS problem focuses on the coarse-grained time scale, the planning period is T_L with the resolution Δt_L. The AS is a MIP-based optimization problem due to some binary variables for appliance scheduling. The following is the mathematical

formulation of the AS:

$$\begin{aligned}
&\text{minimize} && \sum_{t_L=1}^{T_L} \xi_{t_L} \cdot S_{t_L}, && (3.24)\\
&\text{subject to} && (3.1)-(3.13),(3.21),\\
&\text{input}\\
& && \{G_{t_L}, D_{t_L}^{base}, \xi_{t_L}\},\ \forall t_L\\
&\text{decision variables}\\
& && \{S_{t_L}, Y_{t_L}, I_{batt,t_L}, q_{m,p,t_L}, r_{m,p,t_L}\},\ \forall m,p,t_L
\end{aligned}$$

where ξ_{t_L} represents the electricity price from the power company. It should be noted that the non-linear part of the equivalent circuit model is omitted to avoid mixing integer variables and non-linear equations and reduce computational complexity. Specifically, the variable for the terminal voltage V_{batt} is fixed to the constant nominal value, and the equations (3.14)-(3.19), (3.22), and (3.23) are removed. This means that the transient response and complex I-V characteristics are omitted in the AS. However, the following CGEM recalculates the battery schedule incorporating the non-linear part of the equivalent circuit model. The objective function is minimizing electricity costs. The obtained solution of the AS contains the schedules for the shiftable appliances, the purchased energy, the battery system, and the wasted energy. Only the solution of the shiftable appliances, $D^{shft}t_L$ and qm,p,t_L, is applied to the system. The rest solutions are discarded, and the following problems recalculate them.

3.4.3 Coarse-Grained Energy Management

The CGEM refers to the outer loop for the battery scheduling using the same time scale as the AS. The non-linear part of the battery model is integrated into the CGEM problem. Still, the capacitances C_{TS} and C_{TL} are removed since their time constants are very fast: 20 s to 4 min, and it is useless to consider them in the longer time scale. The values of resistances are aggregated as the total resistance R_{total}, as given by:

$$R_{total} = R_S + R_{TS} + R_{TL}, \tag{3.25}$$

$$V_{batt} = N_s \cdot V_{OC} - I_{batt} \cdot \frac{N_s \cdot R_{total}}{N_p}. \tag{3.26}$$

The CGEM is a non-linear programming (NLP) problem because it includes the non-linear equations (3.14) - (3.17). The CGEM's formulation is finally described as

follows:

$$\begin{aligned}
&\text{minimize} && \sum_{t_L=1}^{T_L} \xi_{t_L} \cdot S_{t_L}, && (3.27)\\
&\text{subject to} && (3.1)-(3.3),(3.12)-(3.17),(3.21),(3.25),(3.26),\\
&\text{input}\\
&&& \{G_{t_L}, D_{t_L}^{base}, D_{t_L}^{shft}, \xi_{t_L}\},\ \forall t_L\\
&\text{decision variables}\\
&&& \{S_{t_L}, Y_{t_L}, I_{batt,t_L}\},\ \forall t_L
\end{aligned}$$

where the objective is the same as that of the AS, i.e., electricity cost minimization. The solution of the CGEM includes the schedules for the battery system, the purchased energy, and the wasted energy. It is worth noting that the battery schedule obtained by the CGEM is more practical than that of the AS, as the CGEM incorporates the non-linear effect of the battery system, which is omitted in the AS problem.

To further refine the battery schedule in FGEM, the reference values for battery energy E^{ref} are set based on the obtained solution, as given by:

$$E^{ref} = \frac{1}{1000} \cdot I_1^{batt} \cdot V_1^{batt} \cdot \frac{\Delta t_S}{3600}. \tag{3.28}$$

Using E^{ref} as reference working points, the following FGEM calculates the fine-grained battery schedule preventing a greedy solution, e.g., anyway discharging or charging the battery system based on current renewable generation.

3.4.4 Fine-Grained Energy Management

The FGEM refers to the inner loop for the battery system to compensate for high fluctuations in PV generation. The planning period should be short such as 15 min, denoted by T_S. To be consistent with the coarse-grained time scale, the period T_S should be the same as the resolution of the coarse-grained time scale Δt_L

In FGEM, the appliance schedule obtained from AS is used as input $D_{t_S}^{shft}$. Apart from the AS and CGEM, the FGEM introduces the full equations of the equivalent circuit to consider fast battery dynamics. Besides, the trajectory of the battery output should keep a similar curve to the solution of the coarse-grained time scale to capture the daily change in demand and PV generation. Therefore, using the reference value E^{ref}, the outputs of the battery charge/discharge are constrained by:

$$E_{t_S} - E^{ref} \leq \varepsilon \cdot |E^{ref}|,\ \forall t_S \tag{3.29}$$

where ε represents the acceptable error from E^{ref}, and its typical value is 5%.

The FGEM is an NLP problem since it includes the non-linear parts of the battery model. Finally, the mathematical formulation of the FGEM is given by:

$$\begin{aligned}
&\text{minimize} && \sum_{t_S=1}^{T_S} \xi_{t_S} \cdot S_{t_S}, && (3.30)\\
&\text{subject to} && (3.1)-(3.3),(3.12)-(3.23),(3.29),\\
&\text{input}\\
& && \{G_{t_S}, D_{t_S}^{base}, D_{t_S}^{shft}, \xi_{t_S}, E^{ref}\},\ \forall t_S\\
&\text{decision variables}\\
& && \{S_{t_S}, Y_{t_S}, I_{batt,t_S}\}.\ \forall t_S
\end{aligned}$$

The objective function is minimizing electricity costs, the same as other problems. The solution to the FGEM involves determining the optimal schedule for the battery, as well as calculating the purchased energy and the wasted energy.

The proposed framework applies the optimal solutions to the targeted system. It uses a complete equivalent circuit model to simulate the actual behavior of the battery for the system simulation. It is worth mentioning that simulating the battery system is a crucial step in the actual implementation, as the internal state of the battery is not directly measurable. The simulation step helps to understand the battery's SOC and transient responses.

3.5 Simulation Experiments

This section conducts key simulation experiments with practical assumptions to demonstrate the efficacy of the proposed framework. The experimental setup is first outlined, and the parameter effect of the proposed method is explored. Additionally, the effect of the battery size and PV forecasting error on performance is investigated. Finally, the performance comparison regarding electricity costs with other baseline methods is performed.

3.5.1 Simulation Setup

For all simulation experiments, the simulation period is set to ten days starting at midnight. The parameters of the proposed method are outlined below. The coarse-grained time scale encompasses a 24 h planning period ($T_L = 96$ [900s]) with a 15 min resolution ($\Delta t_L = 900$ [s]). Besides, the fine-grained time scale covers a 15 min planning period ($T_S = 900$ [s]) with a 1 s resolution ($\Delta t_S = 1$ [s]). The commercial solver CPLEX v20.1 is used to solve the AS which is the MIP optimization problem. Also, the open-source NLP solver IPOPT v3.14 [99] is employed to solve the CGEM and FGEM which are

Table 3.1: Parameters settings of battery system.

Description	Symbol	Value
Initial SOC	SOC^{init}	0.5 (50%)
Terminal SOC	SOC^{term}	0.5 (50%)
Min. SOC	$\underline{SOC}$	0.2 (20%)
Max. SOC	$\overline{SOC}$	1 (100%)
Min. current	$\underline{I_{batt}}$	$-0.5 \cdot C_{nom}$ (50% of capacity)
Max. current	$\overline{I_{batt}}$	$0.5 \cdot C_{nom}$ (50% of capacity)
Number of series cells	N_s	25
Number of parallel cells	N_p	191
Nominal voltage	V_{cell}	4.1 [V]
Nominal capacity	C_{cell}	0.85 [Ah]
Battery capacity	-	15 [kWh]

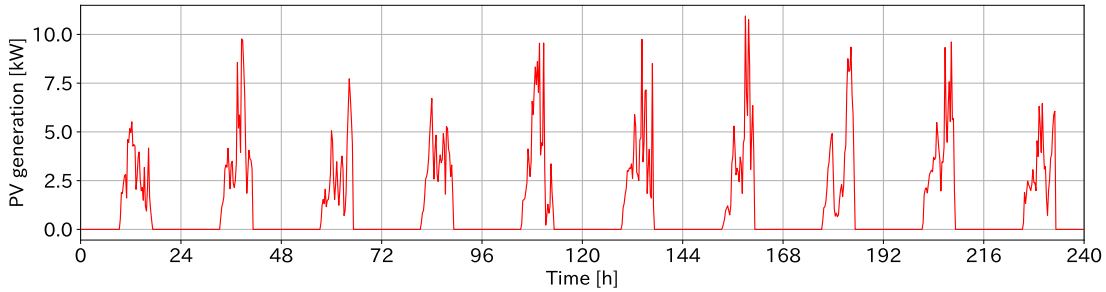

Figure 3.8: PV generation used in simulation, measured at University of Oldenburg from June 18 to July 27.

NLP problems. The computing platform is a modern laptop with 16 GB of DDR3 RAM and a two-core Intel Core-i7 6600U CPU, 2.60 GHz.

The parameters of the battery system are listed in Table 3.1. The coefficients $\{a_n, \forall n = 1...21\}$ are sourced from the literature [76]. The acceptable error of the battery output between the CGEM and FGEM, ε, is set to 5%. A time-of-use (TOU) price commonly used in Japan is used as input: 21.66 ¥/kWh (7 a.m. - 11 p.m.) and 10.7 ¥/kWh (11 p.m. - 7 a.m.) [100].

The PV generation was measured and collected with a resolution of 1 s from June to July 2015 at the University of Oldenburg [75]. From these periods, June 18 to 27, i.e., ten days, are chosen as input for the simulation, as shown in Fig. 3.8. Moreover, to simulate a 15 kWp PV system, the PV generation profiles are amplified by a constant value. It is worth noting that the weather during the simulated days was mostly cloudy. On cloudy days, PV generation tends to fluctuate significantly, making PV forecasting especially challenging. Therefore, high forecasting errors can be expected in this simulation, which represents a worst-case scenario and shows the worst-case performance

Table 3.2: Parameters for smart appliances, washing machine, tumble dryer, and dishwasher.

Appliance	Total energy	Operating time	Configuration time	Shiftable time
Washing machine	0.22 kWh	45 min	8 a.m. - 10 a.m.	7 h
Tumble dryer	1.86 kWh	75 min	8 a.m. - 10 a.m.	7 h
Dishwasher	1.88 kWh	75 min	12 p.m. - 15 p.m.	8 h

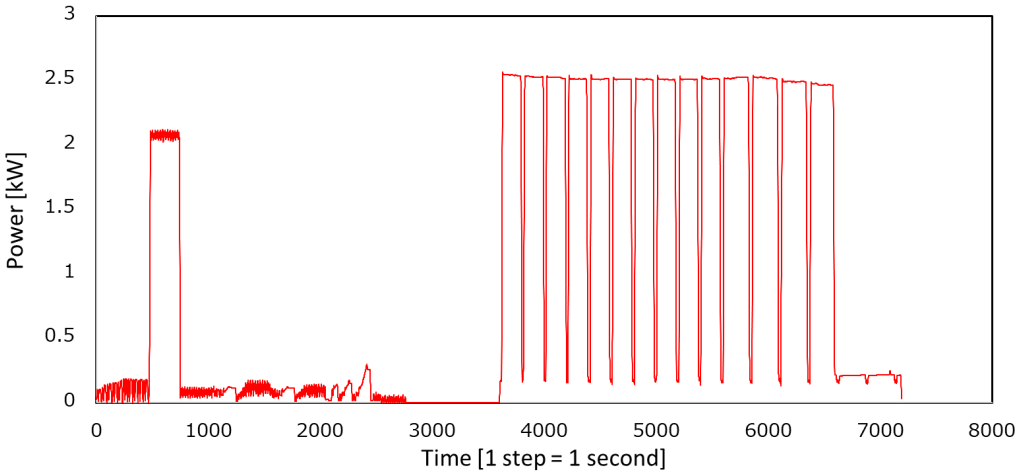

Figure 3.9: Power profiles of washing machine (- 3000 s) and tumble dryer (3000 - 7500 s).

of the proposed method. As for PV forecasting, the PV nowcasting model [75] is used to get the fine-grained PV generation forecasts, which exhibit an average forecasting error of 12% even under cloudy conditions. Since this work does not include a specific forecasting model for the coarse-grained time scale, the coarse-grained PV forecast is manually produced by adding Gaussian-distributed errors to the measured profiles, with an average error of 20%.

The demand profiles of non-shiftable appliances are derived from the Dutch Residential Energy Dataset (DRED) [101], which was collected at a 1 s resolution from July to December 2015. For the purposes of simulation, demand profiles over ten days are extracted from the DRED ranging from July 5 to 14. Also, these are scaled up by a constant value, with the mean daily consumption of non-shiftable appliances set to 50.1 kWh. The parameters of the shiftable appliance are detailed in Table 3.2, with three types of shiftable appliances (dishwashers, washing machines, and tumble dryers) each operated once daily. There are four appliances of each type, totaling twelve shiftable appliances. The configuration time is randomly generated within the range specified in Table 3.2. The deadlines are determined by the shiftable time plus the configuration time. The dataset [102] provides the power profiles of the shiftable appliances with 1

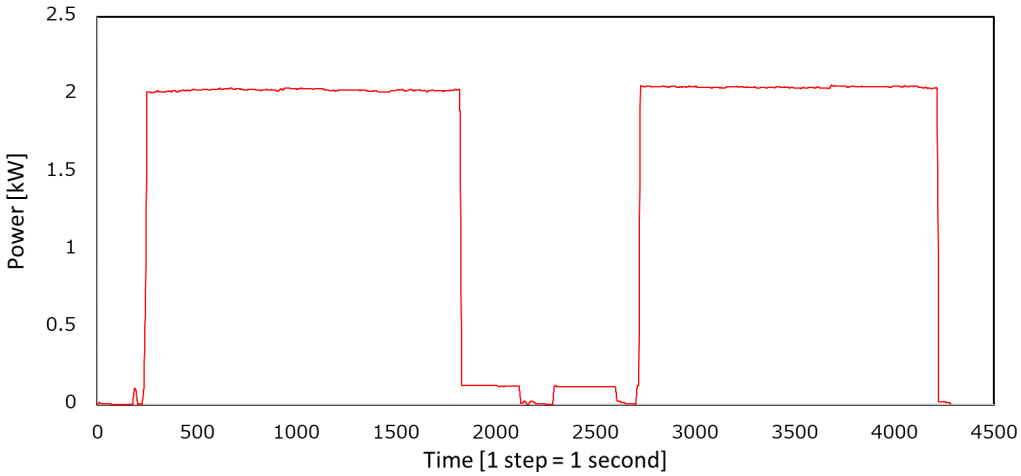

Figure 3.10: Power profiles of dishwasher.

s resolution, with representative examples of the washing machine, tumble dryer, and dishwasher shown in Fig. 3.9 and Fig. 3.10, respectively.

3.5.2 Results

Comparison with Baseline Scheduling Methods

In order to evaluate the efficacy of appliance and battery scheduling, this section compares the proposed framework to several baseline methods, described as follows:

1) **Using Shiftable Appliances As Soon As Possible (ASAP):** Shiftable appliances are not scheduled through optimization. When their configuration time arrives, the appliances are immediately turned on. The schedules of the battery system are optimized by the CGEM and FGEM.
2) **No Battery Scheduling (NBS):** The CGEM and FGEM are excluded from the proposed method. Only AS stage is employed, and the battery system follows the fixed schedule, charging at a constant C-rate of 10% from 11 p.m. - 7 a.m. and discharging at a constant C-rate of 5% from 7 a.m. - 11 p.m.
3) **ASAP-NBS:** This method combines ASAP and NBS, and therefore no optimization problem is solved.

Table 3.3 presents the results of electricity costs for ten days and the improvement rates of the proposed framework compared to the other methods. The proposed framework achieved the lowest electricity cost of all methods, with a maximum improvement rate of 48.1%. Appliance scheduling can help to fill the energy gap between generation and demand, leading to reduced electricity costs. Battery scheduling is also a significant factor in reducing electricity costs. When the battery system is charged and discharged at a constant current like in the NBS method, the battery system is unable to maintain

Table 3.3: Electricity cost and its improving rates of proposed method within ten days compared to three methods, ASAP, NBS, and ASAP-NBS.

Method	Proposed	ASAP	NBS	ASAP-NBS
Electricity cost within ten days [¥]	3004	3319	4408	5784
Improving rate of electricity cost of proposed	-	9.5%	31.9%	48.1%

Table 3.4: Electricity cost and computational time for different lengths of planning period.

Planning period [h]	Electricity costs [¥]	Computational time [s]		
T_L		AS	CGEM	FGEM
6	3194	0.95	0.19	3.11
12	3106	1.63	0.27	3.03
24	3004	4.32	0.43	3.51
36	3044	8.65	0.63	3.12
48	3055	17.59	0.94	3.24

the balance between renewable generation and demand, resulting in increased power purchase to meet energy demand.

Effect of Planning Period on Coarse-Grained Time Scale

In this section, the effect of the planning period on the coarse-grained time scale was investigated. For the proposed method, the planning period T_L is changed from 6 to 48 h.

Table 3.4 shows the electricity costs within ten days and the average computational time for each optimization problem. As can be seen in the table, electricity costs decrease for the first 24 h of the planning period but increase when the planning period exceeds 24 h. This is due to changes in the solution of the battery schedule for the 36 and 48 h planning periods. The end state of the battery's SOC after a ten-day simulation is 53.1% when using a 24 h period. However, it is 65.1% and 65.8% when using 36 and 48 h planning periods, respectively. That means that when using a longer input, the remaining energy in the battery also increases. When the 36 and 48 h period is chosen, some shiftable appliances of the last day are shifted outside the evaluation period. Whereas, employing 24 h periods allows these appliances to be scheduled within the same day.

Moreover, the computational time increases as the planning period become longer. In the case of the 48 h planning period, the computational time for the AS problem significantly increases due to the need to schedule more smart appliances. However, the sum of computational times is much less than the length of the time resolution

Table 3.5: Average AS's computational time for different numbers of smart appliances.

Shiftable appliances per day	Computational times of AS [s]
6	2.13
12	4.32
18	6.67
24	8.79
30	10.39

$\Delta t_L = 900$ [s], making the proposed framework applicable for all simulated planning periods. The planning period of 24 h is the most efficient in this case study, achieving good performance in terms of both computational complexity and solution quality.

Effect of Number of Smart Appliances

Next, the impact of the number of smart appliances on computational time was examined. The number of each type of smart appliance was increased from 2 to 10, resulting in a total of 6 to 30 appliances.

Table 3.5 shows the average computational time for each optimization problem, which increases with adding more appliances. However, the computational time remains appropriately short, as it consistently meets the requirements of $\Delta t_L = 900$ [s]. Thus, the proposed framework can be applied to a smart PV system comprising multiple buildings and up to 30 or more smart appliances.

Effect of PV Forecasting Error and Battery Size

In this section, the system performance under different battery sizes and PV forecasting errors was analyzed. Various coarse-grained forecasts of PV generation were employed, with an average forecasting error of 20%, 30%, or 40%. As for the fine-grained time scale, two different schemes were compared, including energy forecasting [75] and power forecasting, also presented in [75]. The average forecasting error for the 15 min periods of energy and power forecasting was 12% and 20%, respectively. In addition, assuming that the PV forecast method works ideally, the method with a forecasting error of 0% is employed as the perfect forecasting. The battery capacity was also changed from 3 to 18 kWh to investigate the sizing effect.

Fig. 3.11 shows the electricity costs within ten days with different PV forecasting errors and battery capacities. The values of the electricity costs are given in Table 3.6. The black line in Fig. 3.11 represents the electricity costs in the case of perfect forecasting. The blue and red lines indicate the results of power and energy forecasting, respectively. As shown by these results, the electricity costs are not significantly improved, when the battery capacity is larger than 12 kWh. This is because the errors in

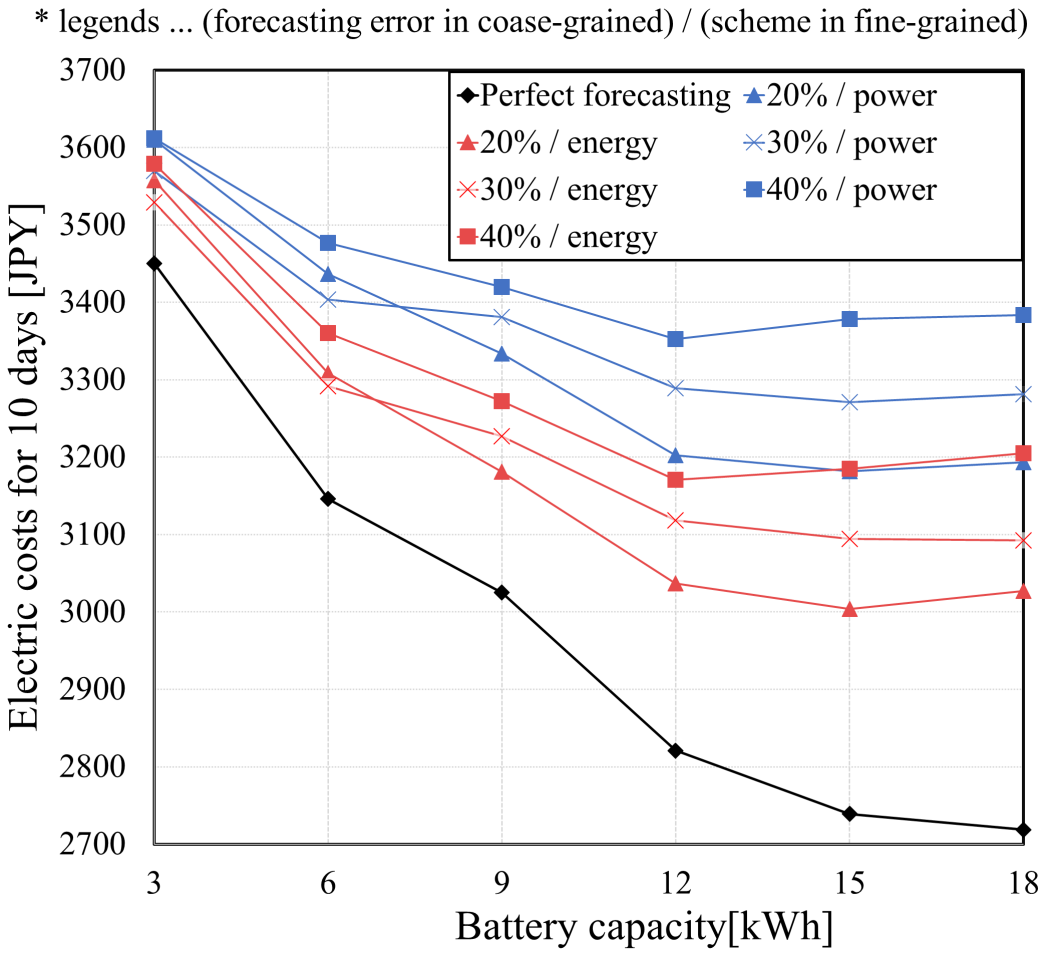

Figure 3.11: Electricity costs within ten days for different scenarios of PV forecasting errors and different battery capacities.

misinterpreting future PV generation profiles impact the performance greatly as the battery size increases. In other words, the wrong battery operation due to PV forecasting error outweighs the effect of reduced electricity costs by large battery capacity. From the perspective of expensive initial costs, it is not advisable to choose a larger battery size.

The forecasting error for the coarse-grained time scale has a significant impact on electricity costs. Specifically, the smaller the forecasting error, the lower the electricity costs. The coarse-grained forecasting error has little effect on the electricity costs when the battery capacity is 3 or 6 kWh. However, when the battery capacity is larger than 9 kWh, the gap in electricity costs between different errors widens. Besides, the effect of fine-grained PV forecasting errors on electricity costs is greater than the coarse-grained ones. A 10% improvement in the fine-grained forecast errors can lead to a 30 - 50%

Table 3.6: Electricity cost values in ¥with different PV forecasting errors and battery capacities.

Battery capacity [kWh]	Perfect forecasting	Forecasting scheme for coarse-grained					
		Energy forecasting (error <12%)			Power forecasting (error <20%)		
		Forecast error for fine-grained			Forecast error for fine-grained		
		20%	30%	40%	20%	30%	40%
3	3450	3558	3529	3579	3610	3570	3612
6	3146	3309	3292	3360	3437	3404	3477
9	3025	3181	3227	3272	3334	3381	3420
12	2821	3037	3118	3171	3202	3289	3353
15	2739	3004	3094	3185	3182	3271	3379
18	2719	3027	3092	3205	3193	3281	3384

reduction in battery size to achieve the same amount of the electricity costs. Thus, the accuracy of the forecasting scheme for the fine-grained time scale is a crucial factor in the system performance of EMS.

Effect of Multi-Time Scale Structure

To determine the necessity of the multi-time scale structure, the proposed framework was compared to two single-time scale methods:

1) **Only Coarse-grained Optimization (OC):** AS and CGEM in the coarse-grained time scale are only executed. The solution is directly applied to the system without solving FGEM. OC has 24 h planning period with 15 min resolution.
2) **Only Fine-grained Optimization (OF):** FGEM in the fine-grained time scale is only executed. The smart appliances are operated as soon as possible similar to the ASAP method, and CGEM is removed. OF has 15 min planning period with 1 s resolution.

Note that the parameters of OC and OF, i.e., the planning period and the time resolution, are determined based on the characteristics of the available PV forecasting methods. As mentioned in Section 3.3.3, the accuracy of long-term PV forecasting is worse when time resolution is less than minutes (e.g., 5 min) [94]. On the other hand, short-term PV forecasting based on a sky image and physics-based model can provide accurate profiles with 1 s resolution; however, when the forecasting period is over 15 min, the forecasting accuracy is rapidly degrading [75]. To align the target time scales for each PV forecasting approach and perform the comparative experiment under the realistic assumption, the parameters of OC and OF are set as above.

Table 3.7 presents the results of the electricity costs for ten days and the improvement rate of the proposed method compared to OC and OF. The proposed framework achieved the best performance, with a maximum improvement rate of 47.5% in electricity costs. This demonstrates the effectiveness of the multi-time scale structure in

Table 3.7: Comparison of electricity cost and its improving rate for proposed method, OC, and OF.

Method	Proposed	OC	OF
Electricity cost for ten days [¥]	3004	3183	5717
Improving rate of electricity costs of Proposed	-	5.6%	47.5%

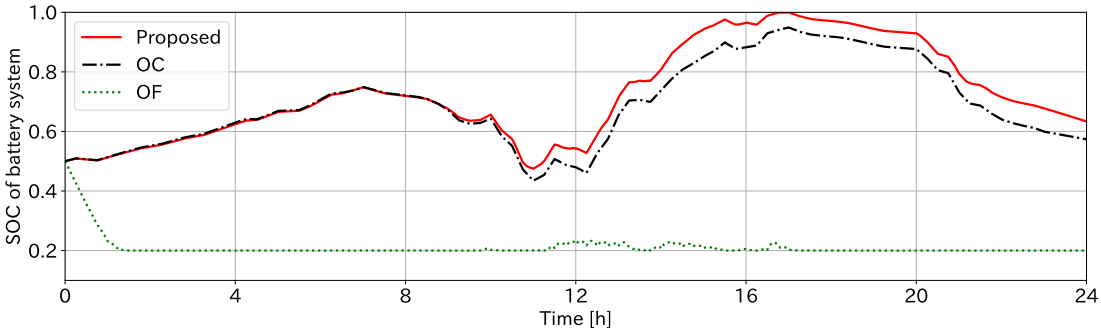

Figure 3.12: SOC profiles of June 18 for three methods, Proposed, OC, and OF, with 15 kWh battery system.

reducing electricity costs.

Figs. 3.12 and 3.13 show the results of the SOC profiles and the battery power profiles for the same day. OF clearly demonstrates myopic optimization, meaning that the battery system is discharged to reduce electricity costs as long as there is still energy remaining inside the battery. Since OF only knows about the upcoming 15 min (T_S) without the coarse-grained time scale, its solution is not optimized for long-term changes in PV generation and demand load. In comparison to the proposed method and OC, the proposed method reaches a higher SOC level. Although OC provides a solution that accounts for long-term changes in energy profiles, accumulated errors in PV fluctuation at the fine-grained time scale result in fewer opportunities to charge the battery with PV generation. Furthermore, the battery solution of the proposed framework not only considers the long-term changes by following the reference values of the coarse-grained time scale but also compensates for the fast PV fluctuations by solving FGEM with fine-grained PV forecasting data. Overall, the multi-time scale structure leads to better performance in energy management.

The proposed framework primarily focuses on the fast and slow dynamics of PV generation and a battery system. Though energy demand is also highly volatile, its time scales are of many minutes and distinct from the time scales of PV generation and a battery system. Consequently, fluctuations in energy demand can be absorbed in the coarse-grained optimization loop of the multi-time step approach. As simulation results

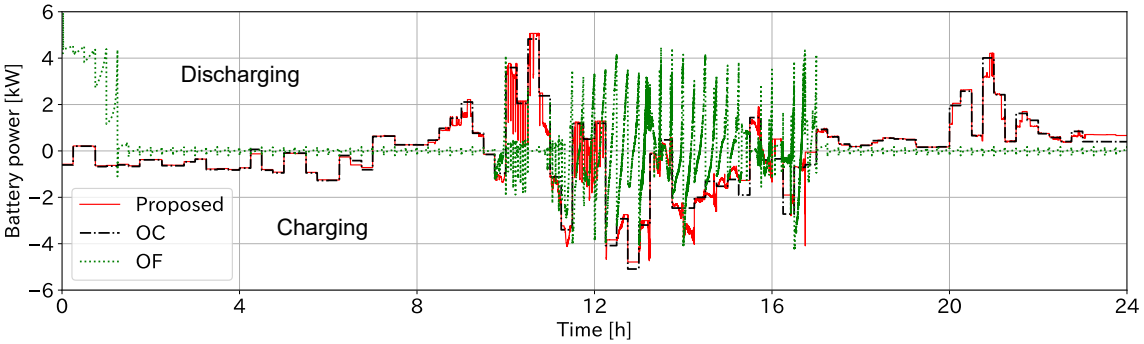

Figure 3.13: Battery power profiles of June 18 for three methods, Proposed, OC, and OF, with 15 kWh battery system; Positive value represents discharging, otherwise charging.

indicate, the quick response of battery charging and discharging enables the system to effectively manage energy demand fluctuations.

3.6 Summary

This chapter has presented a multi-time scale energy management framework for a smart photovoltaic (PV) system. A model predictive control (MPC) strategy with PV generation forecasting as input is adopted to address highly fluctuating PV generation. Furthermore, the proposed framework employs a multi-time scale structure comprising coarse-grained and fine-grained time scales. As for the coarse-grained time scale, the schedules of smart appliances are optimized to move their operating time, and the battery outputs are also optimized to handle daily changes in the energy balance. For the fine-grained time scale, the schedule of the battery system is fine-tuned by incorporating an accurate battery model and fine-grained PV forecasting model. Finally, the proposed framework solves three optimization problems internally connected, which take into account fast and slow system dynamics. Simulation results show that the proposed framework can reduce electricity costs under various scenarios by up to 47.5% compared to baselines. Additionally, the impact of PV forecasting error and battery capacity on the performance of the proposed framework is also analyzed. If an accurate PV forecasting model were integrated, electricity costs could be significantly reduced, even with a small battery system. In summary, the proposed framework affords EMS with real-time control capabilities, resulting in a solution that is highly accurate and enables a reduction in the size of an expensive battery system.

Further work related to this chapter involves extending the proposed framework to incorporate heat ventilation and air conditioning (HVAC) systems. A multi-objective optimization will be investigated to minimize system cost and maximize user comfort. The first step of this expansion is proposed and discussed in Chapter 4.

In future work, more types of demand and renewable energy should be explicitly

considered in the framework. For instance, electric vehicles (EVs) are critical energy components that need to be optimized since they have high capacity and potentially great flexibility. Meanwhile, wind power is promising renewable energy as well as solar power. To minimize system costs and enhance decarbonization, the characteristics of these additional resources should be considered in the optimization. On the other hand, this work does not consider the workload-dependent battery dynamics such as degradation and complex SOC changes. The time constant of such battery dynamics is generally minute-level, which is longer than the 1 s resolution that the fine-grained time scale employs. Integrating battery dynamics into the short-term time scale will not be effective because of the high complexity and the need for a longer planning period more than 15 min. It is also not suitable to integrate it into the long-term time scale due to inconsistency with the time constants of the demand load scheduling. The latter requires a much longer planning period (8 - 24 h), and its time constant is even larger than that of the battery dynamics. Hence, developing a mid-term (semi-fine-grained) time scale, which covers more than one hour period with a minute resolution, would efficiently improve the solution quality of the battery scheduling without computational complexity increase.

Chapter 4

Comfort-Aware Electrical and Thermal Energy Management Framework

In the building sector, heating, ventilation, and air-conditioning (HVAC) systems occupy a significant portion of end-use energy consumption. The reduction of HVAC operations will reduce electricity costs greatly; however, it suffers the thermal comfort of occupants in the building. The consideration of both electricity costs and thermal comfort is required in EMS. This chapter presents an electrical and thermal energy management framework for smart buildings[1]. The objective of the proposed framework is to improve the trade-off relationship between electricity costs and thermal comfort. This chapter extends the online energy management framework proposed in Chapter 3 to consider HVAC scheduling and thermal comfort. The equivalent circuit model to represent the building thermal part and HVAC coefficient of performance (COP) model is introduced. In addition, to estimate optimal temperature set points for maximizing thermal comfort, the proposed framework integrates a low-complexity thermal comfort estimator. The simulation results show that the proposed framework can find a solution that improves both electricity costs and thermal comfort compared to baseline methods.

4.1 Motivation and Objective

Heating, ventilation, and air-conditioning (HVAC) systems account for a significant proportion ($> 40\%$) of a building's energy consumption [104]. To reduce the electricity costs of buildings, smarter management and scheduling of HVAC systems are required. However, the HVAC systems also affect the thermal comfort of the occupants due to

[1]This chapter is a refined and reproduced version of the paper to be published in IEICE Transactions on Fundamentals of Electronics, Communications and Computer Sciences [103] copyrighted by IEICE.

indoor climate change, which influences their productivity and health. Therefore, the main concern of HVAC management is how to reduce electricity costs and maximize thermal comfort simultaneously.

In contrast, an energy management system (EMS) that optimizes photovoltaic (PV) generation, a battery system, and appliances is promising for realizing efficient energy utilization [63]. The EMS coordinately manages these components and provides essential functions for the cost-effective utilization of renewable generation. Easy access to weather forecasts, demand load, and PV generation through the internet of things (IoT) enables the EMS to serve as the main core of the energy infrastructure that satisfies occupants' preferences in real-time. Moreover, thermal comfort can be managed by the EMS that schedules HVAC systems.

Combining the HVAC scheduling and the EMS can reduce electricity costs while maximizing thermal comfort. For example, if occupants are not in the building, the HVAC system can be stopped to reduce electricity costs. Besides, PV generation can meet HVAC demand during sunny daytime. Once a battery system is charged, the flexibility of HVAC control is greatly enhanced by discharging the battery without increasing energy consumption. In this way, co-scheduling all energy subsystems, including PV panels, battery storage systems, and HVAC systems, is a promising solution.

This chapter develops a comfort-aware electrical and thermal energy management framework for a smart building by extending the framework proposed in Chapter 3. The framework proposed in Chapter 3 employs a multi-time scale model predictive control (MPC) to schedule a battery system and shiftable appliances with PV generation forecasts. However, this work only focuses on the electrical part, and its objective is only to minimize electricity costs. In the real system, thermal comfort should be considered for occupant satisfaction. To address this issue, the proposed framework optimizes the HVAC schedule and other energy sources. The building's thermal dynamics and HVAC system are mathematically formulated as the optimization problem. In addition, a thermal-comfort estimation model proposed in [105] is introduced to predict optimal temperature set points. The objective of the proposed method is to minimize electricity costs and maximize thermal comfort simultaneously. The simulation results show the effectiveness of the proposed framework in terms of improving the trade-off relationship between electricity costs and thermal comfort.

The main contributions of this work are shown below:

- The thermal dynamics of a building are modeled by an equivalent circuit model, and an interaction between the electrical and thermal parts is formulated.
- Thermal-comfort estimation model is introduced to predict optimal indoor temperature set points for thermal-comfort maximization.
- A multi-objective function is defined to minimize electricity costs and maximize thermal comfort simultaneously.
- Simulation results show that the trade-off between electricity costs and thermal comfort obtained by the proposed framework is superior to that of the baseline

method.

The remainder of this chapter is structured as follows. Section 4.2 reviews relevant literature on HVAC management. Section 4.3 explains the proposed framework with the extension for building thermal and HVAC management. Section 4.4 presents a mathematical formulation of the multi-time scale optimization problem. Section 4.5 presents simulation results demonstrating the effectiveness of the proposed method, and finally, Section 4.6 summarizes this chapter and outlines future directions.

4.2 Related Works

There have been numerous studies on the scheduling of energy components in buildings. Qayyum et al. [106] proposed an optimal scheduling method based on mixed-integer linear programming (MIP) for time-deferrable appliances such as dishwashers and tumble dryers with PV generation profiles. Telouw et al. [70] developed a multi-objective MIP problem to optimize operating costs and CO_2 emissions through the scheduling of both electrical and thermal energy storage. Duman et al. [107] also formulated a MIP-based home EMS to optimize the schedule of PV generation, electric vehicles, batteries, HVAC systems. Their approach can minimize system costs and maximize thermal comfort in the day ahead manner. However, these day-ahead approaches can result in unexpected cost increases due to uncertainties such as load demand and renewable energy in real-time. In addition, thermal conditions, such as indoor temperature and humidity, can also change due to external disturbances that are difficult to predict before the day. Real-time optimization is, therefore, necessary to manage HVAC systems.

Much research has been investigated on model predictive control (MPC), one of the promising schemes for HVAC management in EMS. The MPC approach iteratively computes optimal control input based on system prediction models and forecasting information at every time step. Ostadijafari et al. [108] investigated a nonlinear economic MPC for a smart building that includes HVAC systems, PV generation, flexible appliances, and a battery system. Their works goal is to minimize electricity costs under time-dependent price signals while tracking comfort temperature ranges based on occupancy information. However, they assumed that the exact value of PV generation and comfort temperature is perfectly known beforehand, even though such information should be unknown in advance. Cui et al. [109] focused on a MIP-based receding horizon approach to optimize battery and HVAC operations. They only minimized system costs composed of electricity expenses and battery degradation costs and did not consider thermal comfort. Perez et al. [110] proposed an integrated MPC scheme to minimize the peak demand by scheduling HVAC and time-shiftable appliances. Their main concern was to shave the power peak and did not take comfortable indoor temperature tracking into account. Killian et al. [111] proposed a comprehensive home EMS that includes many variables and constraints for thermal and electrical energy storage as well as appliances and PV generation. The mixed-integer quadratic programming

(MIQP)-based MPC is solved to obtain an optimal schedule with a resolution of 15 min to improve human comfort and reduce operating costs. However, these works still assume impossible situations where the amount of renewable generation is completely known in advance. In addition, they regarded the HVAC scheduling as just an energy-reduction problem without addressing thermal comfort issues: Only room temperature constraints were considered; getting to a comfortable temperature was not intended. Therefore, a comprehensive approach that incorporates predictive information for renewable generation and thermal comfort is required.

Compared to the studies mentioned earlier, the proposed framework performs both day-ahead and real-time scheduling to deal with unpredictable uncertainties and reflect the latest information of the system. Moreover, integrating the thermal comfort model, which estimates optimal temperature set points, allows the HVAC scheduling to manage thermal comfort appropriately.

4.3 Comfort-Aware Energy Management Framework

This section describes an overview of the proposed framework, detailed system models, and thermal comfort estimation model.

4.3.1 Overview of Proposed Framework

Fig. 4.1 overviews the proposed framework whose key idea is to employ an MPC approach considering a multi-time scale structure. The main development of the MPC and multi-time scale structure has been completed in Chapter 3. The overview of the framework is as follows. The proposed framework follows the MPC approach, which iterates prediction and optimization for the targeted system. In addition, two different time scales, coarse-grained and fine-grained time scales, are considered to capture fast and slow system dynamics. First, the framework obtains PV generation forecasting profiles and thermal-comfort estimation for the next day. Then, the energy subsystems, which include appliances, an HVAC system, and a battery system, are scheduled on a coarse-grained time scale for a longer period such as 24 h of a planning period with 15 min resolution. After that, a short-term scheduling loop for a battery system incorporates the solution at a fine-grained resolution for a shorter period such as 15 min of a planning period with 1 s resolution. These optimization problems are mathematically formulated and solved by an optimization solver. Finally, the obtained schedules are applied to the target system. Although Chapter 3 also proposed the online energy management framework [59], this chapter extends it to control an HVAC system with thermal-comfort estimation to minimize electricity costs and maximize thermal comfort at the same time.

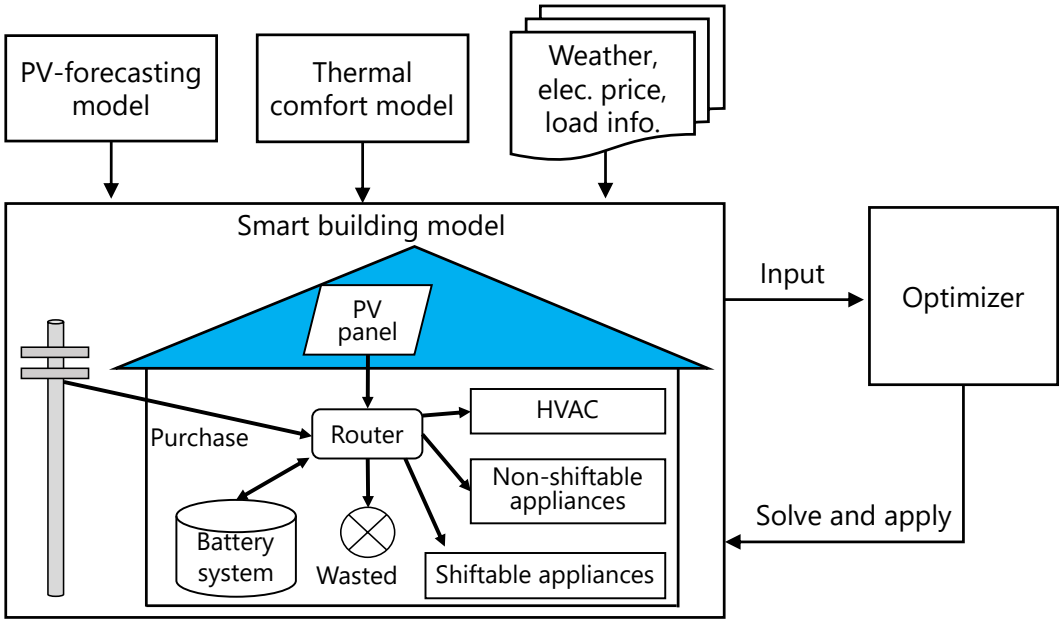

Figure 4.1: Overview of proposed online energy management framework.

4.3.2 Model Development

Smart Building Model

The targeted smart building model is illustrated in Fig. 4.1. It consists of PV panels, various appliances (both shiftable and non-shiftable), a battery system, and a HVAC system. An inverter-based control system, referred to as a power router [57, 58], manages the flow of electrical energy within the building. This model only purchases electricity from the power grid during shortages and stores excess photovoltaic generation in the battery system. If the battery is already fully charged, the excess energy is not sold to the grid but rather goes to waste. This is because allowing a reverse power flow can destabilize the grid.

PV generation forecasting

The generation of electricity from PV panels can be highly variable due to meteorological factors. Therefore, it is necessary to have a PV generation forecast in order to match energy production with demand. As previously mentioned in Section3.3.4, a PV-nowcasting model [75] has been introduced that can predict short-term generation based on sky images, neural network models, and a physics-based thermal model [97]. This model can predict power output at a resolution of one second every minute for 15 min periods, which helps to compensate for the high variability of PV generation. Additionally, a day-ahead PV forecast covering a 24 h period is also used to schedule

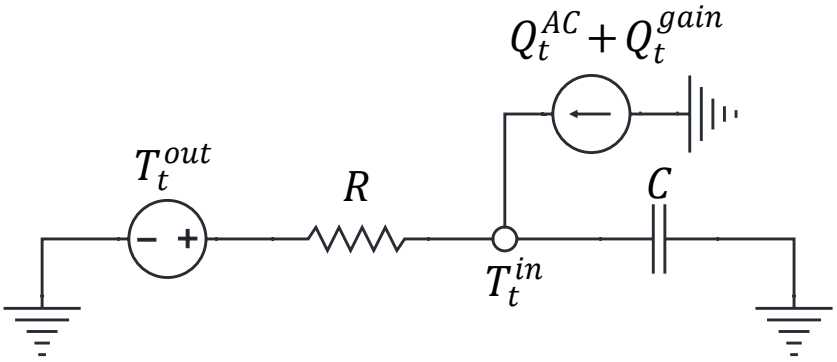

Figure 4.2: Equivalent circuit model for thermal dynamics of buildings.

battery and demand loads efficiently. These forecasts are available from meteorological information providers. Together, these two PV forecasts provide sufficient planning for online energy management.

Battery System

Similar to Chapter 3, a lithium-ion battery system with an equivalent circuit model [76] is incorporated in order to accurately predict the battery's state of charge (SOC) and nonlinear current-voltage characteristics. This model is used in both optimization and simulation to improve the accuracy of battery dynamics and reduce energy loss during charging and discharging. It also allows for a more accurate estimation of the battery's internal state.

Appliances

Two categories of appliances are considered: non-shiftable and shiftable. Shiftable appliances can be rescheduled to different times in order to minimize electricity costs. Each shiftable appliance can be characterized by four parameters [98]: (1) operating time, (2) configuration time, (3) deadline (the time by which its operation must be completed), and (4) power profiles. Shiftable appliances must be scheduled from their configuration times until their deadlines while taking into account the preferences of the occupants.

Thermal Dynamics of Building and HVAC System

In the proposed framework, the thermal dynamics of a building are modeled using a thermal equivalent circuit model [112], as shown in Figure 4.2. This model treats the thermal behavior of a building as an analogy for its electrical behavior. The characteristics of the building are represented by thermal resistance R and thermal capacity

C, which are determined based on building data sheets. The time constant τ, which represents the thermal response speed, is calculated as:

$$\tau = R \cdot C, \tag{4.1}$$

Let t be a time index. Using these parameters, the indoor temperature for the next time step, denoted by $T^{in}t+1$, can be calculated as:

$$T_{t+1}^{in} = \left(1 - \frac{\Delta t}{\tau}\right) \cdot T_t^{in} + \frac{\Delta t}{\tau} \cdot \left\{T_t^{out} - 1000 \cdot R \cdot \left(Q_t^{AC} + Q_t^{gain}\right)\right\}, \ \forall t \tag{4.2}$$

where Δt is the length of the time resolution. T_t^{out} is the outdoor temperature, Q_t^{AC} is the thermal gain due to an HVAC system, and Q_t^{gain} represents external sources of thermal gain such as internal heat and solar radiation. The relationship between the thermal power of the HVAC system and its electrical power is expressed as:

$$Q_t^{AC} = -P_{AC} \cdot COP \cdot u_t, \ \forall t \tag{4.3}$$

where P_{AC} is the rated power and COP is the coefficient of performance (COP) of the HVAC system. It is assumed that the HVAC system has an inverter that allows for continuous control of its power output from 0% to 100%. The manipulated variable u_t is introduced and scheduled in a range from 0 (0%) to 1 (100%) to control the power output of the HVAC system. The power consumption of the HVAC, D_t^{hvac}, at time t is calculated as:

$$D_t^{hvac} = P_{AC} \cdot u_t. \ \forall t \tag{4.4}$$

4.3.3 Thermal-Comfort Estimation

PMV and PPD Indices

To evaluate the thermal comfort of the building, Fanger's model [19] is utilized, which includes the predicted mean vote (PMV) and the predicted percentage of dissatisfied (PPD), both of which are commonly used in real-world applications. The PMV is an index that reflects the occupants' thermal sensations on a scale ranging from -3 (too cold) to +3 (too warm). A PMV of 0 indicates the most comfortable thermal environment for the occupants. The PMV is calculated using a nonlinear complex function based on environmental and occupant parameters such as indoor temperature, humidity, wind speed, radiant temperature, metabolic rate, and clothing insulation. Once the PMV is determined, the PPD, which is the percentage of people feeling thermal discomfort in the thermal environment, is derived using the following empirical equation [19]:

$$PPD = 100 - 95^{(-0.03353 \cdot PMV^4 - 0.2179 \cdot PMV^2)}. \tag{4.5}$$

When the PMV is 0.0, the PPD is minimized (5%), meaning that only 5% of people feel discomfort. Since the proposed framework controls the indoor temperature through HVAC scheduling, approximating Fanger's model (PMV) as a function of the indoor temperature is sufficient for real-time operation purposes.

Thermal-Comfort Estimator

To estimate the comfortable indoor temperature, a low-complexity thermal-comfort estimation technique is introduced, which has been proposed in [105]. To reduce computational time and storage requirements, their work integrated a simple linear regression (LR) model and an efficient data management method. In this work, the LR model is used to represent the relationship between PMV and indoor temperature. Since the comfortable temperature will be different for each time step, the LR model is built for each time step, as defined by:

$$PMV_t = \theta_t^0 + \theta_t^1 \cdot T_t^{in}, \ \forall t \tag{4.6}$$

where θ_t^0 and θ_t^1 are the coefficients of the LR model, and these weights are refined at every time step. Moreover, to increase the accuracy and reduce the data used to train this model, the data management method was also developed in [105]. The idea is to construct two-time scale windows, a coarse-grained and fine-grained window, for model fitting and refinement. The coarse-grained window first chooses the profiles of the last x days as a training dataset, and then, for the target time step t, the fine-grained window extracts near-term data (from $t-y$ to $t+y$ steps) from the coarse-grained dataset. The reason why the coarse-grained and fine-grained time windows are used is as follows: Fanger's factors for human conditions (e.g., metabolic rate and clothing) are almost constant for the last few days, while such environmental factors as humidity and air velocity are generally similar for a given time slot between consecutive days. Thus, the extracted data by these time windows should have a high correlation with each other, which will help to fit the LR model effectively.

Set Points Derivation

This section explains how to drive set points of indoor temperature using the LR model of PMV. An example of the fitted LR model is shown in Fig. 4.3. The PMV is fitted as the LR model (the red line) based on the historical data points shown as the black points in the figure. To control the HVAC model for thermal-comfort maximization, the optimal temperature set point and its upper/lower bounds are calculated based on the fitted LR model. When the PMV is 0, that temperature can be the most comfortable. On the other hand, according to the ASHRAE's 55 standards [113], PPD's acceptable limit is less than 10%, corresponding to a PMV of ± 0.5. Based on the model (4.6), the optimal temperature set points $T_{est,t}^{set}$ and the upper/lower bounds, denoted by $T_{est,t}^{upper}$ / $T_{est,t}^{lower}$, are obtained as follows:

$$T_{est,t}^{set} = -\theta_t^0/\theta_t^1, \ \forall t \tag{4.7}$$

$$T_{est,t}^{upper} = \left(-\theta_t^0 + 0.5\right)/\theta_t^1, \ \forall t \tag{4.8}$$

$$T_{est,t}^{lower} = \left(-\theta_t^0 - 0.5\right)/\theta_t^1. \ \forall t \tag{4.9}$$

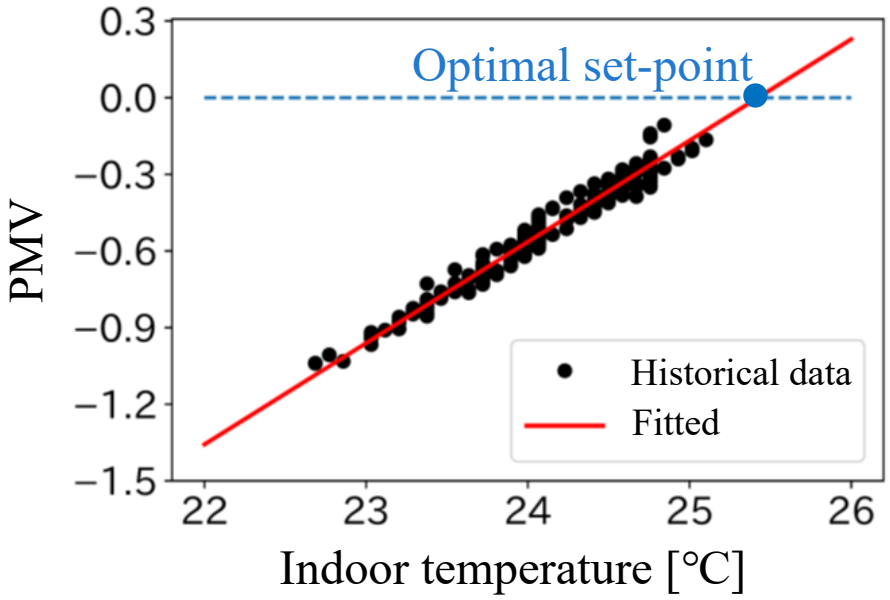

Figure 4.3: Example of linear regression between PMV index and indoor temperature.

These values are used in the objective function and in the constraints of the optimization problem.

4.4 Mathematical Formulation of Comfort-Aware Electrical and Thermal Energy Optimization

This section mathematically formulates an optimization problem for energy management that includes a thermal part of the building. Note that this framework is an extended version of the multi-time scale energy management framework proposed in Chapter 3 for thermal and comfort optimization. Hence, please refer to Section 3.4 for a detailed explanation of the multi-time scale structure and the mathematical formulation.

4.4.1 Overview of Control Flow

Fig. 4.4 shows the proposed framework's comfort-aware multi-time scale optimization flow. It consists of multiple optimization stages for each purpose, considering two different time scales: coarse-grained and fine-grained. This allows simultaneous consideration of long- and short-term system dynamics, reducing computational complexity while maintaining high solution quality. This framework also employs an MPC approach, as mentioned in Section 4.3, to consider the latest system states and handle forecast errors. Its feedback structure has the potential to compensate for uncertainty in

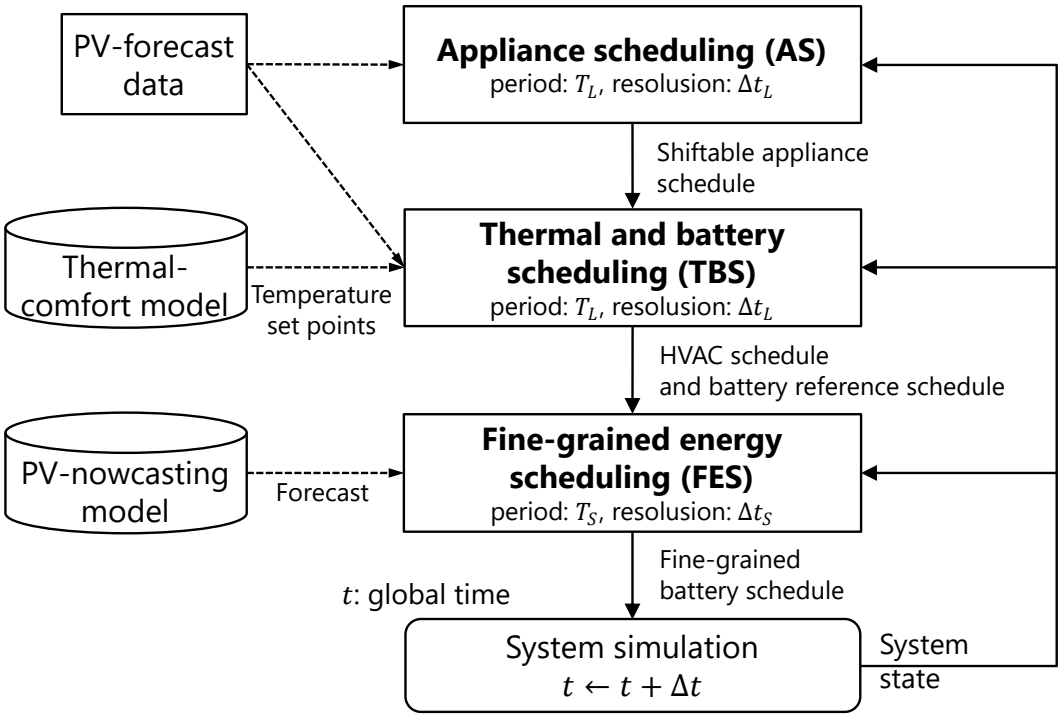

Figure 4.4: Block diagram of comfort-aware multi-time scale optimization flow.

the variation of load demand, PV forecasting errors, and thermal dynamics.

The mathematical formulation of the multi-time scale optimization flow is as follows: Let T_L and T_S be the planning periods for the coarse-grained and fine-grained time scales. Δt_L and Δt_S represent the time resolutions of the coarse- and fine-grained time scales. The proposed framework iteratively performs the following process every internal period Δt_L based on the MPC approach. First, the PV forecasting and thermal-comfort estimation models are used to obtain PV generation profiles and temperature set points. Then, the appliance scheduling (AS) stage decides the shiftable-appliance schedule. Next, the thermal and battery scheduling (TBS) stage calculates the battery and HVAC schedules. These schedules are obtained for a planning period of T_L (e.g., 24 h) with a coarse-grained resolution of Δt_L (e.g., 15 min). After that, the fine-grained energy scheduling (FES) stage provides precise control for a planning period of Δt_S (e.g., 15 min) with a resolution of Δt_S (e.g., 1 s). Based on these processes, the proposed method can deal with the scheduling of appliances, HVAC, and a battery system in real-time.

The main extension in this chapter is the inclusion of the thermal part of energy management in the TBS. The AS and FES are identical to the optimization problems described in Sections 3.4.2 and 3.4.4; refer to them for the detailed formulation of the AS and FES. This chapter primarily discusses the extended part of the framework in the following sections.

4.4.2 Appliance Scheduling

In the AS, the ON-OFF schedules of shiftable appliances are optimized by solving the MIP problem. As described in Section 3.4.2, the optimization problem that is based on mixed-integer linear programming (MIP) is formulated by:

$$\begin{aligned}
&\text{minimize} && \sum_{t_L=1}^{T_L} \xi_{t_L} \cdot S_{t_L}, \\
&\text{subject to} && (3.1)-(3.13),(3.21), \\
&\text{input} \\
& && \{G_{t_L}, D_{t_L}^{base}, \xi_{t_L}\},\ \forall t_L \\
&\text{decision variables} \\
& && \{S_{t_L}, Y_{t_L}, I_{batt,t_L}, q_{m,p,t_L}, r_{m,p,t_L}\},\ \forall m,p,t_L
\end{aligned} \tag{4.10}$$

where m and p are the shiftable appliance index and the operation phase of the shiftable appliance. In addition, G_{t_L} is the PV generation, $D_{t_L}^{base}$ is the base demand, ξ_{t_L} is the electricity price, S_{t_L} is the energy purchased, Y_{t_L} is the wasted energy, I_{batt,t_L} is the current of the battery system, q_{m,p,t_L} is the operation flag of the shiftable appliances, and r_{m,p,t_L} is the finish flag of the shiftable appliance. To capture such long-term system dynamics as PV generation and electricity prices, T_L and Δt_L are typically set for 24 h and 15 min. The objective function of appliance scheduling is to minimize electricity costs, and the AS solution contains optimal schedules for shiftable appliances and a battery schedule. However, the obtained battery schedule is discarded, and only appliance schedules are employed. The HVAC and battery scheduling are solved in the next TBS with these equivalent circuit models, and this decomposition significantly reduces the time complexity.

4.4.3 Thermal and Battery Scheduling

The TBS aims to find optimal HVAC and battery schedules for the same time scale as the AS. It takes as input the shiftable-appliance schedules obtained by the AS, denoted by $D_{t_L}^{shft}$, and optimal temperature set-points T_{est,t_L}^{set}, with upper/lower bounds $T_{est,t_L}^{upper}/T_{est,t_L}^{lower}$, discussed in Section 4.3.3. The TBS is mathematically formulated as

follows:

$$\text{minimize} \qquad \omega \cdot J_{cost} + (1-\omega) \cdot J_{comfort} + P_e \sum_{t_L=1}^{T_L} s_{t_L}, \tag{4.11}$$

subject to

$$(3.2)-(3.3), (3.12)-(3.17), (3.21), (3.25), (3.26), (4.1)-(4.4),$$

$$J_{cost} = \frac{\sum_{t_L=1}^{T_L} \xi_{t_L} \cdot S_{t_L}}{Bill_{max}}, \tag{4.12}$$

$$J_{comfort} = \frac{\sum_{t_L=1}^{T_L} O_{t_L} \cdot (T_{t_L}^{in} - T_{est,t_L}^{set})^2}{|T_{max}^{error}|}, \tag{4.13}$$

$$T_{est,t_L}^{lower} - s_{t_L} \leq T_{t_L}^{in} \leq T_{est,t_L}^{upper} + s_{t_L}, \ \forall t_L \tag{4.14}$$

$$0 \leq s_{t_L}, \ \forall t_L \tag{4.15}$$

$$S_{t_L} + G_{t_L} + B_{t_L} = D_{t_L}^{base} + D_{t_L}^{shft} + D_{t_L}^{hvac} + Y_{t_L}, \ \forall t_L \tag{4.16}$$

input

$$\{G_{t_L}, D_{t_L}^{base}, D_{t_L}^{shft}, \xi_{t_L}, T_{est,t_L}^{set}, T_{est,t_L}^{upper}, T_{est,t_L}^{lower}, O_{t_L}, Q_{t_L}^{gain}, T_{t_L}^{out}\}, \ \forall t_L$$

decision variables

$$\{S_{t_L}, Y_{t_L}, I_{batt,t_L}, u_{t_L}, s_{t_L},\}, \ \forall t_L$$

where B_{t_L} is the battery power and O_{t_L} is a binary variable that is 1 if the room is occupied, and 0 otherwise. The slack variable s_{t_L} is introduced to avoid violating the comfort temperature range. In the objective function (4.11), the first term J_{cost}, defined by (4.12), represents electricity costs. The second term $J_{comfort}$, defined by (4.13), represents the error between the indoor temperature and the optimal set points. ω is a weighting parameter that controls the trade-off between J_{cost} and $J_{comfort}$. These functions are normalized by their maximum possible values, $Bill_{max}$ and $T^{error}max$, in order to treat them equally in the weighted sum [114]. The third term in the objective function is a penalty term that prevents the room temperature from violating the temperature bounds $T_{est,t_L}^{lower}/T_{est,t_L}^{upper}$. The constant P_e is a large penalty value (e.g., set to 1000). The variable s_{t_L} is a non-negative slack variable that represents the excess value when $T_{t_L}^{in}$ exceeds the limits T_{est,t_L}^{upper} or T_{est,t_L}^{lower}, and these constraints are defined by the formulas (4.14) and (4.15). The equation (4.16) states that the energy balance within the system must be maintained at all times, taking into account HVAC power consumption. Overall, the objective of this problem is to minimize electricity costs and maximize thermal comfort.

The TBS formulates a co-scheduling problem for the HVAC and battery systems. Including the battery in this optimization allows for greater flexibility in balancing electricity costs and thermal comfort. As the battery model includes nonlinear equations, the TBS problem is solved using a nonlinear programming (NLP) solver. The resulting

HVAC schedule is applied to the system and serves as input for the FES (denoted by $D_{t_S}^{hvac}$), and the battery power trajectory E^{ref} is used as reference values in the FES, which is defined as follows:

$$E^{ref} = \frac{1}{1000} \cdot I_1^{batt} \cdot V_1^{batt} \cdot \frac{\Delta t_S}{3600}. \tag{4.17}$$

4.4.4 Fine-Grained Energy Scheduling

The FES realizes short-term battery scheduling to interpolate the coarse-grained schedules. Similar to Section 3.4.4, the optimization problem is formulated based on NLP with the goal of minimizing the mismatch between demand and PV generation, as shown in the following:

$$\begin{aligned}
&\text{minimize} && \sum_{t_S=1}^{T_S} \xi_{t_S} \cdot S_{t_S}, \\
&\text{subject to} && (3.2)-(3.3),(3.12)-(3.23),(3.29),(4.16), \\
&\text{input} \\
& && \{G_{t_S}, D_{t_S}^{base}, D_{t_S}^{shft}, D_{t_S}^{hvac}, \xi_{t_S}, E^{ref}\},\ \forall t_S \\
&\text{decision variables} \\
& && \{S_{t_S}, Y_{t_S}, I_{batt,t_S}\}.\ \forall t_S
\end{aligned} \tag{4.18}$$

The objective of the FES is to minimize electricity costs, which helps to minimize the energy mismatch between the demand load and PV generation. The FES typically uses 15 min periods for T_S, as the accuracy of PV forecasts tends to degrade significantly when the prediction period exceeds 15 min [75]. Since the dynamics of the battery typically has a time constant of a few seconds, the time resolution Δt_S is set to 1 sec. The proposed framework applies a precise battery power schedule, optimized by the FES, to the targeted system.

4.5 Simulation Experiments

In this section, the proposed framework is validated based on several case studies with real measured data of summer days. First, an experimental setup is described, and then, the results show the effectiveness of the proposed framework in terms of thermal comfort and electricity costs.

4.5.1 Simulation Setup

To evaluate the performance of the HVAC scheduling and thermal comfort estimation, a simulation experiment was conducted over a period of five days (August 1 to August

5), assuming hot summer conditions. It is worth noting that the system performance of other components, such as the multi-time scale structure, battery modeling, and PV forecasting, has already been validated in Chapter 3. The target system is a smart building, as described in Section 4.3.2, that has a contract for real-time electricity pricing with ComEd in the US [115]. The size of the PV panel is set to 4 kWp, with a mean absolute error of 25% for long-term PV forecasts and 12% for short-term forecasts [75]. The battery system has a capacity of 4 kWh, and the parameters of the circuit model were chosen from the literature [76]. The daily demand for non-shiftable and shiftable appliances is approximately 18 kWh, excluding HVAC. The DRED dataset was used as the demand profile for non-shiftable appliances [101]. In addition, the dishwasher, clothes washer, and tumble dryer were treated as shiftable appliances and scheduled to run once per day using their power profiles [102].

For the thermal modeling, the thermal resistance R is set to 5.20×10^{-3} K/W, and the thermal capacitance is set to 4.03×10^{6} J/K. This results in a time constant of 20925 s for the building. The rated power and COP of the HVAC system are set to 2 kW and 2.5, respectively. The simulation assumed the hottest sunny days of a Japanese summer, with an average outdoor temperature of $28°C$. The thermal comfort data used in the simulation is taken from a public survey dataset [116], which includes PMV values for 24 office occupants over the course of a year. The target residential building is assumed to be occupied from 8 am to 12 pm and 1 pm to 6 pm on all days.

The proposed framework has parameters that are set to 24 h for T_c, 15 min for Δt_c and T_f, and 1 s for Δ. The optimization flow in Fig. 4.4 is executed every 15 min. To control the trade-off between electricity costs and thermal comfort, the weight coefficient ω is changed within a range of 0 to 1. For the time window of thermal-comfort estimation, x and y are set to 15 and 3, following the literature [105]. IPOPT v3.14 and CPLEX v20.1 are used to solve NLP and MIP problems. It should be noted that the total solution time for the three optimization problems (AS, TBS, and FGEM) averages less than 10 s on a modern laptop PC with an Intel Core-i7 6600U CPU and 16 GB of DDR3 RAM. Therefore, the solution can be obtained in real-time, even though the mathematical solvers are not fully optimized for runtimes.

4.5.2 Results

Performance Comparison on Trade-off between Electricity Costs and Thermal Comfort

First, the proposed framework was compared with a method that employs a fixed set-point assuming a typical thermostat controller [109, 117], while the proposed framework adaptively decides the temperature set points based on thermal-comfort estimation. Generally, the thermostat controller follows a pre-determined indoor temperature as much as possible to enforce occupants' orders. To reproduce this, the fixed set-point scheme employs the modified version of the proposed framework, of which $T^{set}_{est,t}$ is set

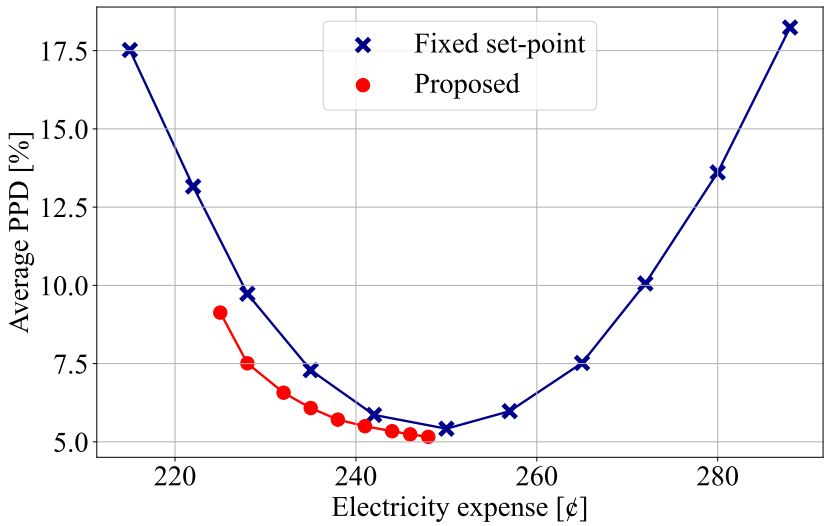

Figure 4.5: Trade-off relationship between average PPD and electricity costs for proposed and fixed set-point method.

to the pre-fixed set point and the weight ω is always set to 0.9.

Table 4.1 shows the results of the total electricity costs and average PPD as a comfort criterion over five days. Note that the best value of PPD is 5%, which means the percentage of occupants dissatisfied with the thermal environment. The results of the proposed method show that the weight coefficient ω controlled the importance of the electricity costs and the average PPD. The larger the weight ω, the lower the electricity costs, and the worsen the PPD. Meanwhile, for the fixed set-point method, the higher the temperature set points the lower the electricity costs since this scheme simply reduces the HVAC operation without thermal-comfort consideration, and vice versa. Fig. 4.5 plots the result of Table 4.1 and shows the relationship between the electricity costs and the average PPD for the different methods. As shown in Fig. 4.5, the line of the proposed method is always superior to the line of the fixed set-point method. This is because the thermal-comfort estimation model provides suitable temperature set points and because the proposed method effectively schedules the HVAC system. From these results, the proposed framework can realize a better trade-off relationship between the electricity costs and the thermal comfort than the baseline. Compared to the baseline, the proposed method reduces the electricity costs by up to 14.0% while achieving the same thermal comfort.

Detailed Profiles

Figure 4.6 shows the performance of the proposed framework in terms of indoor temperature, electricity costs, HVAC power consumption, and battery power, with different values of the weight coefficient ω. Three operating modes were obtained: Eco, Bal-

Table 4.1: Total electricity costs and average PPD over five days in August for proposed and fixed set-point methods.

Method	**Proposed framework with thermal-comfort estimation**									
	$\omega = 0.1$	$\omega = 0.2$	$\omega = 0.3$	$\omega = 0.4$	$\omega = 0.5$	$\omega = 0.6$	$\omega = 0.7$	$\omega = 0.8$	$\omega = 0.9$	
electricity cost [¢]	248	246	244	241	238	235	232	228	225	
Average PPD [%]	5.16	5.24	5.34	5.5	5.71	6.08	6.57	7.51	9.13	
Method	Fixed set-point method									
	23.0°C	23.5°C	24.0°C	24.5°C	25.0°C	25.5°C	26.0°C	26.5°C	27.0°C	27.5°C	28.0°C
electricity cost [¢]	288	280	272	265	257	250	242	235	228	222	215
Average PPD [%]	18.24	13.61	10.06	7.52	5.98	5.42	5.86	7.29	9.73	13.16	17.52

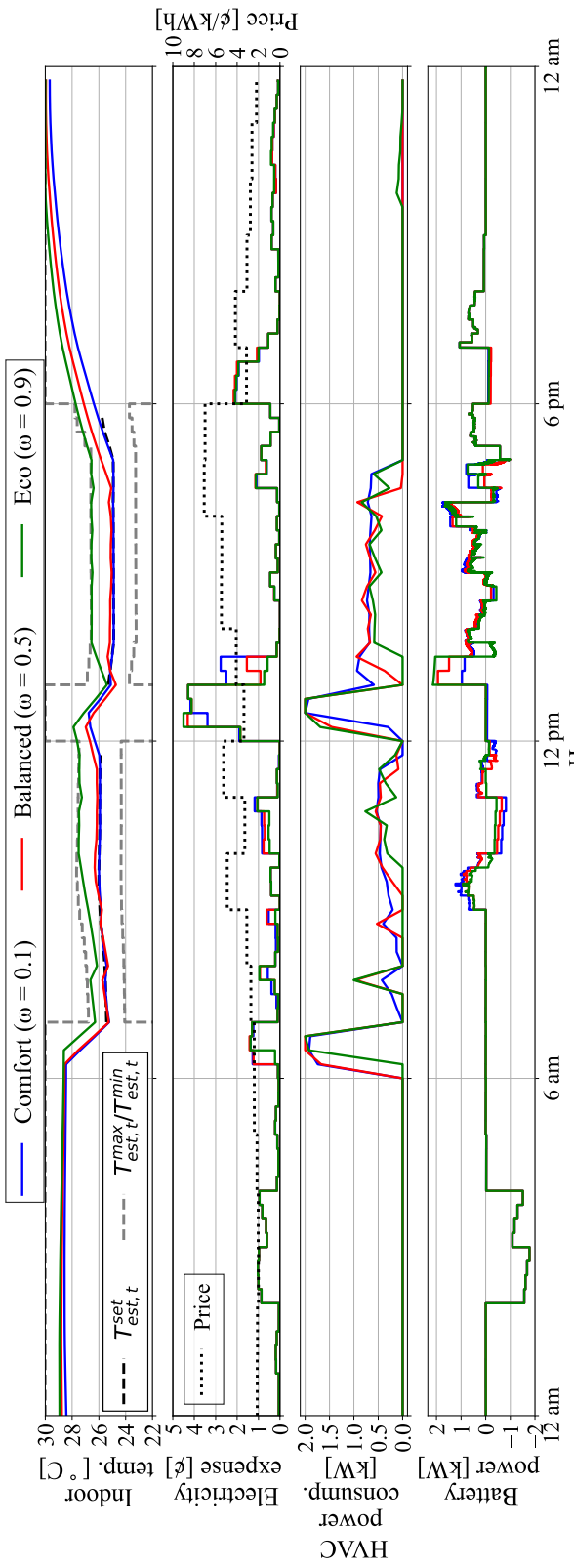

Figure 4.6: Detailed profiles for different modes of August 2, including indoor temperature, electricity costs, HVAC power, and battery power (positive battery power represents discharging, otherwise charging).

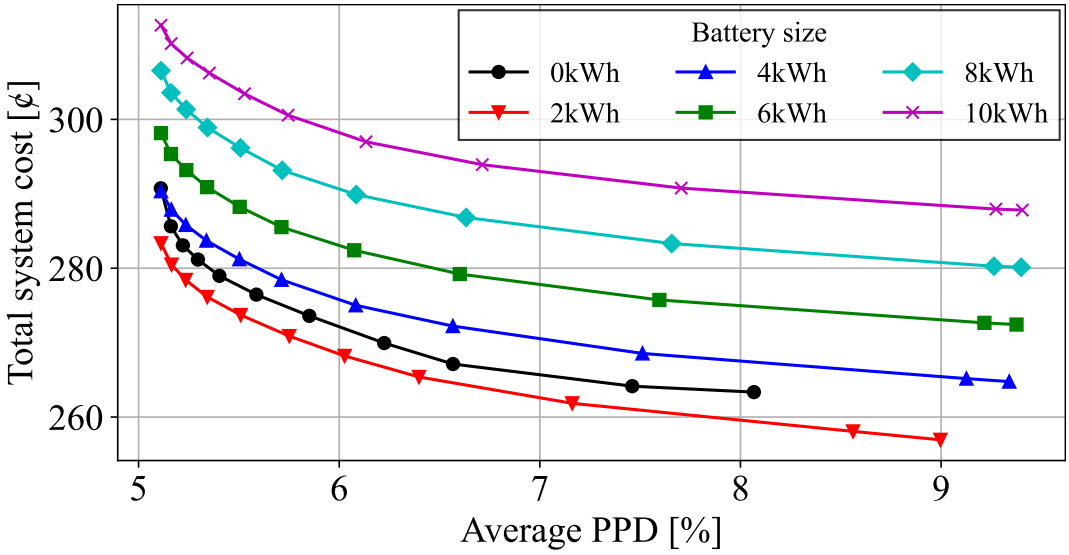

Figure 4.7: Battery size impact on total system cost and average PPD over five days simulation.

anced, and Comfort, corresponding to $\omega = 0.1, 0.5$, and 0.9, respectively. The indoor temperature set point $T_{est,t}^{set}$, upper bound T_{est}^{upper}, and lower bound T_{est}^{lower} were adaptively estimated over time. In the Comfort mode, the temperature was kept close to the set point $T_{est,t}^{set}$ to improve thermal comfort, while in the Eco mode, the temperature was kept close to the upper bound T_{est}^{upper} to minimize electricity costs. As shown in the bottom three figures, electricity was mainly purchased around 3 am and 12 pm, when electricity prices (black dotted line) were low. The HVAC system was also scheduled more frequently during these low-price periods and before the arrival of occupants. The battery system was charged during low-price periods (3 am and 10 am) and discharged during high-price periods (1 pm to 7 pm). Importantly, for different modes, the electricity cost was almost the same from 2 pm to 5 pm, although the HVAC power consumption is different. The optimization of the battery discharge helped minimize electricity costs during the high-price period and ensure the proper operation of the HVAC system while meeting thermal constraints. The co-scheduling of the HVAC and battery systems allowed for the reduction of electricity costs while maintaining thermal comfort. It can be seen that the electricity usage and indoor temperature were successfully controlled according to the chosen mode, and the relationship between electricity costs and thermal comfort was effectively managed.

Effect of Battery Size

This section conducted a size analysis of the battery storage system. The total system cost is defined by adding the battery cost to the electricity costs. The battery cost

is assumed to be a daily depreciation cost, calculated based on a battery initial cost (132$/kWh [118]), the battery capacity, and its lifetime (18 years with one daily battery cycle [54]). Fig. 4.7 shows the trade-off between the system cost and the average PPD with different battery capacities. Each point of the curves corresponds to different weights: $\omega = 0.01, 0.1, 0.2, 0.3, 0.4, 0.5, 0.6, 0.7, 0.8, 0.9, 0.99$ from the left. As shown in Fig. 4.7, battery introduction greatly impacts the trade-off. In this system configuration, the optimal battery size is 2 kWh in terms of the trade-off improvement. Comparing battery sizes of 0 and 2 kWh, the trade-off is improved. However, when the battery is larger than 2 kWh, the trade-off is worse than in the no-battery case. This is because the increase in the battery cost exceeds the reduction of electricity costs from a larger battery size due to the high initial cost of the battery. Since the battery's initial cost is decreasing every year [118], this phenomenon will eventually be reversed. Finally, the battery size should be carefully chosen, considering both electricity and battery costs.

4.6 Summary

This chapter has presented a comfort-aware electrical and thermal energy management framework with a thermal comfort estimator. The proposed framework aims to improve a trade-off relationship between electricity costs and thermal comfort in smart buildings. The framework extended the online energy management system described in Chapter 3 to include heating, ventilation, and air conditioning (HVAC) management. Thermal comfort is modeled following Fanger's index, predicted mean vote (PMV) and predicted percentage of dissatisfaction (PPD). A thermal model based on equivalent circuits is introduced to capture thermal dynamics, and a thermal comfort estimator is employed to predict optimal temperature set points for the HVAC system using historical data. As described in Chapter 3, the proposed framework considers the multi-time scale structure composed of the coarse-grained and fine-grained time scales. The coarse-grained time scale is used for HVAC management, as buildings' typical thermal time constants are longer than an hour. In addition, a multi-objective function was developed to simultaneously reduce electricity costs and improve thermal comfort. The results indicate that the proposed method can achieve a maximum reduction in electricity costs of 14.0% while maintaining the same levels of thermal comfort. Therefore, the proposed method effectively balances the trade-off between electricity costs and thermal comfort, resulting in improvements compared to baseline methods that do not include HVAC management.

One of the challenges in implementing the proposed framework in existing systems is the need for various functions, such as data processing, data transmission, and fast decision-making. The proposed framework can play a central role in energy management systems by providing practical solutions for managing the operation of the entire system. As the first step in this direction, Zhao et al. [119] implemented the HVAC management developed in this research in a campus building.

This work used adaptive temperature set points based on Fanger's model. However,

there is often a discrepancy between Fanger's model and actual comfort in practical situations. Therefore, one area for future work is to incorporate the preferences of occupants based on their choices and sensor information. On the other hand, it is also important to consider an accurate HVAC model, assuming that the HVAC system is ideal, for example, with a constant COP. This should be a key direction for achieving an energy-efficient framework in the future.

Chapter 5

Duck Curve Improving Strategy for Resource Aggregator Based on Dynamic Pricing

With the rapid increase in solar power adoption and the rise of prosumers, the power system confronts complex challenges. In particular, the duck curve is a worldwide problem on the energy supply-side, which shows the imbalance between photovoltaic (PV) generation and electricity demand. To address this issue, a resource aggregator (RA) has emerged to provide flexible solutions by acquiring and utilizing demand-side flexibility (DSF) through demand response (DR) programs such as dynamic pricing. This chapter presents a duck curve improving strategy for the RA that dispatches dynamic pricing to the prosumers and leverages a battery power station owned by the RA[1]. The proposed strategy is based on a model-free deep reinforcement learning (DRL) algorithm to optimize each prosumer's retail prices and schedule usage of the RA's battery power station. The reward function of the proposed strategy is designed to maximize overall social welfare, considering the RA's profit, the prosumer's cost, and the improvement of the duck curve. The simulation experiments are conducted to demonstrate the system performance of the proposed DRL-based strategy using actual wholesale price, demand, and PV generation data. The results show that the proposed strategy can improve the standard deviation and peak-to-average ratio of net load by up to 57.1% and 20.8%, respectively.

5.1 Motivation and Objective

The high market penetration of installed solar renewable generation has turned many consumers into prosumers. Although the increase in prosumers who install PV gener-

[1]This chapter is a refined and reproduced version of the paper presented in part at the Proceedings of ACM BuildSys [120].

ation systems does accelerate the decarbonization of the power grid, it can also cause a severe problem, namely, the duck curve [121] as shown in Fig. 5.1. This graph illustrates an example profile of a net load, which is defined as the total power consumption minus PV generation, of an entire grid on a given day in a scenario with high PV penetration. The timing imbalance between demand peak and solar production causes a steep curve of net load and demand peak valley. The duck curve problem is also becoming severe in Japan [122] and other regions with high levels of PV penetration [123], even given reduced demand in the COVID-19 pandemic period [124]. To cope with the duck curve, an independent system operator (ISO) has to augment delivered power with conventional supply sources like gas or coal power plants. However, the sudden start-up of traditional sources increases carbon emissions and makes the power grid inefficient and expensive.

The conventional solution to the duck curve is the development of supply-side flexibility that includes retrofitting fossil fuel power plants [125], adjusting PV module orientation in solar plants [126], and improving the efficiency of the unit commitment schedule in electric power production [127]. However, these supply-side approaches have limitations in solving the duck curve due to the continuous growth of PV penetration levels in most countries [3]. PV generation is intermittent and non-dispatchable, and its production quantity often changes on an hourly, daily, and seasonal basis. This variability leads to a significant cost paid to develop the capability of grid flexibility [128]. Besides, a day-ahead market usually treats the duck curve problem [129], but the duck curve is also becoming a critical issue in real time. The forecasting of PV generation is generally a difficult task, especially day-ahead forecasting [130]. Therefore, in a power system with a high penetration of PV, the risk of the mismatch with the day-ahead forecasting (over-estimation and under-estimation) is not small and cannot be ignored in real-time. Recently, demand-side flexibility has become attractive because recent prosumers have control over many types of flexible loads such as schedulable appliances, batteries, and electric vehicles (EVs), to manage intermittent renewable energy [59].

As for the demand-side flexibility, battery systems are promising to reshape the load curve locally [131]. The demand-side installation of PV panels accounts for a large share of whole PV capacity, e.g., 30% in the U.S. [132], i.e., the demand-side PV such as a rooftop and behind-the-meter PV panels is a major factor of the duck curve as well as utility-scale PV. Although the supply side has no access to demand-side PV information, the demand side can locally monitor PV generation and effectively schedule its own battery. In order to solve the duck curve effectively, the use of demand-side batteries is also important.

One of the efficient solutions to induce demand-side flexibility is the implementation of a demand response (DR) program as described in Chapter 1. To implement DR programs, a resource aggregator (RA) plays a critical role in efficiently coordinating the end-user response [133]. The RA is one of the market participants and is responsible for many roles, such as market participation, controlling own energy resources, and DR

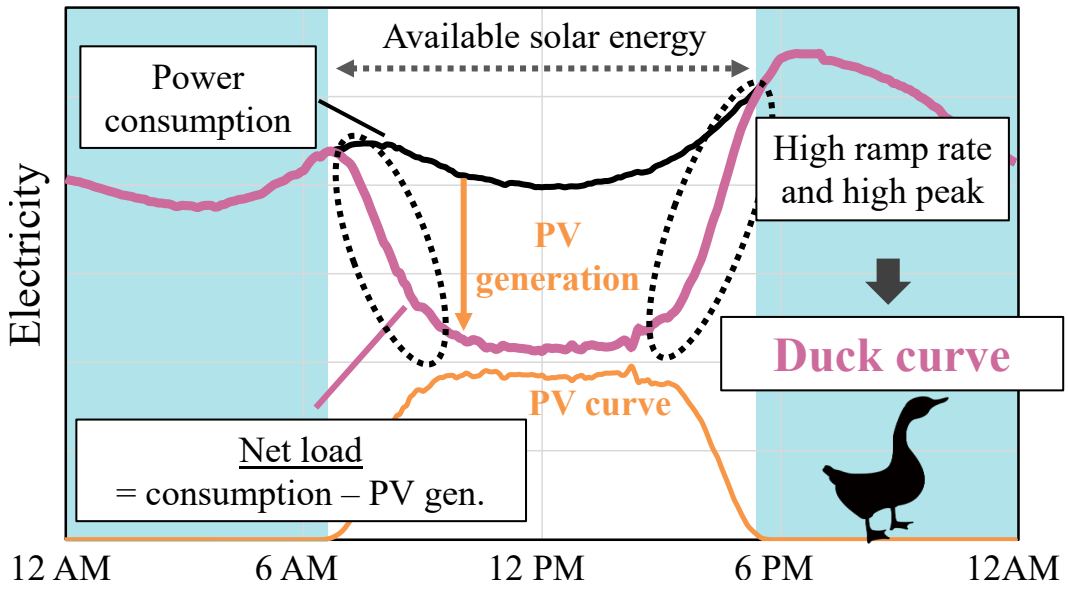

Figure 5.1: Example of typical duck curve graph.

implementation to prosumers, as an integrator between the market and prosumers [134]. The RA usually aggregates the energy resources such as energy storage facilities [135] and prosumer demand controlled by DR programs and provides ancillary services to the grid. The business model of the RA is to earn revenue through electricity retailing to prosumers and to receive remuneration from the ISO by providing ancillary services such as duck curve improvement. The power aggregation of many prosumers is suitable for efficient DR programs and achieving demand-side flexibility. As introduced in the following section, there has been much research on the mechanism design of DR programs as an RA strategy. However, few studies have aimed to improve the duck curve with real-time RA strategies.

This chapter proposes a model-free DRL-based strategy for RAs to improve the duck curve aimed at tackling computer complexity, environmental uncertainty, and privacy concerns for prosumers. The RA's action includes dynamic pricing for end-users (prosumers) and the power-use scheduling of a battery power station owned by RA. The target system is a hierarchical energy market composed of ISO, RA, and prosumers. The RA should be aware of not only maximizing its own profits but also minimizing the prosumer's cost because a bad end-user experience can lead to contract cancellation. Consequently, the objective of the proposed method is to maximize social welfare, including the RA's profit, the prosumer's cost savings, and the improvement of the duck curve. The proposed strategy is based on a model-free deep reinforcement learning (DRL) approach aimed at tackling computer complexity, environmental uncertainty, and privacy concerns for prosumers, as discussed in the following section. The performance of the proposed method is demonstrated by comparing it with specific baselines.

The impact of different scenarios and parameters on its performance is also investigated. This is the first study aiming to improve the duck curve with real-time RA strategies.

The main contributions of this work are as follows.

- A model-free DRL-based algorithm is proposed to make the RA learn the optimal strategy for solving the duck curve. The trained strategy can calculate dynamic pricing and battery scheduling (DP-BS) in real-time without complete knowledge of the prosumers.
- A hierarchical energy market model [136] is extended to include prosumers with a PV panel and a battery system.
- The response of prosumers to retail electricity prices is modeled as two price-responsive devices: elastic load and battery use. This modeling helps to mimic a real-world system as a proof-of-concept for the proposed method.
- The design of the reward function is carefully explored to improve the duck curve.
- Simulation experiments are conducted to demonstrate the performance of the proposed strategy from multiple aspects, such as a mitigation of the duck curve, balancing of prosumer cost and RA profit, and the RA's battery size.

This chapter is a refined and extended version of the paper [120] by developing the demand load model of prosumers to represent realistic responses to retail prices. Moreover, the effectiveness of the proposed method is investigated by comparing it with several baselines and including an optimization-based approach and a rule-based one. In addition, as a significant expansion of the experimental results, a whole-year simulation and a sensitivity analysis for the battery size and weight parameters of the objective are conducted to discuss the effectiveness of the proposed method.

The remainder of this chapter is as follows. Section 5.2 describes the related works of strategies for the RA such as the demand response. Section 5.3 presents the problem setting and system models, and Section 5.4 provides the proposed RA's strategy for improving the duck curve. In Section 5.5, a simulation is conducted to obtain results for verifying the performance of the proposed method. Finally, Section 5.6 summarizes this chapter and shows future works.

5.2 Related Works

Many studies have been conducted on the implementation effect of DR. Jiang et al. [137] proposed an RTP model based on the matrix of electricity price elasticity that expresses the relationship between retail prices and customer response. Wang et al. [138] developed a fairness-aware RTP mechanism based on an optimization approach and established a residential user evaluation system with indicators for user characteristics. Yang et al. [139] proposed the energy optimization method based on an integrated DR program by a multi-energy provider to achieve a win-win strategy for a utility provider and its customers. Taherian et al. [140] integrated load forecasting and a meta-heuristic-based RTP model to maximize the profit of utility providers and minimize the electricity

costs of both proactive and reactive customers. The aforementioned studies have investigated the pricing mechanism and implementation scheme, but they mainly focused on the demand-side profitability for the RA and customers and lack the pricing scheme to improve the supply-side problem, especially for the duck curve.

Many researchers have focused on improving the duck curve through energy management and demand response coordinated by aggregators. First, related works that assume cooperative scenarios are introduced, i.e., the demand-side load is managed by a central optimizer. Jovanovic et al. [141] investigated the potential of demand-side flexibility exploited from large fleets of EVs to minimize ramp-up requirements. Howlader et al. [142] proposed an optimal thermal unit commitment considering RTP and demand-side load based on mixed-integer linear programming (MILP) to fill peak and off-peak gaps in the duck curve. Calero et al. [143] demonstrated the feasibility and potential of pre-cooling strategies in residential households for mitigating the duck curve. Yoon et al. [144] formulated a dynamic pricing DR strategy for building heating, ventilating, and air conditioning (HVAC) systems to reduce peak load as a single-level optimization model. It is doubtful that these cooperative scenarios are feasible in reality, since the end-users may feel discomfort by the privacy issue and having their own devices controlled by someone else. There is also the privacy issue raised by giving detailed information on end-user systems to the central optimizer. The proposed strategy does not control the prosumer's devices directly and aims to flatten the prosumer's demand through a dynamic pricing DR program and scheduling of the RA's battery usage.

Next, related works that assume non-cooperative scenarios are described, i.e., aggregators indirectly controlling end-users through DR programs. Ferdous et al. [145] proposed a nonlinear programming (NLP)-based optimization problem to perform optimal dynamic pricing by electricity retailers. Zhang et al. [146] formulated the vehicle-to-grid (V2G) concept under dynamic pricing as a Stackelberg game to mitigate the ramp event in the duck curve. The leader is a distribution system operator (DSO) that conducts charging price DR programs, and the followers are EVs that calculate the optimal charging schedule individually. Sheha et al. [129] also proposed a Stackelberg game framework to solve the duck curve by iterating dynamic pricing and demand-side scheduling. They assumed that households optimize both battery systems and HVAC systems to minimize electricity costs under dynamic pricing. All of these works proposed model-based approaches based on mathematical optimization. However, these approaches made the impractical assumption of having complete knowledge of the end-user systems, and the computational cost is expensive. Moreover, they require forecast profiles of solar generation and power consumption over the planning period. Since the model-based approach is deterministic, uncertainties such as forecasting errors may cause a failure to improve the duck curve.

There are several approaches to address various uncertainties in a model-based optimization approach. Stochastic optimization accounts for the uncertainties by considering a large number of scenarios [147] or reduced scenario [148]. However, the

computational complexity of stochastic models is generally expensive, and the accurate probability distribution of uncertain variables is necessary, which is a time-consuming process. Robust optimization obtains the solution within certain sets of uncertain variables in the worst-case scenario [149] and upper/lower bounds [150]. However, the obtained solution tends to be conservative, and the accurate range of uncertain variables needs to be known in advance, which is an unpractical setting. Both stochastic and robust optimization are model-based approaches, and customer response to dynamic pricing, which is generally a nonlinear and complex phenomenon, is difficult to model. Meanwhile, model-free approaches, such as reinforcement learning, can learn from data not only uncertainties but also nonlinear relationships.

This chapter addresses the above research challenges, focusing on model-free reinforcement learning (RL) and deep reinforcement learning (DRL). RL is an area of machine learning attempting to learn which actions are the best in environments from the data without expert knowledge of the system [151]. In particular, DRL, which combines RL and deep neural networks, is known to perform well in decision-making for high-dimensional problems such as power systems [152]. Several studies have proposed an aggregator strategy using RL and DRL. Qiu et al. [153] proposed a DRL approach to determine EV charging prices in the EV aggregator. Still, their strategy is tailored to DR programs for EV charging, and they do not consider prosumer households. Lu et al. [136] proposed a model-free price-based DR strategy for the electricity retailer based on Q-learning, a typical RL algorithm. Kuang et al. [154] proposed an optimal incentive-based DR strategy based on DRL for a virtual power plant (VPP) while considering the customer's risk attributes. However, these studies did not consider the duck curve problem or prosumers who use renewable generation, and they did not support selling back surplus energy to the aggregator. Therefore, it is concluded that there is no significant study on the duck-curve-improvement RA's strategy, using the RL/DRL algorithm and considering prosumers.

5.3 Problem Description

This section presents a detailed problem setting and system model. As shown in Fig. 5.2, the target system is a hierarchical energy market composed of supply-side and demand-side sectors [136]. The recent development of ICT (information and communication technology) enables bi-directional communication of information between these entities in real-time. On the supply side, the wholesale electricity market (WEM) is where electricity is traded, sending agreed wholesale electricity prices to the entire system on a real-time basis. The ISO is responsible for monitoring the grid state and resolving issues such as the duck curve by offering supply-side and grid-side flexibility. The demand side consists of RA, a battery power station, and prosumers. It is assumed that the RA owns a controllable battery power station as an energy storage system and joins the WEM. The RA aggregates the net load by the prosumers and the battery power

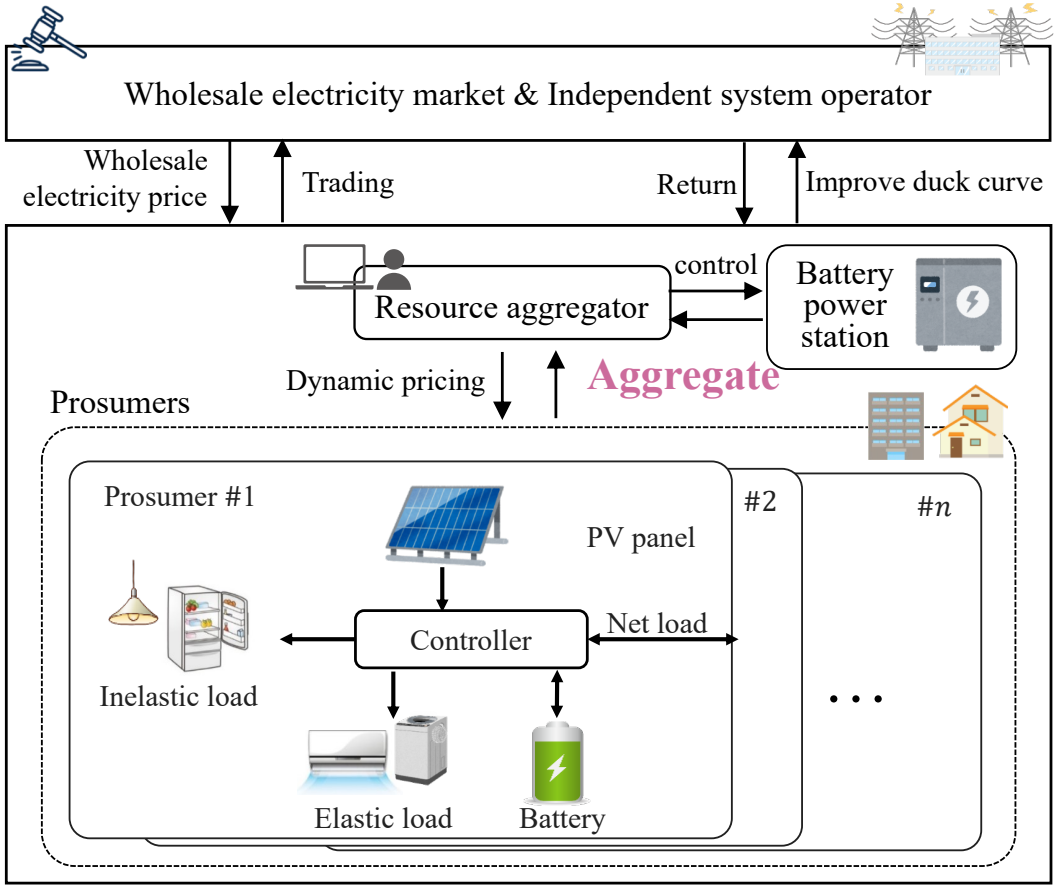

Figure 5.2: Overview of hierarchical energy market.

station and then trades it with the WEM and the ISO. The prosumers individually control energy demand based on their own systems states and retail prices.

This work focuses on the real-time strategy of the RA, including the dynamic pricing to the prosumers and the battery power station scheduling. In this chapter, this problem is denoted by *Dynamic Pricing and Battery Scheduling (DP-BS)*. As mentioned in Section 5.1, this chapter addresses the DP-BS problem by employing a model-free DRL approach. All the proposed strategy is implemented in the RA with a DRL-based algorithm and neural networks. In a practical case, dynamic pricing and battery scheduling by the RA are executed as the following procedures. At each time step, the WEM and the ISO provide a profile of wholesale electricity prices and the requirement for flattening the duck curve to the RA. Then, the RA will collect information about the net load and the battery SOC from each prosumer. The proposed strategy trained by the DRL algorithm computes the retail prices and the schedule of the RA's battery power station. The battery power station of the RA will operate based on the obtained schedule, and the prosumers decide on schedules of their demand and a battery based on the retail price

set by the RA. After that, the RA aggregates the total net load calculated by summing up the power output of the RA's battery power station and the net load of each prosumer and trades it with the WEM and the ISO. Finally, the RA settles the cost of prosumers, the profit of the RA, and the remuneration obtained by flattening the duck curve. All the information that the RA collected is stored in a database of the RA, and the RA trains the neural network based on the DRL algorithm every specific time interval, e.g., 1 week.

The goal of the RA's strategy is to maximize the following social welfare in the hierarchical energy market: (1) maximizing revenue from electricity retailing to the prosumers, (2) minimizing the electricity bill of the prosumers, and (3) maximizing the remuneration for the duck curve improvement given by the ISO. It is worth mentioning that maximizing the social welfare and the profitability of the RA are not in conflict; in fact, they point in the same direction. For example, if a prosumer's cost minimization is not considered, the prosumers feel discomfort and may terminate their contract with RA. On the other hand, the RA can get remuneration by tackling supply-side concerns such as the duck curve, and it will benefit the RA. Thus, RA has the motivation to improve the social welfare, which includes supply-side and prosumers benefits, rather than maximizing only its profits.

Participation in such programs is also valuable to the prosumers. In dynamic pricing programs, electricity retail prices go up and down, depending on the situation such as the emergence of the duck curve. Prosumers can reduce their electricity costs by scheduling demand and batteries according to changes in retail prices. Since the RA considers the cost minimization of the prosumers in the objectives, it is guaranteed that the retail price will not always be too high. Besides, in the assumption, the RA agents get remuneration from the ISO based on how much net load is flattened. Generally, part of the obtained remuneration will be distributed to the prosumers, and this also helps to reduce the prosumer costs. Finally, this system model to solve the duck curve benefits both the supply and demand sides. In the following section, the system model is mathematically described.

5.3.1 Prosumer Model

The operation of the elastic load and the battery is expected to be automatically or manually controlled in response to the surrounding state and the retail price announced by the RA.

Load Model

The prosumers have the inelastic load and the elastic load. The inelastic load refers to base power demand that does not change with respect to retail prices, such as lights, refrigerators, and elevators. The elastic load is a price-responsive load, which is mainly a shiftable load, such as HVAC, clothes washers, and dishwashers: the scheduled energy

is curtailed according to the retail price, a part of the curtailed elastic load will be shifted to a later time slot [98].

Let $t \in T$ be a time index for a day, and let $n \in N$ be a prosumer index. The total load demand $e_{t,n}^{dm}$ of the prosumer n at time t is defined by the elastic load $e_{t,n}^{elas}$, the curtailed load $e_{t,n}^{curt}$ and the shifted load $e_{t,n}^{shft}$, given by:

$$e_{t,n}^{dm} = e_{t,n}^{inelas} + e_{t,n}^{elas} - e_{t,n}^{curt} + e_{t,n}^{shft}, \ \forall t,n \tag{5.1}$$

where the inelastic load $e_{t,n}^{inelas}$ is the base load and can be inferred from a historical load pattern, and $e_{t,n}^{elas}$ is originally scheduled energy of the elastic load. The curtailed load $e_{t,n}^{curt}$ and the shifted load $e_{t,n}^{shft}$ are variables that depend on the retail price determined by the RA.

The load curtailment is modeled by using price elasticity originating from economic theory [155]. The price elasticity shows the prosumer's sensitivity to the price, which means the percentage change of electricity demand when the price increases by 1%. The curtailment of the elastic load is represented by the price elasticity $\xi_{t,n}$ of prosumer n at time t as follows:

$$e_{t,n}^{curt} = e_{t,n}^{elas} \cdot \xi_{t,n} \cdot \frac{-(\lambda_{t,n} - \mu_t)}{\mu_t}, \ \forall t,n \tag{5.2}$$

where $\lambda_{t,n}$ and μ_t are the retailed electricity price for each prosumer n and wholesale electricity price, respectively. The price elasticity $\xi_{t,n}$ is usually negative, and a high absolute value means that the end-user reacts strongly to the price [156].

It is assumed that the part of the curtailed energy $e_{t,n}^{curt}$ is shifted later with a certain probability based on the current retail price and an elapsed period. This assumption comes from the following analysis of prosumer behavior. The prosumer generally schedules its demand load to the lower retail price period to minimize electricity costs [157]. The load shifting is characterized by a deadline time at which the load shift must be completed [98]. To model the shifted load, an auxiliary variable $u_{t,k,n} \in 0,1$ is introduced: when $u_{t,k,n}$ is 1, the curtailed energy $e_{k,n}^{curt}$ of prosumer n at time k is scheduled again at time t. Then, the shifted load $e_{t,n}^{shifted}$ is modeled as follows:

$$e_{t,n}^{shft} = \sum_{k=1}^{t-1} u_{t,k,n} \cdot e_{k,n}^{curt}. \ \forall t,n \tag{5.3}$$

Thus, $e_{t,n}^{shifted}$ means the sum of the scheduled energy that is curtailed at time k ($1 \leq k \leq t-1$). The upper and lower bounds of the retailed electricity price are denoted by λ^{ub} and λ^{lb} and define a patience period of prosumer n as S_n. Here, the auxiliary variable $u_{t,k,n}$ is set by the following probability:

$$\mathrm{P}(u_{t,k,n} = 1) = \frac{\lambda^{ub} - \lambda_{t,n}}{\lambda^{ub} - \lambda^{lb}} + \frac{t-k}{S_n}, \ \forall t,k,n \tag{5.4}$$

where $\mathrm{P}(u_{t,k,n}=1) \in \{0,1\}$ is the probability that $u_{t,k,n}$ becomes 1, i.e., the probability that the curtailed energy at time k is shifted at time t as a part of $e_{t,n}^{shifted}$. If the retail price is lower than the assumed maximum price, there is a higher probability that the curtailed load is shifted to the current time slot. At the same time, the longer time elapses from the load curtailment, the higher the probability. Note that the probability $\mathrm{P}(u_{t,k,n}=1)$ is clipped so that it ranges from 0 (0%) to 1 (100%).

Dissatisfaction Model

The dissatisfaction level of each prosumer is different according to their preferences, and it is generally modeled by a utility function that is an important concept in microeconomic [158]. There are several types of utility functions; due to their tractability, this work uses a quadratic function of the amount of curtailed load caused by the retail prices [159]. The dissatisfaction function $U_{t,n}$ of prosumer n at time t is defined by:

$$U_{t,n} = \alpha_n \cdot (e_{t,n}^{curt})^2 + \beta_n \cdot e_{t,n}^{curt},\ \forall t,n \tag{5.5}$$

where $\alpha_n \leq 0$ and $\beta_n \geq 0$ are predetermined parameters that vary for each prosumer. The greater the amount of energy curtailed, the greater the prosumer's dissatisfaction. Note that the larger energy curtailment (the higher dissatisfaction) leads to lower electricity bills, and thus there is generally a trade-off between electricity costs and dissatisfaction.

Battery Model

The charge/discharge dynamics of the battery of each prosumer are defined by:

$$SOC_{t+1,n}^{bat} = \begin{cases} SOC_{t,n}^{bat} + \dfrac{\eta_{ch,n}^{bat} \cdot e_{t,n}^{bat}}{C_n^{bat}}, & \text{if } e_t^{bat} \geq 0 \\ SOC_{t,n}^{bat} + \dfrac{e_{t,n}^{bat}}{\eta_{disch,n}^{bat} \cdot C_n^{bat}}, & \text{otherwise} \end{cases} \tag{5.6}$$

where $SOC_{t,n}^{bat}$ is the state-of-charge (SOC) of the prosumer n's battery at time t, $e_{t,n}^{bat}$ is the charge/discharge energy taking a positive value when charging and a negative value when discharging, and C_n^{bat} is the capacity of the prosumer n's battery. $\eta_{ch,n}^{bat}$ and $\eta_{disch,n}^{bat}$ are the charging and discharging efficiencies of the battery, respectively. The range of the charge/discharge energy is constrained by:

$$e_n^{lb,bat} \leq e_t^{bat} \leq e_n^{ub,bat},\ \forall t,n \tag{5.7}$$

$$e_n^{lb,bat} = C_{disch,n}^{rate,bat} \cdot C_n^{bat} \cdot \Delta t,\ \forall n \tag{5.8}$$

$$e_n^{ub,bat} = C_{ch,n}^{rate,bat} \cdot C_n^{bat} \cdot \Delta t,\ \forall t,n \tag{5.9}$$

where $C_{ch}^{bat,rate}/C_{disch}^{bat,rate}$ indicates a maximum charging/discharging power rate and Δt is the length of the time step. Here, $e_n^{lb,bat}$ and $e_n^{ub,bat}$ mean the upper/lower bounds of the charge/discharge energy defined in the equations (5.8) and (5.9).

The battery controller of the prosumers also tends to be price-responsive in the typical management problem [160]. This work assumes that the prosumers control the battery operation based on a rule-based controller that responds to the retail price. To judge whether the retail price is high or not, each prosumer sets a price threshold λ_n^{th} calculated by:

$$\lambda_n^{th} = \lambda^{lb} + (\lambda^{ub} - \lambda^{lb}) \cdot h_n, \ \forall n \tag{5.10}$$

where h_n is a predetermined coefficient for each prosumer n. The rule-based controller has four operation modes depending on the current price and PV generation. If the retail price is lower than the threshold, then the system switches to the charge mode, and the prosumer charges the battery with electricity purchased from the RA (mode 1). Otherwise, it switches to the discharge mode, and the prosumer discharges the battery to meet the load demand (mode 2). Other rules include stopping the charging/discharging when the battery capacity is full/empty (mode 3) and charging the surplus PV generation to the battery as much as possible regardless of the electricity price (mode 4).

To sum up, the charge/discharge energy for each mode is given as follows:

$$e_{t,n}^{bat} = \begin{cases} e_n^{ub,bat} \cdot \dfrac{\lambda_n^{th} - \lambda_{t,n}}{\lambda_{t,n}^{th} - \lambda^{lb}}, & \text{(mode 1)} \\ e_n^{lb,bat} \cdot \dfrac{\lambda_{t,n} - \lambda_n^{th}}{\lambda^{ub} - \lambda_n^{th}}, & \text{(mode 2)} \\ 0, & \text{(mode 3)} \\ e_{t,n}^{pv} - e_{t,n}^{dm}, & \text{(mode 4)} \end{cases} \tag{5.11}$$

where $e_{t,n}^{pv}$ is the PV generation of prosumer n at time t. Note that this work assumes an obviously simplistic model for the battery controller, as defined by the equations (5.10) and (5.11), which is only an imitation of prosumer behavior. However, this model is used as a proof of concept for the proposed DRL method. The DRL algorithm can be applied and is also considered effective for the practical battery controller due to the model-free nature of DRL, which can learn the prosumer behavior based on observations without specific models.

Objective

The objective of the prosumer is to minimize their electricity bill and their dissatisfaction. First, the net load $e_{t,n}^{net}$ of prosumer n at time t is calculated by:

$$e_{t,n}^{net} = e_{t,n}^{dm} - e_{t,n}^{pv} + e_{t,n}^{bat}. \ \forall t, n \tag{5.12}$$

Here, the positive net load is denoted by $e^{net,+},t,n$, and the negative net load is denoted by $e_{t,n}^{net,-}$ to distinguish between buying and selling. Finally, the objective of each prosumer is to minimize the total cost $C_{t,n}^{pro}$, defined by:

$$\text{minimize} \quad \sum_{t=1}^{T} C_{t,n}^{pro}, \tag{5.13}$$

$$C_{t,n}^{pro} = \lambda_{t,n} \cdot e_{t,n}^{net,+} - \kappa_t \cdot e_{t,n}^{net,-} + U_{t,n}, \ \forall t,n \tag{5.14}$$

where κ_t is the electricity price for selling the surplus energy. The first term means the electricity cost, the second term is the revenue from selling the surplus energy, and the third term is the dissatisfaction of the prosumer.

5.3.2 Resource Aggregator Model

Pricing Model

This work assumes that the RA sells electricity to each prosumer at a time-varying retail price $\lambda_{t,n}$ and buys the surplus electricity from the prosumers at a purchase price κ_t. The retail prices $\lambda_{t,n}$ also vary for each prosumer, and the purchase price κ_t is generally equal to the wholesale electricity price μ_t. Then, the RA trades the aggregated electricity at a wholesale electricity price μ_t notified every time step by the WEM. Constraints for retail prices are introduced to avoid unfair pricing to the prosumers, given by:

$$\lambda^{lb} \leq \lambda_{t,n} \leq \lambda^{ub}, \ \forall t,n \tag{5.15}$$

$$\lambda^{lb} = \nu \cdot \mu_{min}, \tag{5.16}$$

$$\lambda^{ub} = \nu \cdot \mu_{max}, \tag{5.17}$$

where ν is a coefficient for the price limit, and μ_{min}/μ_{max} is the minimum/maximum wholesale electricity prices for the day, defined by the equations (5.16) and (5.17), respectively. The retailed electricity price $\lambda_{t,n}$ for prosumer n at time t is decided by the proposed strategy.

Battery Power Station Model

The RA controls the charge/discharge amount of the battery power station to provide flexibility to the total net load. The dynamics of the battery power station are specified by the following equation as well as the prosumer's battery:

$$SOC_{t+1}^{ra} = \begin{cases} SOC_t^{ra} + \dfrac{\eta_{ch}^{ra} \cdot E_t^{ra}}{C^{ra}}, & \text{if } E_t^{ra} \geq 0 \\ SOC_t^{ra} + \dfrac{E_t^{ra}}{\eta_{disch}^{ra} \cdot C^{ra}}, & \text{otherwise} \end{cases} \tag{5.18}$$

$$C_{disch}^{rate,ra} \cdot C^{ra} \cdot \Delta t \leq E_t^{ra} \leq C_{ch}^{rate,ra} \cdot C^{ra} \cdot \Delta t, \ \forall t \tag{5.19}$$

where SOC_t^{ra} is the SOC of the RA's battery power station and E_t^{ra} is the charge/discharge energy taking a positive value when charging and a negative value when discharging. η_{ch}^{ra} and η_{disch}^{ra} are the charging and discharging efficiencies of the battery power station, respectively. C^{ra} is the battery capacity, and $C_{ch}^{rate,ra}/C_{disch}^{rate,ra}$ indicates the maximum charging/discharging power rate. The charge/discharge energy E_t^{ra} is also controlled by the proposed strategy.

Objective

The objective of the RA is to maximize social welfare, which includes the RA's profit maximizing, the prosumer's cost-minimizing, and the improvement of the duck curve. The RA profits from the electricity trade and the total net load E_t^{net} is defined by:

$$E_t^{net} = \sum_{n=1}^{N} e_{t,n}^{net} + E_t^{ra}. \ \forall t \tag{5.20}$$

Finally, the objective function of the RA is defined by

$$\text{maximize} \quad \sum_{t=1}^{T} \omega_1 \cdot P_t^{ra} - \omega_2 \cdot \sum_{t=1}^{T} \sum_{n=1}^{N} C_{t,n}^{pro} + (1-\omega_1-\omega_2) \cdot \sum_{t=1}^{T} R_t^{duck}, \tag{5.21}$$

$$P_t^{ra} = \sum_{n=1}^{N} \left(\lambda_{t,n} \cdot e_{t,n}^{net,+} - \kappa_t \cdot e_{t,n}^{net,-} \right) - \mu_t \cdot E_t^{net}, \ \forall t \tag{5.22}$$

where ω_1 and ω_2 are weight parameters used to adjust the importance for each term, and these range from 0 to 1. P_t^{ra} is revenue through the electricity retail, and R_t^{duck} is remuneration for the duck curve improvement. To improve the duck curve, the design of R_t^{duck} is very important. The detailed formulation of R_t^{duck} is described in Sec. 5.4.

5.3.3 Dynamic Pricing and Battery Scheduling Problem

The central (cooperative) DP-BS problem in the RA can be formulated as a nonlinear programming (NLP) problem as follows:

$$\begin{aligned} \underset{v}{\text{maximize}} \quad & (5.21), \\ \text{subject to} \quad & (5.1)-(5.11),(5.12),(5.14), \\ & (5.15)-(5.20),(5.22), \end{aligned}$$

where v is a set of decision variables that includes $\{\forall t,n : e_{t,n}^{bat}, e_{t,n}^{shifted}, \lambda_{t,n}, E_t^{ra}\}$.

It is challenging to solve the problem due to the following reasons. First, uncertain future information such as wholesale electricity prices and net load is necessary to solve this optimization problem. This information is essentially unknown in advance, and

related prediction errors result in large costs. Second, the RA has no access to detailed models of prosumers due to privacy concerns. Without the prosumers response model, the solution to the problem will be unreliable. Third, the computational complexity of NLP is generally quite high. Thus, solving this NLP-based problem is not realistic in practice. This work addresses this issue by employing a model-free DRL approach.

5.4 Deep Reinforcement Learning-Based Strategy

5.4.1 Overview

To solve the DP-BS problem, a model-free DRL algorithm is employed. The reasons for using DRL to solve the DP-BS problem are twofold: its adaptive capability and model-free nature. First, in a DRL paradigm, learning policy proceeds adaptively in response to changes in the dynamic environment, taking into account uncertainties, e.g., wholesale prices and net load change. Second, DRL methods can learn an optimal policy to make a decision through observable interactions without detailed system models. This model-free nature requires no knowledge of the detailed system models of each prosumer, i.e., privacy concerns can be resolved. Moreover, once trained, decision-making by DRL takes negligible computation time, typically less than one second, without the need to solve complex problems like NLP.

In a DRL problem, a decision-maker is called an agent, while a surrounding follower interacting with the agent is called an environment. The agent-environment interactions must be modeled as a Markov Decision Process (MDP) to apply DRL methods. The MDP consists of a set of a state, an action, a transition probability, and a reward function [161]. Following the transition probability, the environment's state s moves to a new state s' under an action of the agent a. The reward is a numerical score that evaluates whether the action taken is good or not. To choose appropriate actions, the agent learns a policy π_θ parameterized by θ, which is a way of decision-making that maximizes the reward function. The typical procedure of the RL framework at time t is for the agent to take action a_t in the environment based on the policy and then feed back the reward r_t and new state s_{t+1} to the agent. The DRL algorithm updates the policy based on the transition information (s_t, a_t, r_t, s_{t+1}).

5.4.2 Formulation of Markov Decision Process

The DP-BS problem is reformulated as the MDP to handle the problem by the DRL algorithm. Fig. 5.3 shows the proposed DRL framework for the DP-BS problem. The agent is the RA, and the environment is the ISO with the WEM, the battery power station, and the prosumers. Unlike the central NLP problem defined in Section 5.3.3, the proposed strategy only optimizes the retail prices and the usage of the RA's battery

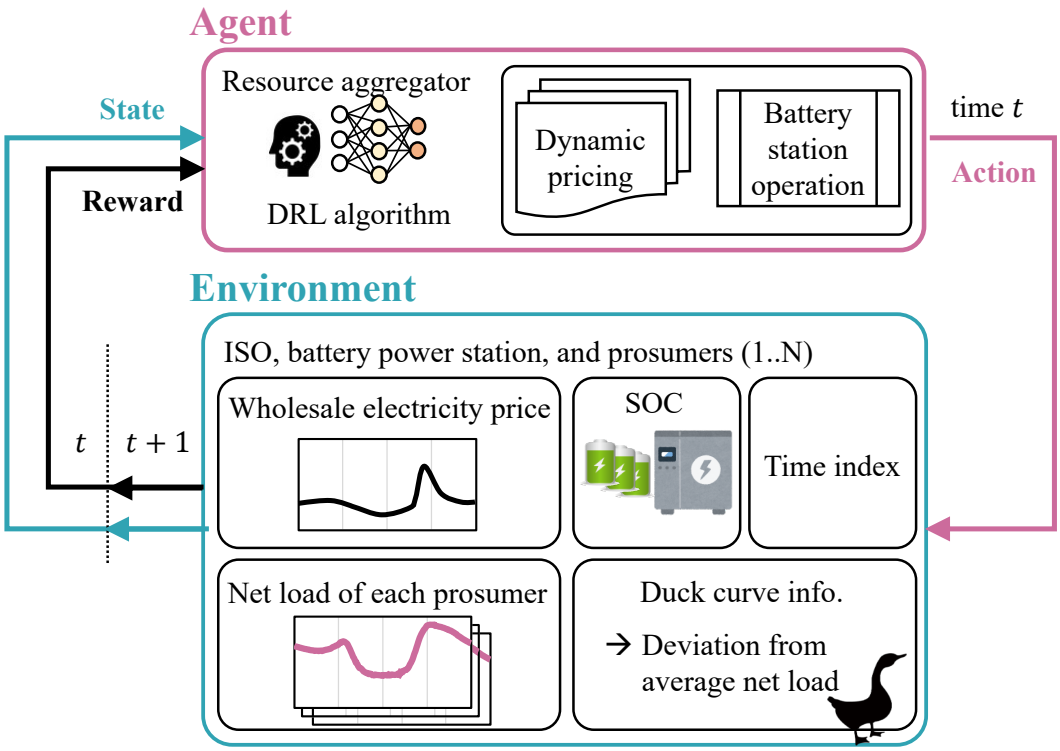

Figure 5.3: Illustration of DRL framework for DP-BS problem.

power station. Note that the formulation does not require a model of the transition probabilities since the proposed method is a model-free method that learns from data.

State

The state observations consist of seven kinds of information for the ISO, the prosumers, and the battery power station: time slot index $t' = t \mod T$, the wholesale electricity price μ_t, the net load for each prosumer $e^{net}_{t,n}$, the sum of the remaining curtailed energy $\Sigma^{t-1}_{k=1} e^{curt}_{k,n}$, SOC of the prosumer's battery / the battery power station $SOC^{bat}_{t,n}/SOC^{ra}_{t}$, and the deviation E^{dev}_t between the total net load and daily average net load calculated by the following equations.

$$E^{dev}_t = \sum_{n=1}^{N} e^{net}_{t,n} - E^{avg}_{day}, \ \forall t \tag{5.23}$$

$$E^{avg}_{day} = \sum_{t=1}^{T} \sum_{n=1}^{N} \frac{e^{net}_{t,n}}{N}, \tag{5.24}$$

where E^{avg}_{day} is the daily average of the net load. The deviation will provide an important basis for improving the duck curve. Note that this work assumes the value of the daily

average of the net load E_{day}^{avg} is known in advance. Although the specific forecasting method for E_{day}^{avg} is out-of-scope of this work, it can be forecasted directly using short-term forecasting that has already been developed in the literature [162], which has high accuracy. Accordingly, the state s_t at time t is set as

$$s_t = (t', \mu_t, e_{t,1}^{net}, \ldots, e_{t,N}^{net}, \Sigma_{k=1}^{t-1} e_{k,n}^{curt}, \ldots, \Sigma_{k=1}^{t-1} e_{k,n}^{curt}, SOC_{t,1}^{bat}, \ldots, SOC_{t,N}^{bat}, SOC_t^{ra}, E_t^{dev}). \tag{5.25}$$

Action

The RA decides the retail price for each prosumer $\lambda_{t,n}$ and the operation of the battery power station E_t^{ra}, aiming to maximize social welfare. This work assumes that the action space is continuous, and its range is constrained by the upper/lower bound as given in the formulas (5.15) and (5.19). Thus, the actions of the RA a_t at time t are given by

$$a_t = (\lambda_{t,1}, \ldots, \lambda_{t,N}, E_t^{ra}). \tag{5.26}$$

Reward Function

The objective of the RA agent is to improve social welfare. Hence, the following reward r_t at time t is used:

$$r_t = \omega_1 \cdot P_t^{ra} - \omega_2 \cdot \sum_{n=1}^{N} C_{t,n}^{pro} - (1 - \omega_1 - \omega_2) \cdot R_t^{duck}. \ \forall t \tag{5.27}$$

Note that the value of the weights ω_1 and ω_2 should be carefully chosen based on each entity's preferences. The adjustment method of the weights is out-of-scope of this work; however, the effect of the weight value choices is verified in Section 5.5.

The design of an appropriate reward function is critical to training and deploying the DRL agent efficiently. Here, four different reward terms are defined as R_t^{duck} to improve the duck curve (Table 5.1). The content of the duck curve is a large peak valley deviation of the net load and a steep change of net load for consecutive time slots. The power generation cost of power plants for flexibility is typically defined as a quadratic function of the net load [163]. Thus, The proposed reward term is a quadratic penalty function for deviation from a daily average, the net load difference for consecutive time slots, and the total net load. In addition, no reward term for the duck curve improvement R_t^{no} is defined to compare the effect of R_t^{duck}. The effectiveness of the proposed terms is validated in Section 5.5.

5.4.3 Algorithm Design

The agent is trained to solve the DP-BS problem using Proximal Policy Optimization (PPO) [164], which is one of the state-of-the-art DRL algorithms. This is because the

Table 5.1: Proposed reward terms for improving duck curve.

Reward	Description
$R_t^{avg} = (E_t^{net} - E_{day}^{avg})^2$	Quadratic penalty of deviation between current net load and daily average net load
$R_t^{diff} = (E_t^{net} - E_{t-1}^{net})^2$	Quadratic penalty of net load difference for consecutive time slots
$R_t^{quad} = (E_t^{net})^2$	Quadratic penalty of total net load
$R_t^{no} = 0$	No reward for duck curve improvement

performance of the PPO algorithm is compatible with or better than other state-of-the-art DRL algorithms in the DRL benchmark for tasks with a continuous action space.

PPO is an actor-critic policy gradient method parameterized by neural networks and improves the stabilization of learning by preventing a large policy update. To do this, the ratio of the old to the new policy is clipped, and a lower update bound, i.e., a pessimistic bound, is chosen. At the k-th iteration, the parameter θ of a policy π_θ is updated by

$$\underset{\theta}{\text{maximize}} \qquad \hat{\mathbb{E}}[L^C(\theta)], \tag{5.28}$$

$$L^C(\theta) = \min \begin{pmatrix} \dfrac{\pi_\theta(a|s)}{\pi_{\theta_k}(a|s)} A^{\pi_{\theta_k}}(s,a), \\ \text{clip}\left(\dfrac{\pi_\theta(a|s)}{\pi_{\theta_k}(a|s)}, 1-\varepsilon, 1+\varepsilon\right) \cdot A^{\pi_{\theta_k}}(s,a) \end{pmatrix}, \tag{5.29}$$

where $\hat{\mathrm{E}}$ denotes the empirical expectation over time steps and L^C is a surrogate objective. Where $A^{\pi_{\theta_k}}$ is the estimated advantage at the k-th iteration and ε is a hyperparameter that denotes the clipping range. The function clip() clips the policy update ratio within $[1-\varepsilon, 1+\varepsilon]$.

PPO is generally implemented with a neural network architecture that shares parameters between the policy and value functions. Here, the value function $V_{\theta_k}(s)$ parameterized by θ_k in the critic network is updated with respect to a mean-squared error of value function L^{VF}:

$$\underset{\theta}{\text{minimize}} \qquad \hat{\mathbb{E}}[L^{VF}(\theta)], \tag{5.30}$$

$$L^{VF}(\theta) = \big(V_\theta(s) - V^{targ}(s)\big)^2, \tag{5.31}$$

where $V^{targ}s$ is a target value from an old value function. Finally, the loss function of PPO L^{PPO} to be maximized is the sum of L^C, L^{VF}, and an entropy bonus S:

$$L^{PPO}(\theta) = \hat{\mathbb{E}}[L^C(\theta) - c_1 \cdot L^{VF}(\theta) + c_2 \cdot S[\pi_\theta(s)], \tag{5.32}$$

Algorithm 1: Training and deployment process of proposed DP-BS strategy based on PPO algorithm.

Initialize policy parameters θ;
Initialize training memory $\mathscr{M}$;
/* Training process */
for *episode = 1, max_episode* **do**
  Initialize the state of the hierarchical energy market; **for** $t = 1, T$ **do**
    Receive initial state s_t;
    Sample action a_t according to π_{θ_k};
    Calculate reward r_t and observe new state s_{t+1};
    Store transition (s_t, a_t, r_t, s_{t+1}) in training memory $\mathscr{M}$;
  Get a mini-batch from training memory $\mathscr{M}$;
  Estimate advantages $A^{\pi_{\theta_k}}$ using any advantage estimation algorithm;
  Optimize loss function L^{PPO} given by the equation (5.32);
  Update θ with any gradient optimizer;
/* Deployment process */
Deploy the trained policy π_θ for the RA;
Perform the DP-BS in the actual system based on π_θ;

where c_1 and c_2 are coefficients.

The pseudocode of the proposed strategy is presented in Algorithm 1. The RA agents in the PPO algorithm are first trained repeatedly, and then the trained agents are deployed in the RA and operate the DP-BS in real time.

5.5 Simulation Experiments

This section presents several simulation experiments to evaluate the proposed DP-BS strategy. The experimental setup and implementation details are first described, and then the performance of the proposed strategy is compared with other baselines in terms of the duck curve improvement and computational complexity. In addition, different scenarios are performed to access the system performance of the proposed strategy.

5.5.1 Simulation Setup

The targeted hierarchical energy market consists of an ISO, an RA, and ten prosumers ($N = 10$). The intervals of dynamic pricing and battery scheduling by the RA were set to 30 min, and an episode length was set to a day, i.e., $T = 48$. The wholesale electricity prices were obtained for the entire year of 2017 from a California ISO [165]. The parameters of the RA are given in Table 5.2. The purchase price κ_t is assumed to be the same value as the wholesale electricity price μ_t at that time. Both weights of ω_1 and ω_2 in the reward function (5.27) were set to 0.2 so that the duck curve improvement

Table 5.2: Parameter setting for RA and prosumers.

Parameter	Symbol	Value
Coefficient for price limit	ν	1.5
Battery capacity [kWh]	C^{ra}	300
Charging efficiency	η^{ra}_{ch}	0.9
Discharging efficiency	η^{ra}_{disch}	0.9
Maximum charging power rate	$C^{ra,rate}_{ch}$	0.3
Maximum discharging power rate	$C^{ra,rate}_{disch}$	0.3
Patience period [30 min]	S_n	6, 12, or 18
Coefficient for utility function	α_n	Rand. value within 1∼4
	β_n	1
Battery capacity [kWh]	C^{bat}_n	10, 15, or 20
PV panel size [kW]	-	10, 15, or 20
Charging efficiency	η^{bat}_{ch}	0.9
Discharging efficiency	η^{bat}_{disch}	0.9
Maximum charging power rate	$C^{bat,rate}_{ch}$	0.3
Maximum discharging power rate	$C^{bat,rate}_{disch}$	0.3
Coefficient for price threshold	h_n	0.5
Average total net load [kW]	-	50
Average ratio of inelastic load to total demand [%]	-	60
Average ratio of elastic load to total demand [%]	-	40

would be considered more important than other terms. However, the effect of weight is also explored in the simulation experiments.

On the other hand, the prosumers are simulated using the building's energy consumption profiles collected by the Building Data Genome Project 2 [166] and PV generation profiles provided by the California Distributed Generation Statistics [167]. The period under study for both profiles covers the entire year of 2017. Note that these datasets were resampled to 30 min intervals and were normalized according to the building site area. The other parameters of the prosumers are also given in Table 5.2. The profile of price elasticity $\xi_{t,n}$ ranges from -0.2 to -0.8 based on the literature [156], and it was manually generated.

The evaluation metrics for improving the duck curve are the average of the standard deviation of the net load, denoted by std, and peak-to-average ratio (PAR) of the total

Table 5.3: Parameters for PPO algorithm.

Parameter	Value
Number of environments in parallel	16
Number of episodes max_episode	20,000
Batch size	128
Training memory size $\mathscr{M}$	2048
Number of epochs	5
Clip range ε	0.1
Discount factor	0.995
Learning rate	0.002
Value function coefficient for loss function c_1	0.5
Entropy bonus coefficient for loss function c_2	3.6e-8
Number of hidden layers	2
Number of neurons	[256,256]
Activation function	ReLu

net load E_t^{net} for each day, as given by

$$std = \sqrt{\frac{\sum_{t=1}^{T} |E_t^{net} - \sum_{t=1}^{T} E_t^{net}/T|^2}{T-1}}, \tag{5.33}$$

$$PAR = \frac{\max(E_t^{net})}{\sum_{t=1}^{T} E_t^{net}/T}, \tag{5.34}$$

where $\max(E_t^{net})$ is a function that finds a maximum value for the total net load.

5.5.2 Implementation and Training Process

The simulator and PPO algorithm are implemented in `python`. The simulator was built on the OpenAI Gym framework [168], which allows us to easily observe the agent-environment interaction. Furthermore, the proposed DP-BS strategy was implemented using the python library `stable-baselines3` [169], which is an open-source DRL framework. The parameters of the PPO were fine-tuned using `Optuna` [170], and the obtained parameters are shown in Table 5.3. In this simulation setting, the neural network is shared for both policy and value functions in actor-critic.

It is worth mentioning that some implementation techniques were made for the DRL framework to stabilize the training and shorten the training time. The value of state observation and actions are normalized within [-1, +1] using min-max normalization. This state-action normalization is required to ensure that the neural network is not too dependent on the scale of the features [171]. The scale of the reward terms in the reward function (5.27) is aligned based on the standard score, which is calculated by the difference

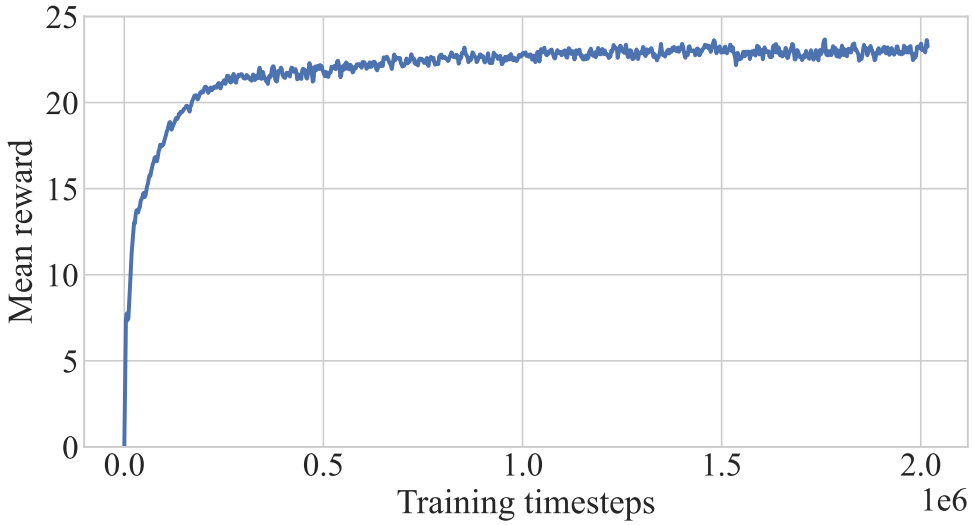

Figure 5.4: Typical training curve of proposed method.

between the value and the mean divided by the standard deviation. This standardization of rewards ensures that the RL agents can be tuned with similar hyperparameters. Firstly, hyperparameter tuning is carefully performed using the previous year's data for representative parameters that include the number of neurons, the number of parallel environments, learning rate, and discounted factor as important hyperparameters [172], and the same parameters are applied for all experiments with the aforementioned normalization and standardization technique.

The configurations of the test-bed machine include Intel(R) Core(TM) i7-10700 CPU @ 2.90 GHz, Nvidia GeForce RTX 2080 Ti GPU, and 16 GB DDR4 RAM. The average execution time of training the neural network is 29.4 min for 2M steps, and the typical training curve is shown in Fig. 5.4. After repeated training with the simulator using a one-month dataset, the trained agent is deployed and makes a decision for the DP-BS in real time.

5.5.3 Results

Comparison with Baseline Methods

First, the proposed strategy is compared with representative baseline methods to evaluate the performance of the duck curve improvement. In all, seven methods were compared:

- **Optimal:** NLP problem defined in Section 5.3.3 with R_t^{avg} over 24 h with 30 min resolution is solved every day. Note that the solution is obtained by the approaches proposed in the literature [173]. Assuming the ideal case of DP-BS, the agent already knows all future input and system configuration and directly controls the

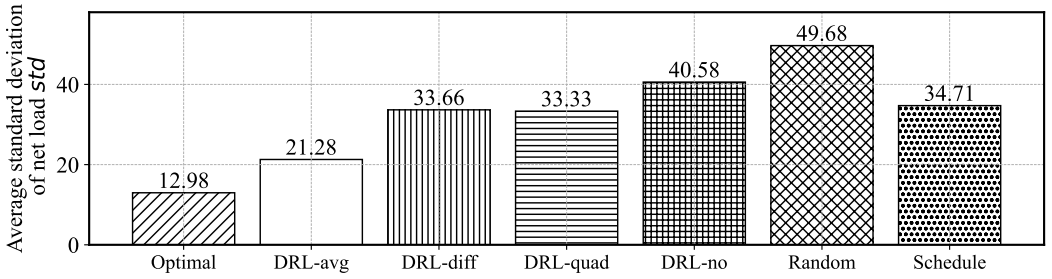

(a) Average standard deviation of net load.

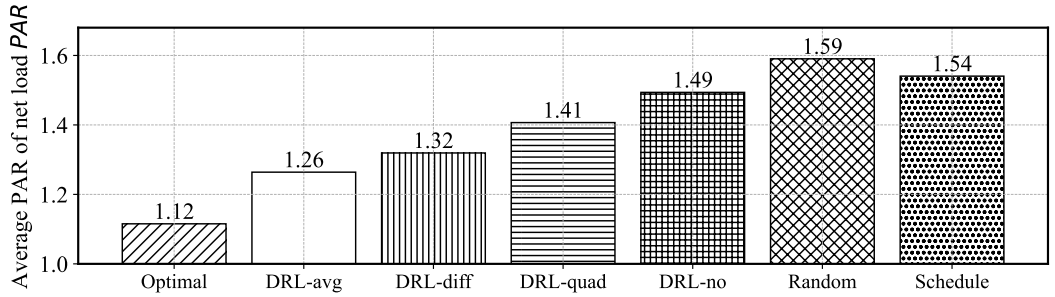

(b) Average PAR of net load.

Figure 5.5: Results of average standard deviation and average PAR of total net load for one week's simulation from August 1 to August 7 compared to baselines and DRL-based method with different reward functions.

prosumer's devices, which include the demand and the battery, as well as the RA's operation. This method provides the ideal solution and the potential of DP-BS.

- **DRL-avg:** Proposed DRL strategy trained with R_t^{avg}.
- **DRL-diff:** Proposed DRL strategy trained with R_t^{diff}.
- **DRL-quad:** Proposed DRL strategy trained with R_t^{quad}.
- **DRL-no:** Proposed DRL strategy trained with R_t^{no}.
- **Random:** Randomly determines the retail price and the battery operation.
- **Schedule:** Following the schedule; retail prices are set to 75% of the price range in peak hours (4 p.m.-9 p.m.), otherwise set to 25% of that. The battery station discharges at a constant rate of 0.2 C during the same peak hours and charges at 0.1 C during another period.

Fig. 5.5a and Fig. 5.5b show the results of standard deviation and PAR of total net load for one week from August 1 to August 7 in 2017. DRL methods were well-trained with the simulator and input profiles for the previous month from July 1 to July 31. From both figures, it can be seen that DRL-avg achieved the best standard deviation and PAR in all methods except for Optimal. In Fig. 5.5a, DRL-avg improved the standard deviation of the total net load by at least 36.2% over DRL-quad and up to 57.1% over Random. In Fig. 5.5b, DRL-avg improved the PAR of total net load by at least 4.5%

over DRL-diff and up to 20.8% over Random. Note that Optimal is an ideal baseline that has complete future knowledge and system models.Even though DRL-avg observes only the current state of the system, this method improved the duck curve in terms of both metrics, and its values were closest to Optimal.

Fig. 5.6 shows the detailed profiles on August 5 using DRL-avg. The upper figure shows the aggregated energy profiles of the RA and the prosumers, where the pre-net load, which is the net load scheduled originally, is calculated by $e_{t,n}^{net,org} = e_{t,n}^{inelas} + e_{t,n}^{elas} - e_{t,n}^{pv}$. The pre-demand, which is the demand scheduled originally, is calculated by $e_{t,n}^{dm,org} = e_{t,n}^{inelas} + e_{t,n}^{elas}$. In the upper figure, there are two bars next to each other every 30 min. The left bars are the energy profiles scheduled originally, and the right bars are the energy profiles after the DP-BS. The positive value means the energy demand including the total demand and battery charging, and the negative energy means the energy supply by PV generation and battery discharging. From the upper figure, comparing the pre-net load $\sum_n e_{t,n}^{net,org}$ to the actual net load E_t^{net}, the actual net load becomes larger than the pre-net load around the noon (11 a.m. - 3 p.m.) and smaller in the morning and the evening (7 a.m. and 4 p.m. - 8 p.m.). This shows that the duck curve that appeared in the pre-net load is smoothed out. The improvement of the duck curve resulted from the following two factors. First, the prosumer contributed to flattening the net load. The actual load demand $\sum_n e_{t,n}^{dm}$ is larger than the pre-net load $\sum_n e_{t,n}^{dm,org}$ around the noon (11 a.m. - 3 p.m.), comparing the two adjacent blue bars in the figure. This means that the prosumer shifted their demand to noon. At the same time, the prosumer charged the battery in the daytime and discharged it in the evening (4 p.m. - 7 p.m.), as represented by the red bars in the figure. Second, the RA's battery power station, which is shown by the green bars in the figure, was scheduled to charge around noon and discharge in the morning and evening. Moreover, the middle figure represents the results of dynamic pricing, and the average prices for all prosumers are plotted. The shaded area means the price deviation among prosumers, and the results show that the trend of the retail prices is similar for each prosumer. The retail prices were set relatively low from noon to 3 p.m. As a result, the prosumers are encouraged to shift their demand and charge the battery in the period 12 p.m. - 3 p.m. Finally, the lower figure shows the SOC profiles of the RA's battery. The DRL-avg method learned to charge when the pre-net load is relatively low (11 a.m.-2 p.m.) and discharge when the pre-net load is relatively high (4 p.m.-8 p.m.).

Fig. 5.7 shows the detailed profiles of prosumer #8 for August 6 to demonstrate how the demand and battery respond to the retail price. Similar to Fig. 5.6, in the upper figure, the left bars are the demand profiles scheduled originally, and the right bars are the actual demand and battery profiles after the retail price announcement; the lower figure shows the retail price of prosumer #8 given by the RA. Firstly, the RA raised the retail price from midnight to morning, decreased it until 3 p.m., and then raised the retail price again. According to the price change, the prosumer #8 shifted their demand from morning (especially around 8 a.m.) to daytime where PV generation is large. As for the

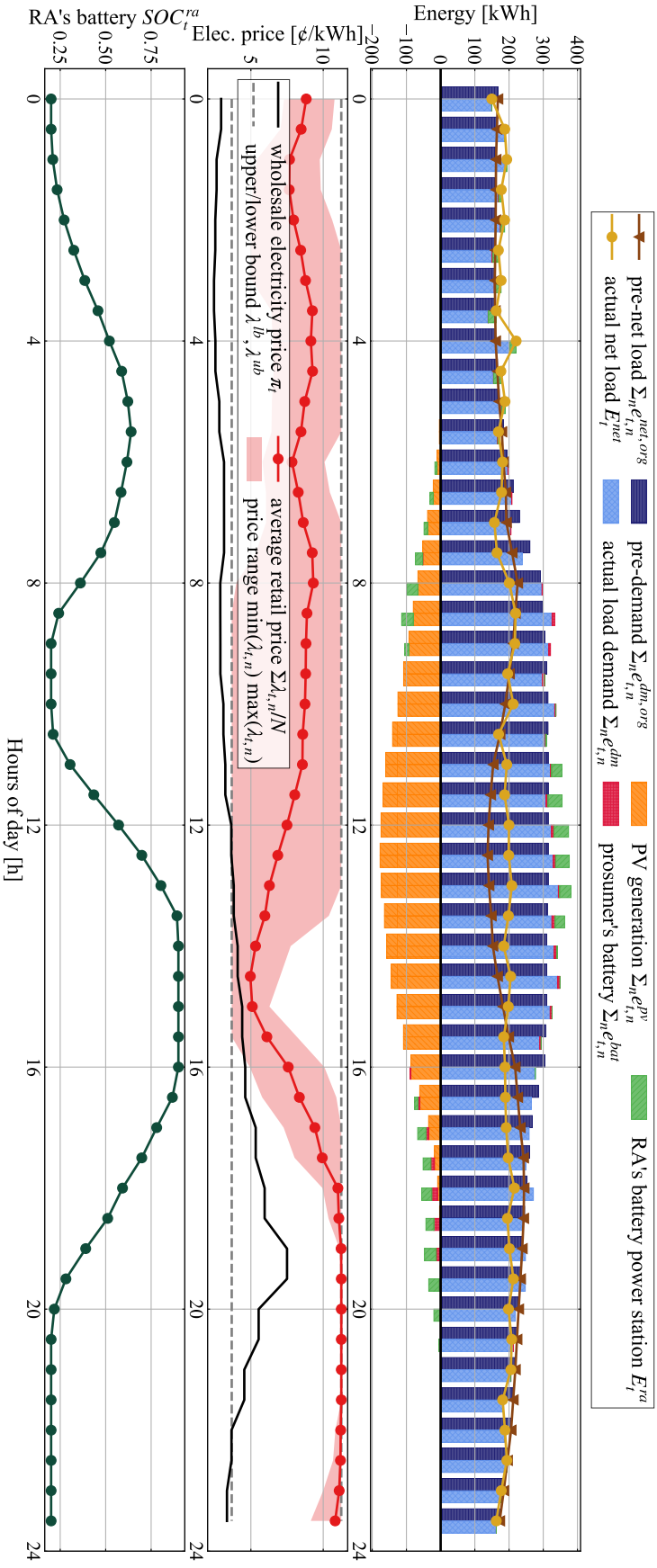

Figure 5.6: Result profile for August 5 using DRL-avg; (upper) energy and net load change every 30 min, (middle) wholesale electricity prices and average retail price for all prosumers with shaded area, indicating max-min values of retail prices at each time step, and (lower) SOC of the RA's battery.

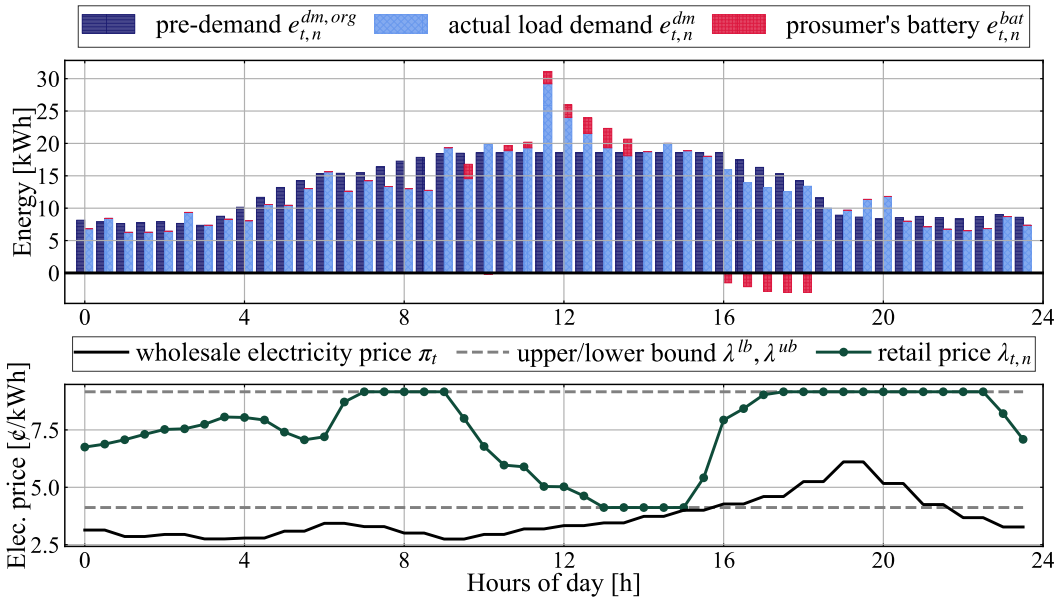

Figure 5.7: Detail profile of prosumer #8 for August 6 using DRL-avg; (upper) demand change and battery energy, (lower) retail price and wholesale price.

battery, the prosumer charged the battery during the lower retail price period (9 a.m. - 1 p.m.) and discharged it during the higher period (4 p.m. - 6 p.m.). Finally, the RA decided on the retail price that made the prosumer increase their net load around noon and reduce it during peak hours for improving the duck curve.

Fig. 5.8 shows the profiles of the net load and the RA's battery power station on another day (August 2). The results show that the DRL agent operated the RA's battery to discharge during peak period (9 a.m. and 6 p.m. - 9 p.m.) while charging to fill the net load valley until the battery capacity was full (11 a.m. 3 p.m.). From these results, the proposed strategy can make an effective decision on the retail prices and the RA's battery schedule in real-time for improving the duck curve.

Whole-Year Simulation

To evaluate the annual performance of the proposed DRL strategy, a whole-year simulation was conducted using five methods: Optimal, DRL-avg, DRL-no, Random, and Schedule. In DRL methods, the training of the agent was iterated every week using data from the previous month corresponding to that week. This iteration allows the agent to consider seasonal changes in the target system, such as wholesale electricity prices and net load change.

Fig. 5.9a and Fig. 5.9b are box plots that show the daily standard deviation and the daily PAR of the total net load for all of 2017. Consequently, the results show the same trend as in Fig. 5.5, and thus DRL-avg achieves reductions in both the standard deviation

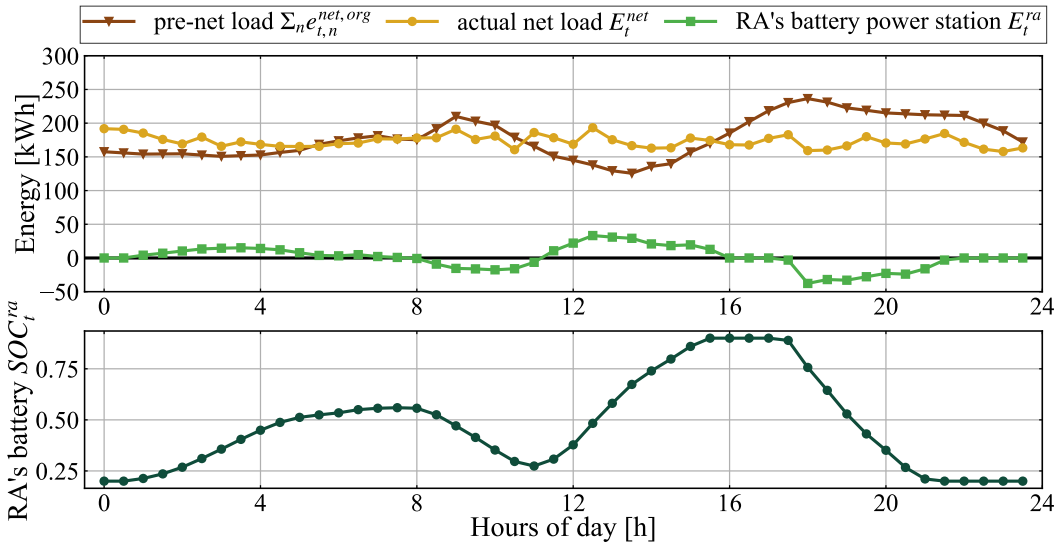

Figure 5.8: Result profile of RA for August 2 using DRL-avg; (upper) total net load change and energy of RA's battery power station, (lower) SOC of RA's battery power station.

and the PAR compared to other baselines. In the best case of DRL-avg, the standard deviation was 10.23, and the PAR was 1.1, which is 73.1% and 21.2% improvement over Random on the same day. Finally, the DRL-avg has the potential to improve the duck curve throughout the year.

Effect of Weight Coefficient

This section discusses the effect of a weight coefficient in the reward function (5.27) on system performance. The simulation period is one week from August 1 to 7 using the DRL-avg method. Both weight coefficients of the RA's profit ω_1 and the prosumer's cost ω_2 changed from 0.0 to 1.0 subject to $\omega_1 + \omega_2 \leq 1$, and the weight of the duck curve improvement was calculated by $(1 - \omega_1 - \omega_2)$. The large weights mean that the corresponding term is considered important.

Fig. 5.10 shows the heat maps of the system performance with different weights over one week: the standard deviation of the net load *std*, PAR of net load, total RA profit, and total prosumer cost. The lower left on the heat map, the greater the importance of duck curve improvement $(1 - \omega_1 - \omega_2)$. The light (yellow) squares mean better values, and the dark (navy) squares mean worse values. As can be seen from the *std* and PAR results, the performance trends of the standard deviation and PAR with respect to the weights are similar. A greater weight of RA's profit increases the standard deviation and PAR of the net load. In terms of the duck curve improvement, the best weight pair is $(\omega_1, \omega_2, 1 - \omega_1 - \omega_2) = (0.2, 0.3, 0.5)$. Furthermore, the relationship between the RA's

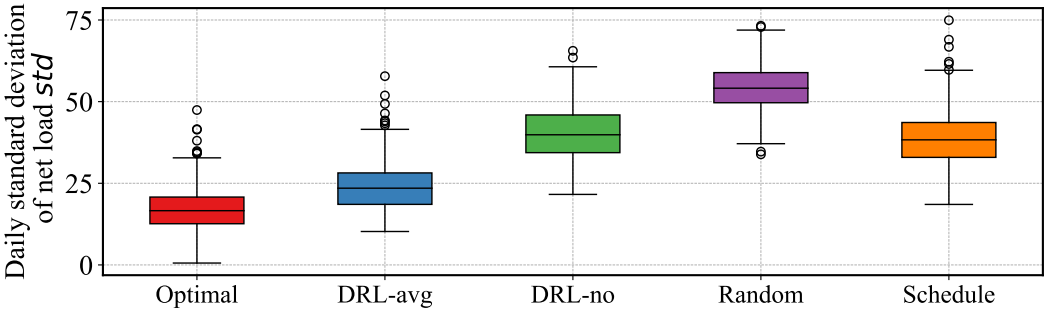

(a) Average standard deviation of net load.

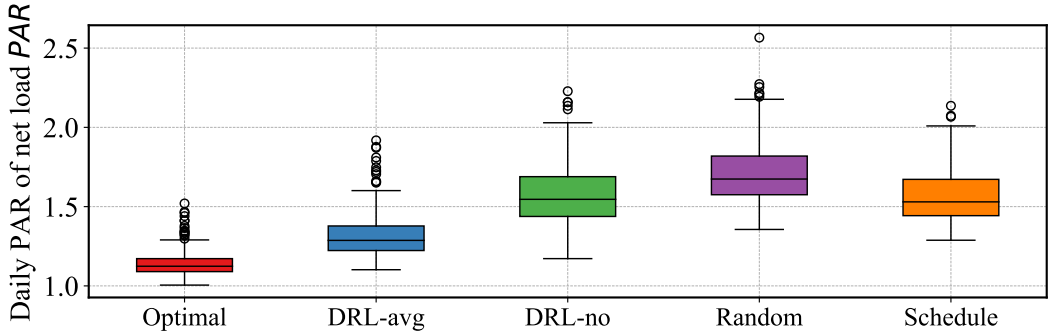

(b) Average PAR of net load.

Figure 5.9: Results of average standard deviation and average PAR for the 2017 whole-year simulation compared to baselines.

profit and the prosumer's cost is clearly a trade-off that can be controlled by adjusting the weight coefficients. Because both of them tend to be extreme values, the weights of RA's profit and the prosumer's cost should be chosen to be as equal as possible. As a result, the preferred operating point can be chosen by referring to these heat maps and adjusting the weight coefficient.

Effect of Battery Power Station Size

In this section, the effect of the battery power station's size on performance for the duck curve improvement is demonstrated. The simulation period is one week from August 1 to August 7 using the DRL-avg method. The battery power station's size was increased from 0 kWh to 1500 kWh.

Fig. 5.11a shows the standard deviation of the total net load for each battery power station size. As can be seen from the results up to 900 kWh, the larger the size of the battery, the more the standard deviation is reduced. However, the standard deviation did not decrease much at sizes larger than 900 kWh and increased in the cases of 1100 kWh and 1500 kWh. Fig. 5.11b is the PAR of the total net load for each battery power station

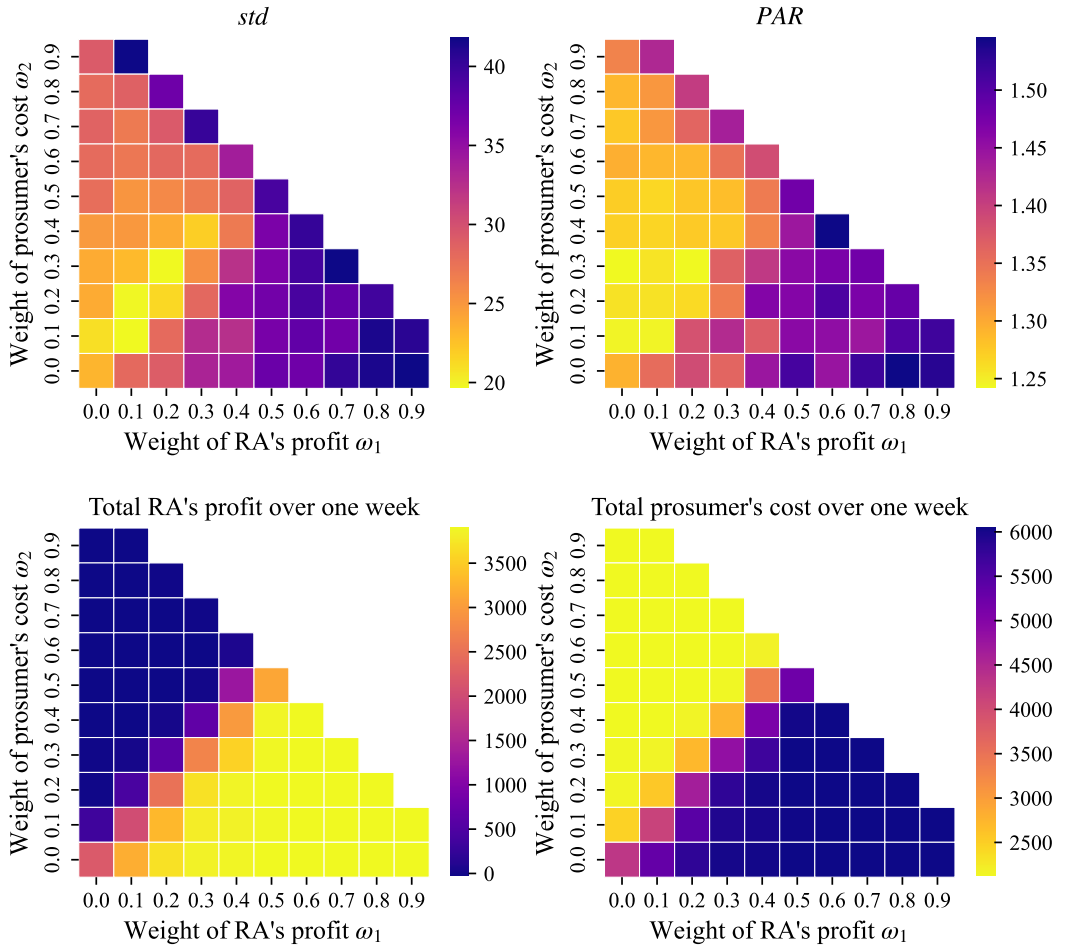

Figure 5.10: Results of system performance with different weights ω_1, ω_2 from Aug. 1 to 7 / Weight of duck curve improvement, standard deviation of net load, PAR of net load, total RA's profit, and total prosumer's cost are shown.

size. These results also show that further improvement with batteries larger than 900 kWh cannot be expected, and in fact, it was worse at 1500 kWh.

This is because the influence of charging and discharging the RA's battery power station on the overall system has increased. The maximum charging/discharging rate is 30% as shown in Table 5.1, i.e., a 1500 kWh battery can manipulate 300 kW for each time slot. This power rate is greater than the average net load of prosumers (also shown in Table 5.1). Besides, the RA's battery size is large enough to flatten the duck curve, and the agents tended to learn to charge and discharge at a large rate. Therefore, when the DRL agent fails to capture the prosumer's response with large errors and decides the battery operation with large charging/discharging, the value of the total net load is greatly affected.

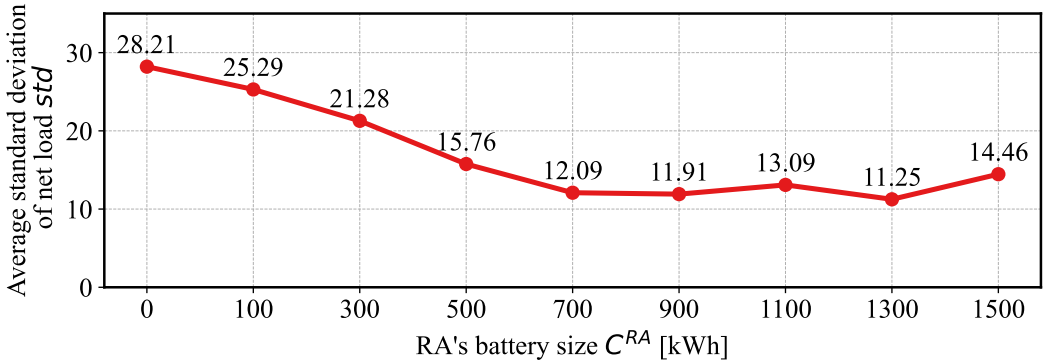

(a) Average standard deviation of net load.

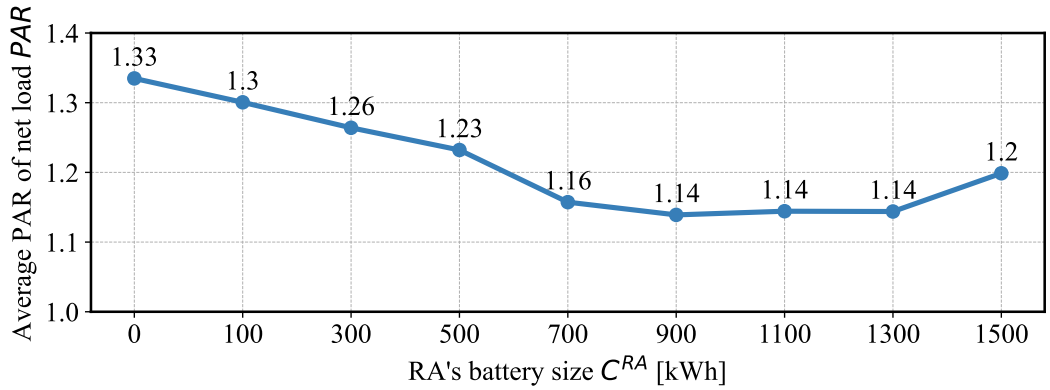

(b) Average PAR of net load

Figure 5.11: Results of average standard deviation and average PAR for one-week simulation from Aug. 1 to 7 with different battery sizes.

Finally, increasing the size of the battery is effective in improving the duck curve, but its effectiveness is limited. No matter how large the battery capacity, charge/discharge timing losses will occur depending on the current net load and wholesale electricity prices. In addition, the larger charge/discharge capacity of the battery also causes an increase in performance errors when the agent incorrectly estimates the response of the environment. Considering that the initial cost of batteries is negligibly expensive relative to the RA's profit, it is also necessary to determine the appropriate size of the battery system.

Time Scalability

This section compares the computational time using the baseline optimization method and the proposed DRL strategy with the different numbers of prosumers. Table 5.4 summarizes the average CPU time at execution (online), i.e., calculating the solution,

Table 5.4: Computational time for training and execution with different numbers of prosumers.

# of prosumers	Optimal (NLP)	Proposed (DRL)	
	Average CPU time at execution (online) [h]	Training time to converge (offline) [h]	Average CPU time at execution (online) [s]
10	0.28	0.16	2.28e-4
20	1.44	0.33	2.31e-4
30	2.94	0.56	2.34e-4
40	4.89	0.77	2.37e-4
50	7.57	0.96	2.39e-4

and the training time to converge the policy (offline). As for the online execution time, the optimization-based method increases the computational time exponentially with the number of prosumers, which is not practical due to the online time limitation ($\Delta t = 30min$). Meanwhile, the proposed DRL strategy takes only a few milliseconds, and it does not scale to the number of prosumers. The offline training time of the proposed DRL strategy remains in the practical range.

5.6 Summary

This chapter has investigated the strategy of the resource aggregator (RA) to improve the duck curve. The dynamic pricing and battery scheduling (DP-BS) problem is solved to maximize social welfare, including the RA's profit, the prosumer's cost, and the improvement of the duck curve. First, the DP-BS problem is formulated as a Markov decision process (MDP) for a hierarchical energy market model. Then, a model-free deep reinforcement learning (DRL) algorithm was proposed to learn the optimal strategy, determining the retail price for prosumers and battery power station charging/discharging. No prior knowledge of the prosumer's details and wholesale electricity prices is required to learn the strategy using the proposed method. Therefore, the proposed method not only addresses the uncertainty of the system but also protects the privacy of the prosumers. The simulation results show that the proposed method with the best reward function can reduce the standard deviation and the peak-to-average ratio (PAR) of the net load by up to 57.1% and 20.8%, respectively, compared to the baselines.

In future work, an optimal energy management method for prosumers should be integrated into the DP-BS problem. Then, a cooperative multi-agent system is considered to improve the duck curve more and more. Moreover, it is important to develop an algorithm for choosing an appropriate weight in the reward function based on the entity's

preferences interactively. Also, the integration with day-ahead scheduling and the detailed modeling of power systems to consider network constraints are one of the future directions for the practical implementation of the proposed approaches.

Chapter 6

Conclusion and Future Work

6.1 Conclusion

With the rapid increase of variable and uncontrollable renewable energy, the energy system requires more flexibility to mitigate grid challenges, such as demand and supply mismatch and high ramp rates. In particular, demand-side flexibility (DSF) is one of the promising solutions to address this issue, which refers to a capacity to change the demand load of end users from their current load patterns. The demand-side distributed energy resources (DER) such as a battery system and controllable demand could be adjusted through a demand response (DR) program that requests the engagement of end users by price signals or incentives. This interaction maximizes the acquisition and utilization of DSF. Therefore, this dissertation presents a system-level energy management methodology for DSF concerning the planning and real-time operation in the demand-side energy management system (EMS) and a DR strategy that exploits DSF for solving supply-side issues. To unlock the potential of DSF, this dissertation has addressed three research questions defined in Chapter 1.

Answer to Question 1: How could prosumers make a plan for their DERs to reduce system costs?

To estimate the annual system performance and achieve low system costs by considering relatively long-term effects such as battery degradation, an operational planning methodology is required for weekly and monthly periods. Chapter 2 mainly focuses on the battery degradation effects and has proposed a battery degradation-aware operational planning method for smart energy systems [32, 174]. The proposed method in this chapter aims to minimize battery degradation without increasing energy purchases. The simulation experiments are conducted for a whole year to evaluate the annual costs composed of the battery aging cost and the electricity costs. The simulation results show that the proposed method can reduce the battery aging costs by up to 14.1% compared

to the baseline. In addition, the proposed method can maintain the same amount of the purchased energy as the baseline. This means that the trade-off relationship between the battery aging cost and the energy purchase is completely improved. It is found that the trade-off improvement was caused by gradually charging the battery system and limiting the maximum battery charging level. Finally, The proposed method can find the optimal operating points of the battery system in terms of the annual costs. Compared to the state-of-the-art that implicitly reduces battery aging effects without specific battery degradation models, the proposed method can calculate the battery aging costs quantitatively and optimizes the battery operational plan considering both the battery aging costs and the electricity costs by introducing the detailed battery degradation model.

Answer to Question 2: How could prosumers operate their DERs in real-time to maximize their preferences?

The real-time operation of DERs by the EMS is required to compensate for the renewable fluctuation and reduce electricity costs. Chapter 3 has proposed a multi-time scale energy management framework for scheduling a battery system and shiftable appliances with variable PV generation [59, 175]. The simulation results show that the proposed framework can reduce electricity costs by up to 47.5% compared to baseline methods. Moreover, under the simulation settings and the computer platform, the proposed framework takes only 20 seconds of computational time at maximum, and it meets the computational requirement greatly. The sensitivity analysis of the proposed framework is also performed. The proposed framework is scalable to both the length of the planning period and the number of shiftable appliances, and the computational capability is sufficiently low for operating the local energy system. Moreover, the impact of PV forecasting error and battery capacity on the performance of the proposed framework is explored. The results show that the integration of accurate PV forecasting can reduce electricity costs significantly, and its effect is equivalent to a 30%-50% reduction in the size of the battery system. The state-of-the-art methods for real-time operation only consider either slow (hours-day) or fast (seconds-minutes) system dynamics and use measured data, a persistence model, or unoptimized models for PV forecasting, and it causes great energy loss. The proposed multi-time scale structure combined with a physics-based well-optimized PV forecasting can capture a mix of fast and slow system dynamics and enables managing both solution quality and computational complexity.

For the operation of the EMS, other objectives such as user preferences and comfort should be considered as well as electricity and system costs. Chapter 4 mainly focuses on thermal comfort maintained by the heating, ventilation, and air conditioning (HVAC) systems and has proposed a comfort-aware electrical and thermal energy management framework [103, 176]. The proposed framework in this chapter is the extended version of the framework proposed in Chapter 3 to schedule HVAC systems while estimating optimal temperature set points. The simulation results show that the proposed framework can solve the comprehensive optimization problem including a battery sys-

tem, shiftable appliances, and HVAC systems with little increase in computational time where the worst case is only one minute for each control loop. Also, compared to the implicit baseline method that does not optimize the HVAC schedule, the proposed method can find a better trade-off relationship between thermal comfort and electricity costs by changing the importance of each objective term. In the best case, the proposed method can achieve a 14.0% reduction in the electricity costs with the same thermal comfort levels as the baseline. Moreover, by conducting the simulation experiments with different battery sizes, the best size for the battery system can be chosen based on the obtained trade-offs. Note that many existing methods in the literature are limited to optimizing individual energy systems such as battery systems, appliances, and so on. Meanwhile, the proposed framework in Chapter 3 and 4 provides comprehensive solutions for general DERs that include PV generation, battery systems, and controllable demands. It has scalability for expansion to other demands and generations, such as wind turbines and EVs.

Answer to Question 3: How could an aggregator encourage prosumers to change their load into the desired shape?

To meet the grid purposes by exploiting DSF, the optimal design of the DR strategy is required. In Chapter 5, an optimal price-based DR strategy on dynamic pricing and battery scheduling has been proposed to improve the specific supply-side issue, the duck curve caused by massive PV introduction [120]. The proposed strategy is developed for an aggregator based on a model-free deep reinforcement learning (DRL) approach to maximize social welfare that includes improvements of the duck curve, profit maximization of the aggregator, and cost minimization of prosumers. The simulation experiments for a whole year are conducted to incorporate the seasonal effects on the PV generation. The results show that the proposed strategy with the carefully designed reward function can reduce the duck curve index: the standard deviation and peak-to-average ratio (PAR) of the net load are reduced by up to 57.1% and 20.8% compared to all baselines. In addition, the performance of the proposed method is close to the ideal method where all information and future input are known in advance. The detailed analysis shows that the proposed strategy often puts low prices and battery charging at noon while choosing high prices and battery discharging in the morning and evening. In this way, the proposed strategy mitigates the duck curve. On the other hand, the proposed method can control the importance of each objective term, and the trade-off relationship between them can be obtained. Finally, the proposed method can be applied to the real world to deal with the challenging issue, the duck curve, and it helps to introduce more solar energy in the energy system. The state-of-the-art strategies from the literature often need a detailed model of prosumers such as the system configuration and the prosumer preferences, and the prosumers would suffer from privacy leakage. It should be stressed that the proposed method can capture the complex prosumer responses to the prices without the detailed privacy information of the prosumers owing to the model-free DRL

approach.

6.2 Future Work

The works presented in this dissertation will be able to extend in several directions.

Uncertainty-aware techniques for operational planning

In Chapter 2, a battery degradation-aware operational planning method for DERs on the demand side has been proposed. The proposed method is solved with the deterministic scenario; however, demand and renewable generation are often affected by stochastic phenomena like abnormal weather conditions. To accurately estimate and design the system performance, it is quite important to deal with this uncertainty even in the planning stage. Therefore, one direction for future work is to develop an uncertainty-aware operational planning method incorporating the uncertainty consideration using stochastic and robust optimization paradigm [177].

Dynamic workload-based reliability improvement of battery system

In Chapter 2, the hourly load profiles were assumed, which are relatively static in change. Thus, the battery degradation addressed in this work is based on the slow and static case. However, battery reliability with respect to degradation and module temperature change is also affected by a more dynamic workload that rapidly changes in minute levels. Hence, another future work is to achieve a reliability improvement of battery systems in the face of dynamic workloads even in the planning phase.

Development of semi-fine-grained time scale for battery scheduling improvement

The two-time scale framework proposed in Chapter 3 does not adequately consider the impact of workload-dependent battery dynamics, including battery degradation and the complex SOC changes [178,179]. Moreover, the current two-time scales do not fit to incorporate them because of the unmatched planning period and time resolution with that battery dynamics. To address this issue, the fine-grained time scale will be divided into two scales: (1) a fine-grained (short-term) time scale with a 15-30 minute period and 1-second resolution to maintain photovoltaic (PV) forecasting accuracy and compensate for PV fluctuations, which is the same as the current one, and (2) a semi-fine-grained (mid-term) time scale with a detailed battery model to improve solution quality in the battery-related part. This mid-term time scale will have a 1-3 hour period and one or a few minutes of time resolution. Finally, the framework will have three-time scales: coarse-grained, semi-fine-grained, and fine-grained time scales, enabling reducing computational complexity while improving solution quality. On the other hand, splitting the

problem may raise another challenge: The mid-term optimization problem requires mid-term PV and demand forecasting techniques that this dissertation has not investigated. The further development of the multi-time scale structure and new forecasting approach is an important future direction.

Many-objective optimization for real-time operation

In Chapter 3 and 4, the real-time operation method for the EMS has been proposed to minimize electricity costs and maximize thermal comfort. In the real world, many different requirements exist, which include reducing carbon footprints, maximizing the self-consumption ratio of renewable generation, and maximizing service quality of EV transportation and appliance operation, etc. These objectives sometimes conflict with each other, and users may compromise with others to improve some metric. Generally, optimization problems with more than three or four objectives are called many-objective optimization, which is a kind of multi-objective optimization [180]. In the context of multi-objective optimization, the Pareto front that shows a set of effective solutions should be explored and constructed so that the users can choose their preferable solution. Thus, another future direction is to develop many-objective optimization that involves more than three objective terms. The construction method for the Pareto front in the real-time operation phase should be investigated.

Introduction of other types of DERs

Another important future work for Chapter 3 and 4 is introducing other DERs. Currently, the proposed framework in these chapters considers PV generation and directly optimizes battery systems, shiftable appliance schedules, and HVAC systems. However, other DERs such as wind generation, electric vehicles (EVs), and so on, are implicitly introduced to the framework as a part of energy profiles. To further enhance energy flexibility on demand sides, introducing more DERs should be explicitly considered with their different characteristics in the optimization.

Improvement of thermal modeling

In Chapter 4, adaptive temperature set points were estimated based on a linear regression model for Fanger's comfort indices. However, in practical cases, there is a gap between Fanger's indices and actual thermal comfort, i.e., comfortable indoor temperature estimated by Fanger's model is often far from optimal indoor temperature. Therefore, one future work will reflect the preferences of occupants based on collected information such as occupancy votes and sensing information in actual buildings. On the other hand, this work made a simple assumption on the HVAC system, e.g., the cost of performance (COP) is set to constant, while it is nonlinear. To capture the realistic behavior of

HVAC systems and optimize their operation effectively, an accurate HVAC model such as physics-based and data-driven models should be integrated into the framework.

Distributed energy management for multiple buildings

Chapter 4 has investigated the electrical and thermal energy management framework. The proposed method is limited to single HVAC scheduling mathematically as an approximation of the whole building's HVAC management. However, the actual building has multiple HVAC systems corresponding to multiple rooms with different thermal parameters and occupancy profiles. Ignoring these heterogeneities in HVAC scheduling is nonsense. Hence, distributed optimization approach for multiple HVAC systems and buildings considering their heterogeneous conditions should be developed in the future.

Fairness consideration in dynamic pricing

Chapter 5 has proposed the dynamic pricing and battery scheduling strategy for the aggregator, and the proposed strategy decides the retail electricity prices for each prosumer. In some cases, the proposed strategy may offer higher prices to one prosumer than others. However, if the prosumer does not accept the pricing, such unfair pricing may cause contract cancellation of the prosumer. Thus, one of the future works is to investigate a dynamic pricing scheme that takes fairness to prosumers into account. Moreover, the scenario where multiple aggregators and prosumers can choose preferable contracts should be investigated.

Incentive-based DR strategy

Chapter 5 has focused on a price-based DR program. Meanwhile, an incentive-based DR is also a promising way to encourage the demand side to change its load patterns. For such incentive-based DR programs, an aggregator contracts with the demand-side prosumer. The main advantage of the incentive-based DR program is to be able to easily estimate the amount of flexibility since the DSF exploitation is based on the contract and the request signals. In future work, a new strategy that integrates price-based and incentive-based DR programs should be investigated to maximize the exploitation of DSF.

Integration of different approaches for three questions towards holistic approach

Three research questions posed in Section 1.3 are closely related to each other. However, all approaches for these questions, shown in this dissertation, are independent. The important future work is to integrate them towards the holistic approach covering operational planning, real-time operation, and DR programs. To do so, the main challenge in the integration is how to deal with the trade-off relationship between their

performance. For example, the proposed method in the planning phase can obtain the long-term battery schedule to reduce battery degradation. This schedule can be used as reference-working points in the real-time operation stage. However, active battery degradation control leads to strict battery charge/discharge limitations and will degrade electricity costs in the real-time operation stage. On the other hand, for example, demand response (DR) programs and demand-side controls (planning and real-time operation) interact with each other. Once the behavior and solution of the demand-side energy management change, the optimal DR program will also be different. In addition, the DR programs affect all entity's criteria, i.e., the electricity costs and preferences for the demand side, the profitability of the aggregator, and the grid stabilization for the supply side. These criteria generally have a trade-off relationship, and finding a reasonable compromise among all entities is difficult. Hence, a methodology to integrate the results shown in this dissertation while balancing their trade-off relationship should be investigated in the future.

Bibliography

[1] I. Dincer, "Renewable energy and sustainable development: A crucial review," *Renewable and Sustainable Energy Reviews*, vol. 4, no. 2, pp. 157–175, 2000.

[2] N. L. Panwar, S. C. Kaushik, and S. Kothari, "Role of renewable energy sources in environmental protection: A review," *Renewable and Sustainable Energy Reviews*, vol. 15, no. 3, pp. 1513–1524, 2011.

[3] IRENA, *Renewable Energy Statics 2021*. Abu, Dubai: The International Renewable Energy Agency (IRENA), 2021.

[4] H. Ritchie, M. Roser, and P. Rosado, "Energy," *Our World in Data*, 2022.

[5] N. Phuangpornpitak and S. Tia, "Opportunities and challenges of integrating renewable energy in smart grid system," *Energy Procedia*, vol. 34, pp. 282–290, 2013.

[6] S. R. Sinsel, R. L. Riemke, and V. H. Hoffmann, "Challenges and solution technologies for the integration of variable renewable energy sources — a review," *Renewable Energy*, vol. 145, pp. 2271–2285, 2020.

[7] J. Lazar, *Teaching the "Duck" to Fly*. Montpelier, Vermont, U.S.: The Regulatory Assistance Project, 2016.

[8] B. Glensk and R. Madlener, "The value of enhanced flexibility of gas-fired power plants: A real options analysis," *Applied energy*, vol. 251, p. 113125, 2019.

[9] X. Fang, S. Misra, G. Xue, and D. Yang, "Smart grid — the new and improved power grid: A survey," *IEEE Communications Surveys & Tutorials*, vol. 14, no. 4, pp. 944–980, 2012.

[10] K. Bruninx, H. Pandžić, H. Le Cadre, and E. Delarue, "On the interaction between aggregators, electricity markets and residential demand response providers," *IEEE Transactions on Power Systems*, vol. 35, no. 2, pp. 840–853, 2020.

[11] F. D'Ettorre, M. Banaei, R. Ebrahimy, S. A. Pourmousavi, E. M. V. Blomgren, J. Kowalski, Z. Bohdanowicz, B. Łopaciuk-Gonczaryk, C. Biele, and H. Madsen, "Exploiting demand-side flexibility: State-of-the-art, open issues and social perspective," *Renewable and Sustainable Energy Reviews*, vol. 165, p. 112605, 2022.

[12] N. O'Connell, P. Pinson, H. Madsen, and M. O'Malley, "Benefits and challenges of electrical demand response: A critical review," *Renewable and Sustainable Energy Reviews*, vol. 39, pp. 686–699, 2014.

[13] IEA, *Heat Pumps*. Paris, France: International Energy Agency (IEA), 2022.

[14] ——, *Global EV Outlook 2022*. Paris, France: International Energy Agency (IEA), 2022.

[15] ——, *World Energy Outlook 2022*. Paris, France: International Energy Agency (IEA), 2022.

[16] P. P. Mishra, A. Latif, M. Emmanuel, Y. Shi, K. McKenna, K. Smith, and A. Nagarajan, "Analysis of degradation in residential battery energy storage systems for rate-based use-cases," *Applied Energy*, vol. 264, p. 114632, 2020.

[17] S. Althaher, P. Mancarella, and J. Mutale, "Automated demand response from home energy management system under dynamic pricing and power and comfort constraints," *IEEE Transactions on Smart Grid*, vol. 6, no. 4, pp. 1874–1883, 2015.

[18] W. Jung and F. Jazizadeh, "Human-in-the-loop HVAC operations: A quantitative review on occupancy, comfort, and energy-efficiency dimensions," *Applied Energy*, vol. 239, pp. 1471–1508, 2019.

[19] P. O. Fanger, *Thermal comfort. Analysis and applications in environmental engineering*. Copenhagen, Denmark: Danish Technical Press., 1970.

[20] R. Shi, S. Li, P. Zhang, and K. Y. Lee, "Integration of renewable energy sources and electric vehicles in V2G network with adjustable robust optimization," *Renewable Energy*, vol. 153, pp. 1067–1080, 2020.

[21] D. Pevec, J. Babic, A. Carvalho, Y. Ghiassi-Farrokhfal, W. Ketter, and V. Podobnik, "Electric vehicle range anxiety: An obstacle for the personal transportation revolution?" in *Proceedings of the 2019 4th International Conference on Smart and Sustainable Technologies (SpliTech)*, 2019, pp. 1–8.

[22] R. Pereira, J. Figueiredo, R. Melicio, V. M. F. Mendes, J. Martins, and J. C. Quadrado, "Consumer energy management system with integration of smart meters," *Energy Reports*, vol. 1, pp. 22–29, 2015.

[23] L. Jia and L. Tong, "Dynamic pricing and distributed energy management for demand response," *IEEE transactions on smart grid*, vol. 7, no. 2, pp. 1128–1136, 2016.

[24] A. Molina, A. Gabaldón, J. A. Fuentes, and C. Álvarez, "Implementation and assessment of physically based electrical load models: Application to direct load control residential programmes," *IEE Proceedings - Generation, Transmission and Distribution*, vol. 150, no. 1, pp. 61–66, 2003.

[25] M. Hosseini Imani, P. Niknejad, and M. R. Barzegaran, "The impact of customers' participation level and various incentive values on implementing emergency demand response program in microgrid operation," *International Journal of Electrical Power & Energy Systems*, vol. 96, pp. 114–125, 2018.

[26] A. Asadinejad and K. Tomsovic, "Optimal use of incentive and price based demand response to reduce costs and price volatility," *Electric Power Systems Research*, vol. 144, pp. 215–223, 2017.

[27] A. Faruqui, "The ethics of dynamic pricing," *Electricity Journal*, vol. 23, no. 6, pp. 13–27, 2010.

[28] X. Han, L. Lu, Y. Zheng, X. Feng, Z. Li, J. Li, and M. Ouyang, "A review on the key issues of the lithium ion battery degradation among the whole life cycle," *eTransportation*, vol. 1, p. 100005, 2019.

[29] W. Gu, Z. Wu, R. Bo, W. Liu, G. Zhou, W. Chen, and Z. Wu, "Modeling, planning and optimal energy management of combined cooling, heating and power microgrid: A review," *International Journal of Electrical Power & Energy Systems*, vol. 54, pp. 26–37, 2014.

[30] F. Ascione, N. Bianco, C. De Stasio, G. M. Mauro, and G. P. Vanoli, "Simulation-based model predictive control by the multi-objective optimization of building energy performance and thermal comfort," *Energy and Buildings*, vol. 111, pp. 131–144, 2016.

[31] P. Denholm, M. O'Connell, G. Brinkman, and J. Jorgenson, "Overgeneration from solar energy in california - a field guide to the duck chart," National Renewable Energy Laboratory (NREL), Golden, CO, USA, Tech. Rep., 2015.

[32] D. Watari, I. Taniguchi, and T. Onoye, "SOH aware system-level battery management methodology for decentralized energy network," *IEICE Transactions on Fundamentals of Electronics, Communications and Computer Sciences*, vol. E103.A, no. 3, pp. 596–604, 2020.

[33] IRENA, *Electricity Storage and Renewables: Costs and Markets to 2030*, Pablo Ralon, Michael Taylor and Andrei Ilas, Harald Diaz-Bone, and Kai-Philipp Kairies, Ed. Abu, Dubai: The International Renewable Energy Agency (IRENA), 2017.

[34] M. Ecker, N. Nieto, S. Käbitz, J. Schmalstieg, H. Blanke, A. Warnecke, and D. U. Sauer, "Calendar and cycle life study of Li(NiMnCo)O2-based 18650 lithium-ion batteries," *Journal of Power Sources*, vol. 248, pp. 839–851, 2014.

[35] P. Keil, S. F. Schuster, J. Wilhelm, J. Travi, A. Hauser, R. C. Karl, and A. Jossen, "Calendar aging of Lithium-Ion batteries," *Journal of the Electrochemical Society*, vol. 163, no. 9, p. A1872, 2016.

[36] M. Dubarry, V. Svoboda, R. Hwu, and B. Y. Liaw, "Capacity and power fading mechanism identification from a commercial cell evaluation," *Journal of power sources*, vol. 165, no. 2, pp. 566–572, 2007.

[37] S. B. Peterson, J. Apt, and J. F. Whitacre, "Lithium-ion battery cell degradation resulting from realistic vehicle and vehicle-to-grid utilization," *Journal of power sources*, vol. 195, no. 8, pp. 2385–2392, 2010.

[38] S. F. Schuster, T. Bach, E. Fleder, J. Müller, M. Brand, G. Sextl, and A. Jossen, "Nonlinear aging characteristics of lithium-ion cells under different operational conditions," *Journal of Energy Storage*, vol. 1, pp. 44–53, 2015.

[39] A. Millner, "Modeling lithium ion battery degradation in electric vehicles," in *Proceedings of the 2010 IEEE Conference on Innovative Technologies for an Efficient and Reliable Electricity Supply (CITRES)*, 2010, pp. 349–356.

[40] Y. Zhang, N. Rahbari-Asr, J. Duan, and M.-Y. Chow, "Day-Ahead smart grid cooperative distributed energy scheduling with renewable and storage integration," *IEEE Transactions on Sustainable Energy*, vol. 7, no. 4, pp. 1739–1748, 2016.

[41] H. Kanchev, D. Lu, F. Colas, V. Lazarov, and B. Francois, "Energy management and operational planning of a microgrid with a PV-Based active generator for smart grid applications," *IEEE Transactions on Industrial Electronics*, vol. 58, no. 10, pp. 4583–4592, 2011.

[42] J. Silvente and L. G. Papageorgiou, "An MILP formulation for the optimal management of microgrids with task interruptions," *Applied Energy*, vol. 206, pp. 1131–1146, 2017.

[43] P. Harsha and M. Dahleh, "Optimal management and sizing of energy storage under dynamic pricing for the efficient integration of renewable energy," *IEEE Transactions on Power Systems*, vol. 30, no. 3, pp. 1164–1181, 2015.

[44] N. Michelusi, L. Badia, R. Carli, L. Corradini, and M. Zorzi, "Energy management policies for Harvesting-Based wireless sensor devices with battery degradation," *IEEE Transactions on Communications*, vol. 61, no. 12, pp. 4934–4947, 2013.

[45] K. Vatanparvar and M. A. A. Faruque, "Electric vehicle optimized charge and drive management," *ACM Transactions on Design Automation of Electronic Systems*, vol. 23, no. 1, pp. 1–25, 2017.

[46] S. Park, L. Zhang, and S. Chakraborty, "Battery assignment and scheduling for drone delivery businesses," in *Proceedings of the 2017 IEEE/ACM International Symposium on Low Power Electronics and Design (ISLPED)*, 2017, pp. 1–6.

[47] S. Kato, I. Taniguchi, M. Fukui, and K. Sakakibara, "A battery degradation aware optimal power distribution on decentralized energy network," in *Proceedings of the 10th IEEE International NEWCAS Conference*, 2012, pp. 409–412.

[48] G. K. Prasad and C. D. Rahn, "Model based identification of aging parameters in lithium ion batteries," *Journal of Power Sources*, vol. 232, pp. 79–85, 2013.

[49] Y.-H. Chiang, W.-Y. Sean, and J.-C. Ke, "Online estimation of internal resistance and open-circuit voltage of lithium-ion batteries in electric vehicles," *Journal of Power Sources*, vol. 196, no. 8, pp. 3921–3932, 2011.

[50] D. Andre, C. Appel, T. Soczka-Guth, and D. U. Sauer, "Advanced mathematical methods of SOC and SOH estimation for lithium-ion batteries," *Journal of Power Sources*, vol. 224, pp. 20–27, 2013.

[51] H.-T. Lin, T.-J. Liang, and S.-M. Chen, "Estimation of battery state of health using probabilistic neural network," *IEEE Transactions on Industrial Informatics*, vol. 9, no. 2, pp. 679–685, 2013.

[52] G. Ning and B. N. Popov, "Cycle life modeling of Lithium-Ion batteries," *Journal of the Electrochemical Society*, vol. 151, no. 10, p. A1584, 2004.

[53] Y. Cui, C. Du, G. Yin, Y. Gao, L. Zhang, T. Guan, L. Yang, and F. Wang, "Multi-stress factor model for cycle lifetime prediction of lithium ion batteries with shallow-depth discharge," *Journal of Power Sources*, vol. 279, pp. 123–132, 2015.

[54] B. Xu, A. Oudalov, A. Ulbig, G. Andersson, and D. S. Kirschen, "Modeling of Lithium-Ion battery degradation for cell life assessment," *IEEE Transactions on Smart Grid*, vol. 9, no. 2, pp. 1131–1140, 2018.

[55] I. Taniguchi, K. Sakakibara, S. Kato, and M. Fukui, "Network topology and battery size exploration for decentralized energy network with MIP base power flow optimization," *IEICE Transactions on Fundamentals of Electronics, Communications and Computer Sciences*, vol. E96.A, no. 7, pp. 1617–1624, 2013.

[56] A. Hirsch, Y. Parag, and J. Guerrero, "Microgrids: A review of technologies, key drivers, and outstanding issues," *Renewable and Sustainable Energy Reviews*, vol. 90, pp. 402–411, 2018.

[57] Y. Li, D. M. Vilathgamuwa, and P. C. Loh, "Design, analysis, and real-time testing of a controller for multibus microgrid system," *IEEE Transactions on Power Electronics*, vol. 19, no. 5, pp. 1195–1204, 2004.

[58] Y. Xu, J. Zhang, W. Wang, A. Juneja, and S. Bhattacharya, "Energy router: Architectures and functionalities toward energy internet," in *Proceedings of the 2011 IEEE International Conference on Smart Grid Communications (SmartGridComm)*. ieeexplore.ieee.org, 2011, pp. 31–36.

[59] D. Watari, I. Taniguchi, H. Goverde, P. Manganiello, E. Shirazi, F. Catthoor, and T. Onoye, "Multi-time scale energy management framework for smart PV systems mixing fast and slow dynamics," *Applied Energy*, vol. 289, p. 116671, 2021.

[60] Varun, R. Prakash, and I. K. Bhat, "Energy, economics and environmental impacts of renewable energy systems," *Renewable and Sustainable Energy Reviews*, vol. 13, no. 9, pp. 2716–2721, 2009.

[61] X. Liang, "Emerging power quality challenges due to integration of renewable energy sources," *IEEE Transactions on Industry Applications*, vol. 53, no. 2, pp. 855–866, 2017.

[62] H. Lund, P. A. Østergaard, D. Connolly, and B. V. Mathiesen, "Smart energy and smart energy systems," *Energy*, vol. 137, pp. 556–565, 2017.

[63] C. Chen, S. Duan, T. Cai, B. Liu, and G. Hu, "Smart energy management system for optimal microgrid economic operation," *IET Renewable Power Generation*, vol. 5, no. 3, pp. 258–267, 2011.

[64] D. Mariano-Hernández, L. Hernández-Callejo, A. Zorita-Lamadrid, O. Duque-Pérez, and F. Santos García, "A review of strategies for building energy management system: Model predictive control, demand side management, optimization, and fault detect & diagnosis," *Journal of Building Engineering*, vol. 33, p. 101692, 2021.

[65] L. Olatomiwa, S. Mekhilef, M. S. Ismail, and M. Moghavvemi, "Energy management strategies in hybrid renewable energy systems: A review," *Renewable and Sustainable Energy Reviews*, vol. 62, pp. 821–835, 2016.

[66] A. Merabet, K. Tawfique Ahmed, H. Ibrahim, R. Beguenane, and A. M. Y. M. Ghias, "Energy management and control system for laboratory scale microgrid based Wind-PV-Battery," *IEEE Transactions on Sustainable Energy*, vol. 8, no. 1, pp. 145–154, 2017.

[67] D. Azuatalam, K. Paridari, Y. Ma, M. Förstl, A. C. Chapman, and G. Verbič, "Energy management of small-scale PV-battery systems: A systematic review considering practical implementation, computational requirements, quality of input data and battery degradation," *Renewable and Sustainable Energy Reviews*, vol. 112, pp. 555–570, 2019.

[68] A. Szumanowski and Y. Chang, "Battery management system based on battery nonlinear dynamics modeling," *IEEE Transactions on Vehicular Technology*, vol. 57, no. 3, pp. 1425–1432, 2008.

[69] Y. Zhang, R. Wang, T. Zhang, Y. Liu, and B. Guo, "Model predictive control-based operation management for a residential microgrid with considering forecast uncertainties and demand response strategies," *IET Generation, Transmission and Distribution*, vol. 10, no. 10, pp. 2367–2378, 2016.

[70] T. Terlouw, T. AlSkaif, C. Bauer, and W. van Sark, "Optimal energy management in all-electric residential energy systems with heat and electricity storage," *Applied Energy*, vol. 254, p. 113580, 2019.

[71] Q. Lu, Z. Zhang, and S. Lü, "Home energy management in smart households: Optimal appliance scheduling model with photovoltaic energy storage system," *Energy Reports*, vol. 6, pp. 2450–2462, 2020.

[72] A. Anees and Y.-P. P. Chen, "True real time pricing and combined power scheduling of electric appliances in residential energy management system," *Applied Energy*, vol. 165, pp. 592–600, 2016.

[73] O. Erdinc, "Economic impacts of small-scale own generating and storage units, and electric vehicles under different demand response strategies for smart households," *Applied Energy*, vol. 126, pp. 142–150, 2014.

[74] K. C. Sou, J. Weimer, H. Sandberg, and K. H. Johansson, "Scheduling smart home appliances using mixed integer linear programming," in *Proceedings of the 2011 50th IEEE Conference on Decision and Control and European Control Conference (ECC)*, 2011, pp. 5144–5149.

[75] D. Anagnostos, T. Schmidt, S. Cavadias, D. Soudris, J. Poortmans, and F. Catthoor, "A method for detailed, short-term energy yield forecasting of photovoltaic installations," *Renewable Energy*, vol. 130, pp. 122–129, 2019.

[76] M. Chen and G. A. Rincon-Mora, "Accurate electrical battery model capable of predicting runtime and I-V performance," *IEEE Transactions on Energy Conversion*, vol. 21, no. 2, pp. 504–511, 2006.

[77] B. Lokeshgupta and S. Sivasubramani, "Multi-objective home energy management with battery energy storage systems," *Sustainable Cities and Society*, vol. 47, p. 101458, 2019.

[78] S. Dorahaki, R. Dashti, and H. R. Shaker, "Optimal energy management in the smart microgrid considering the electrical energy storage system and the demand-side energy efficiency program," *Journal of Energy Storage*, vol. 28, p. 101229, 2020.

[79] R. Godina, E. M. G. Rodrigues, E. Pouresmaeil, J. C. O. Matias, and J. P. S. Catalão, "Model predictive control home energy management and optimization strategy with demand response," *NATO Advanced Science Institutes Series E: Applied Sciences*, vol. 8, no. 3, p. 408, 2018.

[80] A. Parisio, C. Wiezorek, T. Kyntäjä, J. Elo, K. Strunz, and K. H. Johansson, "Cooperative MPC-based energy management for networked microgrids," *IEEE Transactions on Smart Grid*, vol. 8, no. 6, pp. 3066–3074, 2017.

[81] R. Carli, G. Cavone, S. Ben Othman, and M. Dotoli, "IoT based architecture for model predictive control of HVAC systems in smart buildings," *Sensors*, vol. 20, no. 3, 2020.

[82] L. K. Gan, P. Zhang, J. Lee, M. A. Osborne, and D. A. Howey, "Data-driven energy management system with gaussian process forecasting and MPC for interconnected microgrids," *IEEE Transactions on Sustainable Energy*, vol. 12, no. 1, pp. 695–704, 2021.

[83] Y. Zhang, A. Lundblad, P. E. Campana, F. Benavente, and J. Yan, "Battery sizing and rule-based operation of grid-connected photovoltaic-battery system: A case study in sweden," *Energy Conversion & Management*, vol. 133, pp. 249–263, 2017.

[84] D. Arcos-Aviles, J. Pascual, L. Marroyo, P. Sanchis, and F. Guinjoan, "Fuzzy logic-based energy management system design for residential grid-connected microgrids," *IEEE Transactions on Smart Grid*, vol. 9, no. 2, pp. 530–543, 2018.

[85] A. Abreu, R. Bourdais, and H. Guéguen, "Hierarchical model predictive control for building energy management of hybrid systems," *IFAC-PapersOnLine*, vol. 51, no. 16, pp. 235–240, 2018.

[86] A. Lefort, R. Bourdais, G. Ansanay-Alex, and H. Guéguen, "Hierarchical control method applied to energy management of a residential house," *Energy and Buildings*, vol. 64, pp. 53–61, 2013.

[87] X. Jin, J. Wu, Y. Mu, M. Wang, X. Xu, and H. Jia, "Hierarchical microgrid energy management in an office building," *Applied Energy*, vol. 208, pp. 480–494, 2017.

[88] M. Elkazaz, M. Sumner, E. Naghiyev, S. Pholboon, R. Davies, and D. Thomas, "A hierarchical two-stage energy management for a home microgrid using model predictive and real-time controllers," *Applied Energy*, vol. 269, p. 115118, 2020.

[89] L. Ferrarini, G. Mantovani, and G. T. Costanzo, "A distributed model predictive control approach for the integration of flexible loads, storage and renewables," in *Proceedings of the 2014 IEEE 23rd International Symposium on Industrial Electronics (ISIE)*. IEEE, 2014, pp. 1700–1705.

[90] A.-L. Klingler and L. Teichtmann, "Impacts of a forecast-based operation strategy for grid-connected PV storage systems on profitability and the energy system," *Solar Energy*, vol. 158, pp. 861–868, 2017.

[91] C. E. García, D. M. Prett, and M. Morari, "Model predictive control: Theory and practice—a survey," *Automatica: the journal of IFAC, the International Federation of Automatic Control*, vol. 25, no. 3, pp. 335–348, 1989.

[92] G. Ramos Ruiz, E. Lucas Segarra, and C. Fernández Bandera, "Model predictive control optimization via genetic algorithm using a detailed building energy model," *Energies*, vol. 12, no. 1, p. 34, 2018.

[93] A. Parisio, E. Rikos, and L. Glielmo, "A model predictive control approach to microgrid operation optimization," *IEEE Transactions on Control Systems Technology*, vol. 22, no. 5, pp. 1813–1827, 2014.

[94] M. Diagne, M. David, P. Lauret, J. Boland, and N. Schmutz, "Review of solar irradiance forecasting methods and a proposition for small-scale insular grids," *Renewable and Sustainable Energy Reviews*, vol. 27, pp. 65–76, 2013.

[95] H. Goverde, D. Anagnostos, B. Herteleer, J. Govaerts, K. Baert, B. Aldalali, F. Catthoor, J. Driesen, and J. Poortmans, "Model requirements for accurate short term energy yield predictions during fast-varying weather conditions," in *Proceedings of the 31st European Photovoltaic Solar Energy Conference and Exhibition (EUPVSEC)*, 2015, pp. 1556–1559.

[96] K. Lappalainen and S. Valkealahti, "Analysis of shading periods caused by moving clouds," *Solar Energy*, vol. 135, pp. 188–196, 2016.

[97] H. Goverde, D. Anagnostos, J. Govaerts, P. Manganiello, E. Voroshazi, J. Szlufcik, F. Catthoor, J. Poortmans, K. Baert, and J. Driesen, "Accurately simulating PV energy production: Exploring the impact of module build up," in *Proceedings of the 33rd European Photovoltaics Science and Engineering Conference (EUPVSEC)*, 2017, pp. 1643–1646.

[98] N. Sadeghianpourhamami, T. Demeester, D. F. Benoit, M. Strobbe, and C. Develder, "Modeling and analysis of residential flexibility: Timing of white good usage," *Applied Energy*, vol. 179, pp. 790–805, 2016.

[99] A. Wächter and L. T. Biegler, "On the implementation of an interior-point filter line-search algorithm for large-scale nonlinear programming," *Mathematical Programming. A Publication of the Mathematical Programming Society*, vol. 106, no. 1, pp. 25–57, 2006.

[100] Kansai Electric Power Co., Inc., "The Time-of-Use electricity price in the kansai electric power company in japan," https://kepco.jp/ryokin/menu/jikanbetsu/, accessed: 2022-12-1.

[101] A. S. N. Uttama Nambi, A. Reyes Lua, and V. R. Prasad, "LocED: Location-aware energy disaggregation framework," in *Proceedings of the 2nd ACM International Conference on Embedded Systems for Energy-Efficient Built Environments (BuildSys)*, 2015, pp. 45–54.

[102] A. Reinhardt, P. Baumann, D. Burgstahler, M. Hollick, H. Chonov, M. Werner, and R. Steinmetz, "On the accuracy of appliance identification based on distributed load metering data," in *Proceedings of the 2012 Sustainable Internet and ICT for Sustainability (SustainIT)*, 2012, pp. 1–9.

[103] D. Watari, I. Taniguchi, F. Catthoor, C. Marantos, K. Siozios, E. Shirazi, D. Soudris, and T. Onoye, "Thermal-comfort aware online co-scheduling framework for HVAC, battery systems, and appliances in smart buildings," *IEICE Transactions on Fundamentals of Electronics, Communications and Computer Sciences*, vol. E106-A, no. 5, pp. –, 2022 (to appear).

[104] G. Serale, M. Fiorentini, A. Capozzoli, D. Bernardini, and A. Bemporad, "Model predictive control (MPC) for enhancing building and HVAC system energy efficiency: Problem formulation, applications and opportunities," *Energies*, vol. 11, no. 3, p. 631, 2018.

[105] C. Marantos, K. Siozios, and D. Soudris, "Rapid prototyping of Low-Complexity orchestrator targeting CyberPhysical systems: The Smart-Thermostat usecase,"

IEEE Transactions on Control Systems Technology, vol. 28, no. 5, pp. 1831–1845, 2020.

[106] F. A. Qayyum, M. Naeem, A. S. Khwaja, A. Anpalagan, L. Guan, and B. Venkatesh, "Appliance scheduling optimization in smart home networks," *IEEE Access*, vol. 3, pp. 2176–2190, 2015.

[107] A. C. Duman, H. S. Erden, Ö. Gönül, and Ö. Güler, "A home energy management system with an integrated smart thermostat for demand response in smart grids," *Sustainable Cities and Society*, vol. 65, p. 102639, 2021.

[108] M. Ostadijafari, A. Dubey, Y. Liu, J. Shi, and N. Yu, "Smart building energy management using nonlinear economic model predictive control," in *Proceedings of the 2019 IEEE Power & Energy Society General Meeting (PESGM)*, 2019, pp. 1–5.

[109] T. Cui, S. Chen, Y. Wang, Q. Zhu, S. Nazarian, and M. Pedram, "An optimal energy co-scheduling framework for smart buildings," *Integration*, vol. 58, no. May, pp. 528–537, 2017.

[110] K. X. Perez, M. Baldea, and T. F. Edgar, "Integrated HVAC management and optimal scheduling of smart appliances for community peak load reduction," *Energy and Buildings*, vol. 123, pp. 34–40, 2016.

[111] M. Killian, M. Zauner, and M. Kozek, "Comprehensive smart home energy management system using mixed-integer quadratic-programming," *Applied Energy*, vol. 222, pp. 662–672, 2018.

[112] F. Ferracuti, A. Fonti, L. Ciabattoni, S. Pizzuti, A. Arteconi, L. Helsen, and G. Comodi, "Data-driven models for short-term thermal behaviour prediction in real buildings," *Applied Energy*, vol. 204, pp. 1375–1387, 2017.

[113] ANSI/ASHRAE, *Thermal Environmental Conditions for Human Occupancy Standard 55-2013*. Peachtree Corners, GA, USA: The American Society of Heating, Refrigerating and Air-Conditioning Engineers (ASHRAE), 2013.

[114] O. Grodzevich and O. Romanko, "Normalization and other topics in Multi-Objective optimization," in *Proceedings of the Fields-MITACS Industrial Problem-Solving Workshop (FMIPW)*, 2006, pp. 89–101.

[115] ComEd, "Live prices," https://hourlypricing.comed.com/live-prices/, accessed: 2022-3-30.

[116] J. Langevin, P. L. Gurian, and J. Wen, "Tracking the human-building interaction: A longitudinal field study of occupant behavior in air-conditioned offices," *Journal of Environmental Psychology*, vol. 42, pp. 94–115, 2015.

[117] M. Wallace, R. McBride, S. Aumi, P. Mhaskar, J. House, and T. Salsbury, "Energy efficient model predictive building temperature control," *Chemical Engineering Science*, vol. 69, no. 1, pp. 45–58, 2012.

[118] BloombergNEF, "Battery pack prices fall to an average of $132/kwh, but rising commodity prices start to bite," https://about.bnef.com/blog/battery-pack-prices-fall-to-an-average-of-132-kwh-but-rising-commodity\-prices-start-to-bite/, 2021, accessed: 2022-3-25.

[119] D. Zhao, D. Watari, Y. Ozawa, I. Taniguchi, T. Suzuki, Y. Shimoda, and T. Onoye, "A thermal comfort and peak power demand aware VRF heating/cooling management framework: Simulation and on-site experiment," *Journal of Information Processing*, vol. 30, pp. 476–485, 2022.

[120] D. Watari, I. Taniguchi, and T. Onoye, "Improving duck curve by dynamic pricing and battery scheduling based on a deep reinforcement learning approach," in *Proceedings of the 8th ACM International Conference on Systems for Energy-Efficient Buildings, Cities, and Transportation (BuildSys)*, 2021, pp. 232–233.

[121] O. Gandhi, D. S. Kumar, C. D. Rodríguez-Gallegos, and D. Srinivasan, "Review of power system impacts at high PV penetration part i: Factors limiting PV penetration," *Solar Energy*, vol. 210, pp. 181–201, 2020.

[122] Y. Li, W. Gao, and Y. Ruan, "Performance investigation of grid-connected residential PV-battery system focusing on enhancing self-consumption and peak shaving in kyushu, japan," *Renewable Energy*, vol. 127, pp. 514–523, 2018.

[123] P. Olczak, P. Jaśko, D. Kryzia, D. Matuszewska, M. I. Fyk, and A. Dyczko, "Analyses of duck curve phenomena potential in polish PV prosumer households' installations," *Energy Reports*, vol. 7, pp. 4609–4622, 2021.

[124] H. Zhong, Z. Tan, Y. He, L. Xie, and C. Kang, "Implications of COVID-19 for the electricity industry: A comprehensive review," *CSEE Journal of Power and Energy Systems*, vol. 6, no. 3, pp. 489–495, 2020.

[125] Q. Hou, N. Zhang, E. Du, M. Miao, F. Peng, and C. Kang, "Probabilistic duck curve in high PV penetration power system: Concept, modeling, and empirical analysis in china," *Applied energy*, vol. 242, pp. 205–215, 2019.

[126] M. Doroshenko, S. Keshav, and C. Rosenberg, "Flattening the duck curve using grid-friendly solar panel orientation," in *Proceedings of the 9th ACM International Conference on Future Energy Systems (e-Energy)*, 2018, pp. 375–377.

[127] J. Meus, K. Poncelet, and E. Delarue, "Applicability of a clustered unit commitment model in power system modeling," *IEEE Transactions on Power Systems*, vol. 33, no. 2, pp. 2195–2204, 2018.

[128] R. Torabi, A. Gomes, and F. Morgado-Dias, "The duck curve characteristic and storage requirements for greening the island of porto santo," in *Proceedings of the 2018 Energy and Sustainability for Small Developing Economies (ES2DE)*, 2018, pp. 1–7.

[129] M. Sheha, K. Mohammadi, and K. Powell, "Solving the duck curve in a smart grid environment using a non-cooperative game theory and dynamic pricing profiles," *Energy Conversion & Management*, vol. 220, p. 113102, 2020.

[130] M. Q. Raza, M. Nadarajah, and C. Ekanayake, "On recent advances in PV output power forecast," *Solar Energy*, vol. 136, pp. 125–144, 2016.

[131] B. Li, J. Shen, X. Wang, and C. Jiang, "From controllable loads to generalized demand-side resources: A review on developments of demand-side resources," *Renewable and Sustainable Energy Reviews*, vol. 53, pp. 936–944, 2016.

[132] Energy Information Administration (EIA), "Electric power monthly - U.S. energy information administration (EIA)," https://www.eia.gov/electricity/monthly/, 2022, accessed: 2022-9-11.

[133] S. Kerscher and P. Arboleya, "The key role of aggregators in the energy transition under the latest european regulatory framework," *International Journal of Electrical Power & Energy Systems*, vol. 134, p. 107361, 2022.

[134] X. Lu, K. Li, H. Xu, F. Wang, Z. Zhou, and Y. Zhang, "Fundamentals and business model for resource aggregator of demand response in electricity markets," *Energy*, vol. 204, p. 117885, 2020.

[135] K. Liu, Q. Chen, C. Kang, W. Su, and G. Zhong, "Optimal operation strategy for distributed battery aggregator providing energy and ancillary services," *Journal of Modern Power Systems and Clean Energy*, vol. 6, no. 4, pp. 722–732, 2018.

[136] R. Lu, S. H. Hong, and X. Zhang, "A dynamic pricing demand response algorithm for smart grid: Reinforcement learning approach," *Applied Energy*, vol. 220, pp. 220–230, 2018.

[137] J. Jiang, Y. Kou, Z. Bie, and G. Li, "Optimal real-time pricing of electricity based on demand response," *Energy Procedia*, vol. 159, pp. 304–308, 2019.

[138] Z. Wang, M. Sun, C. Gao, X. Wang, and B. C. Ampimah, "A new interactive real-time pricing mechanism of demand response based on an evaluation model," *Applied Energy*, vol. 295, p. 117052, 2021.

[139] Z. Yang, M. Ni, and H. Liu, "Pricing strategy of multi-energy provider considering integrated demand response," *IEEE Access*, vol. 8, pp. 149 041–149 051, 2020.

[140] H. Taherian, M. R. Aghaebrahimi, L. Baringo, and S. R. Goldani, "Optimal dynamic pricing for an electricity retailer in the price-responsive environment of smart grid," *International Journal of Electrical Power & Energy Systems*, vol. 130, p. 107004, 2021.

[141] R. Jovanovic, S. Bayhan, and I. S. Bayram, "A multiobjective analysis of the potential of scheduling electrical vehicle charging for flattening the duck curve," *Journal of Computational Science*, vol. 48, p. 101262, 2021.

[142] H. O. R. Howlader, M. M. Sediqi, A. M. Ibrahimi, and T. Senjyu, "Optimal thermal unit commitment for solving duck curve problem by introducing CSP, PSH and demand response," *IEEE Access*, vol. 6, pp. 4834–4844, 2018.

[143] I. Calero, C. A. Cañizares, K. Bhattacharya, and R. Baldick, "Duck-curve mitigation in power grids with high penetration of PV generation," *IEEE Transactions on Smart Grid*, vol. 13, no. 1, pp. 314–329, 2022.

[144] A.-Y. Yoon, H.-K. Kang, and S.-I. Moon, "Optimal price based demand response of HVAC systems in commercial buildings considering peak load reduction," *Energies*, vol. 13, no. 4, p. 862, 2020.

[145] J. Ferdous, M. P. Mollah, M. A. Razzaque, M. M. Hassan, A. Alamri, G. Fortino, and M. Zhou, "Optimal dynamic pricing for trading-off user utility and operator profit in smart grid," *IEEE Transactions on Systems, Man, and Cybernetics*, vol. 50, no. 2, pp. 455–467, 2017.

[146] J. Zhang, L. Che, L. Wang, and U. K. Madawala, "Game-Theory based V2G coordination strategy for providing ramping flexibility in power systems," *Energies*, vol. 13, no. 19, p. 5008, 2020.

[147] M. Askeland, T. Burandt, and S. A. Gabriel, "A stochastic MPEC approach for grid tariff design with demand-side flexibility," *Energy Systems*, 2020.

[148] A. SoltaniNejad Farsangi, S. Hadayeghparast, M. Mehdinejad, and H. Shayanfar, "A novel stochastic energy management of a microgrid with various types of distributed energy resources in presence of demand response programs," *Energy*, vol. 160, pp. 257–274, 2018.

[149] S. Abapour, B. Mohammadi-Ivatloo, and M. Tarafdar Hagh, "Robust bidding strategy for demand response aggregators in electricity market based on game theory," *Journal of Cleaner Production*, vol. 243, p. 118393, 2020.

[150] Y. Li, K. Wang, B. Gao, B. Zhang, X. Liu, and C. Chen, "Interval optimization based operational strategy of integrated energy system under renewable energy resources and loads uncertainties," *International Journal of Energy Research*, vol. 45, no. 2, pp. 3142–3156, 2021.

[151] R. S. Sutton and A. G. Barto, *Reinforcement Learning, second edition: An Introduction*. Cambridge, MA, USA: MIT Press, 2018.

[152] B. Wang, Y. Li, W. Ming, and S. Wang, "Deep reinforcement learning method for demand response management of interruptible load," *IEEE Transactions on Smart Grid*, vol. 11, no. 4, pp. 3146–3155, 2020.

[153] D. Qiu, Y. Ye, D. Papadaskalopoulos, and G. Strbac, "A deep reinforcement learning method for pricing electric vehicles with discrete charging levels," *IEEE Transactions on Industry Applications*, vol. 56, no. 5, pp. 5901–5912, 2020.

[154] Y. Kuang, X. Wang, H. Zhao, T. Qian, J. Wang, and X. Wang, "Model-free demand response scheduling strategy for virtual power plant considering risk attitude of consumer," *CSEE Journal of Power and Energy Systems*, pp. 1–12, 2021.

[155] P. R. Thimmapuram and J. Kim, "Consumers' price elasticity of demand modeling with economic effects on electricity markets using an Agent-Based model," *IEEE Transactions on Smart Grid*, vol. 4, no. 1, pp. 390–397, 2013.

[156] M. Miller and A. Alberini, "Sensitivity of price elasticity of demand to aggregation, unobserved heterogeneity, price trends, and price endogeneity: Evidence from U.S. data," *Energy Policy*, vol. 97, pp. 235–249, 2016.

[157] K. Vanthournout, B. Dupont, W. Foubert, C. Stuckens, and S. Claessens, "An automated residential demand response pilot experiment, based on day-ahead dynamic pricing," *Applied Energy*, vol. 155, pp. 195–203, 2015.

[158] P. Yang, G. Tang, and A. Nehorai, "A game-theoretic approach for optimal time-of-use electricity pricing," *IEEE Transactions on Power Systems*, vol. 28, no. 2, pp. 884–892, 2013.

[159] P. Samadi, A.-H. Mohsenian-Rad, R. Schober, V. W. S. Wong, and J. Jatskevich, "Optimal Real-Time pricing algorithm based on utility maximization for smart grid," in *Proceedings of the 2010 1st IEEE International Conference on Smart Grid Communications (SmartGridComm)*. IEEE, 2010, pp. 415–420.

[160] K. M. Tsui and S. C. Chan, "Demand response optimization for smart home scheduling under Real-Time pricing," *IEEE Transactions on Smart Grid*, vol. 3, no. 4, pp. 1812–1821, 2012.

[161] M. van Otterlo and M. Wiering, "Reinforcement learning and markov decision processes," in *Reinforcement Learning: State-of-the-Art*, M. Wiering and M. van Otterlo, Eds. Berlin, Heidelberg, Germany: Springer Berlin Heidelberg, 2012, pp. 3–42.

[162] L. Han, Y. Peng, Y. Li, B. Yong, Q. Zhou, and L. Shu, "Enhanced deep networks for Short-Term and Medium-Term load forecasting," *IEEE Access*, vol. 7, pp. 4045–4055, 2019.

[163] M. Tanaka, "Real-time pricing with ramping costs: A new approach to managing a steep change in electricity demand," *Energy Policy*, vol. 34, no. 18, pp. 3634–3643, 2006.

[164] J. Schulman, F. Wolski, P. Dhariwal, A. Radford, and O. Klimov, "Proximal policy optimization algorithms," arXiv:1707.06347 [cs.LG], 2017.

[165] California ISO, "Wholesale electricity prices," http://www.caiso.com/Pages/default.aspx, accessed: 2021-7-19.

[166] C. Miller, A. Kathirgamanathan, B. Picchetti, P. Arjunan, J. Y. Park, Z. Nagy, P. Raftery, B. W. Hobson, Z. Shi, and F. Meggers, "The building data genome project 2, energy meter data from the ASHRAE great energy predictor III competition," *Scientific Data*, vol. 7, no. 1, p. 368, 2020.

[167] The California Solar Initiative (CSI), "California distributed generation statistics," https://www.californiadgstats.ca.gov/downloads/, accessed: 2021-7-19.

[168] G. Brockman, V. Cheung, L. Pettersson, J. Schneider, J. Schulman, J. Tang, and W. Zaremba, "OpenAI gym," arXiv:1606.01540 [cs.LG], 2016.

[169] A. Raffin, A. Hill, A. Gleave, A. Kanervisto, M. Ernestus, and N. Dormann, "Stable-baselines3: Reliable reinforcement learning implementations," *Journal of Machine Learning Research*, vol. 22, no. 268, pp. 1–8, 2021.

[170] T. Akiba, S. Sano, T. Yanase, T. Ohta, and M. Koyama, "Optuna: A next-generation hyperparameter optimization framework," in *Proceedings of the 25th ACM SIGKDD International Conference on Knowledge Discovery & Data Mining (KDD)*, 2019, pp. 2623–2631.

[171] L. Engstrom, A. Ilyas, S. Santurkar, D. Tsipras, F. Janoos, L. Rudolph, and A. Madry, "Implementation matters in deep policy gradients: A case study on PPO and TRPO," arXiv: 2005.12729 [cs.LG], 2020.

[172] M. Andrychowicz, A. Raichuk, P. Stańczyk, M. Orsini, S. Girgin, R. Marinier, L. Hussenot, M. Geist, O. Pietquin, M. Michalski, S. Gelly, and O. Bachem, "What matters in On-Policy reinforcement learning? a Large-Scale empirical study," arXiv: 2006.05990 [cs.LG], 2020.

[173] S. Chen, G. Sun, Z. Wei, and D. Wang, "Dynamic pricing in electricity and natural gas distribution networks: An EPEC model," *Energy*, vol. 207, p. 118138, 2020.

[174] D. Watari, I. Taniguchi, and T. Onoye, "SoH aware battery management optimization on decentralized energy network," in *Proceedings of the 9th ACM/IEEE International Conference on Cyber-Physical Systems (ICCPS)*, 2018, pp. 337–338.

[175] D. Watari, I. Taniguchi, P. Manganiello, H. Goverde, F. Catthoor, and T. Onoye, "An online multi-scale optimization framework for smart PV systems," in *Proceedings of the 36th European Photovoltaic Solar Energy Conference and Exhibition (EUPVSEC)*. WIP, 2019, pp. 1681–1684.

[176] D. Watari, I. Taniguchi, F. Catthoor, C. Marantos, K. Siozios, E. Shirazi, D. Soudris, and T. Onoye, "Thermal comfort aware online energy management framework for a smart residential building," in *Proceedings of the 24th Design, Automation and Test in Europe Conference (DATE)*, 2021, pp. 535–538.

[177] V. Gabrel, C. Murat, and A. Thiele, "Recent advances in robust optimization: An overview," *European Journal of Operational Research*, vol. 235, no. 3, pp. 471–483, 2014.

[178] J. Weniger, T. Tjaden, and V. Quaschning, "Sizing of residential PV battery systems," *Energy Procedia*, vol. 46, pp. 78–87, 2014.

[179] Y. Cao, R. C. Kroeze, and P. T. Krein, "Multi-timescale parametric electrical battery model for use in dynamic electric vehicle simulations," *IEEE Transactions on Transportation Electrification*, vol. 2, no. 4, pp. 432–442, 2016.

[180] H. Ishibuchi, N. Tsukamoto, and Y. Nojima, "Evolutionary many-objective optimization: A short review," in *Proceedings of the 2008 IEEE Congress on Evolutionary Computation (CEC)*, 2008, pp. 2419–2426.